University of Southern Queensland
Faculty of Engineering & Surveying

Temperature Variations in a Free Piston Compression Wind Tunnel

A thesis submitted by

Agung Sugeng Widodo

B.Eng., M.Eng.

in fulfilment of the requirements for the degree of

Doctor of Philosophy

Submitted: July, 2012

Abstract

This dissertation presents an investigation of the free stream stagnation temperature variations in the University of Southern Queensland (USQ) hypersonic wind tunnel (designated TUSQ), a short duration wind tunnel operated as a Ludwieg Tube with free piston compression heating. Because the facility is relatively new and because strong disturbances have previously been observed in similar facilities, a study to investigate the thermal characteristics of the hypersonic flow generated by TUSQ was needed.

This study investigates the temporal and spatial thermal characteristics of the hypersonic flow produced in the TUSQ facility and relates these characteristics to the compression and flow discharge processes within the barrel. Quantification of the flow conditions produced in wind tunnels is important. Without such information, it is difficult to relate wind tunnel results to flight conditions or to perform meaningful computational simulations on the tested configuration.

Three different versions of an aspirating thermocouple probe were developed for this work and a thin film heat flux gauge was also tested. Results with the Mach 6 nozzle show that the flow stagnation temperature decreases with time and thermodynamic simulations accurately reflect the majority of the observed temporal variations when flat plate boundary layer cooling is used to model the heat transfer in the barrel of the facility. Because the flat plate boundary layer cooling model provides a good match to the measured temperature on the nozzle centre line for the majority of the flow duration, it is concluded that significant

mixing must have occurred across the diameter of barrel prior to flow discharge through the nozzle. Measurements in other facilities have indicated the existence of discrete, large scale thermal disturbance which propagated ahead of the piston and potentially compromised the test flow quality, but no such disturbance were detected at the centre line of the nozzle exit in the present work.

The stagnation temperature measurements indicated a core flow region with a radius of almost 80 mm near the start of the test flow. The maximum average spatial gradient of stagnation temperature was registered at about 150 ms after the start of the test flow and had a value of approximately -0.45 K/mm within the core flow region, indicating an average drop in stagnation temperature of about 20 K over the core flow region at this time. Complementary pitot pressure measurements indicate core flow uniformity to within 2 % and a core flow radius of at least 80 mm for the majority of the test flow duration of around 200 ms. Mach number profiles deduced from the pitot pressure measurements are likewise uniform with a Mach number of 5.81 ± 0.05 for the majority of the test flow duration.

A fully-developed turbulent pipe flow model was developed and stagnation temperature fluctuations in the TUSQ facility were estimated to be around 20 K. Although this value is large compared to results from previous experiments in a gun tunnel facility, the value obtained is consistent with the magnitude of the spatial variation in stagnation temperature within the core region of the nozzle exit flow at about 150 ms from the start of the flow. Relatively low frequency fluctuations in the stagnation point heat flux were observed and these appeared to correlate with the stagnation pressure fluctuations, but further effort in this area is required in order to resolve stagnation temperature fluctuations due to the turbulent mixing in the barrel.

Keywords : temperature fluctuations, hypersonic flow, stagnation temperature, free piston compression

Associated Publications

The following publications were produced during the period of candidature:

Widodo, A. and Buttsworth, D., "Deduction of Temperature Fluctuation in Transient Compression Wind Tunnels Using Incompressible Turbulent Flow Data", *Proceeding of ICEE 2009, 3 rd International Conference on Energy and Environment*, 7-8 December 2009. Malacca, Malaysia: pp 6-10.

Widodo, A. and Buttsworth, D., "Stagnation Temperature Measurements in the USQ Hypersonic Wind Tunnel", *17 th Australasian Fluid Mechanics Conference*, Auckland, New Zealand, 5-9 December 2009.

Widodo, A. and Buttsworth, D., "Stagnation Temperature in a Cold Hypersonic a Flow Produced in a Light Piston Compression Facility", *submitted for publication.*

Widodo, A. and Buttsworth, D., "Radial Stagnation Temperature Distribution at the Nozzle Exit of the USQ Hypersonic Wind Tunnel", *submitted for publication.*

Certification of Dissertation

I certify that the ideas, designs and experimental work, results, analyses and conclusions set out in this dissertation are entirely my own effort, except where otherwise indicated and acknowledged.
I further certify that the work is original and has not been previously submitted for assessment in any other course or institution, except where specifically stated.

Agung Sugeng Widodo

0050078029

_____

Signature of Candidate

_____

Date

ENDORSEMENT

_____

Signature of Supervisor/s

_____

Date

Acknowledgments

This project, I believe would not have been possible without the following people. I wish to acknowledge their support in helping me complete this project.

I would like to thank my advisor, Professor David R. Buttsworth for all of his guidance, support, encouragement and willingness to help in any way possible throughout the duration of this work.

I also would like to express thanks to Dr. Sudantha Balage of helping in operational of the University of Southern Queensland Wind tunnel and assistance with the data acquisition and electrical problems.

All of my fellow students with whom I shared office space in P7 for any discussions relating to all sorts of matters which impacted on this work.

I wish to thank Office of Research and Higher Degrees – University of Southern Queensland, the Faculty of Engineering and Surveying – University of Southern Queensland, Indonesian Government and my institution the University of Brawijaya for financial support.

Finally, I would like to express my deep gratitude to my wife Fitri Witanovelasari and my daughters Irene and Tamara also my son Renjiro who were always there for me.

Agung Sugeng Widodo

University of Southern Queensland

July 2012

Contents

List of Figures

List of Tables

List of Notation

Symbols

c_p	constant pressure specific heat
c_v	constant volume specific heat
d	wire diameter
D	diameter
T	temperature
f	friction factor
h	heat transfer coefficient
I	element i
k	thermal conductivity
Nu	Nusselt number
Pr	Prandtl number
Q_w	heat flux at the wall
q	heat flux
R	resistance
Re	Reynolds number
Re_τ	friction velocity Reynolds number
S	scaling factor
T_{aw}	adiabatic wall temperature
T_τ	friction temperature
T_f	flow temperature
T_0	stagnation temperature
T_w	wall temperature

t	time
t_0	time constant
u	velocity
u_τ	friction velocity
V	voltage; velocity
x	rectangular coordinate
y	rectangular coordinate

Greek Symbols

α	thermal diffusivity; film temperature coefficient
δ	boundary layer thickness
ε	eddy diffusivity
γ	specific heat ratio (c_p/c_v)
ν	convection parameter
ρ	density
σ	standard deviation
τ_i	ignition time
τ_r	reaction time
ϕ	diameter; $T_i - T_0$

Subscript

ad	adiabatic
c	centreline
$exit$	exit conditions
i	ignition; initial; element i
$isen$	isentropic
L	half-length of the wire
M	momentum
pit	pitot
r	reaction; reservoir
rms	root mean square

s	surface
p	piston
w	wall
0	stagnation; initial

Superscript

$+$	directed outward from a surface
$'$	fluctuating
$*$	at throat

Overscore

$-$	average
.	per unit time
$*$	at throat

List of Acronyms

BW	Butt-welded
CHAL	Chromega-Alumega
EMF	Electro Motive Force
LICH	Ludwieg tubes with Isentropic Compression Heating
OUGT	The Oxford University Gun Tunnel
RMS	Root Mean Square
RTD	Resistance Temperature Detector
TUSQ	The University of Southern Queensland Wind Tunnel
USQ	University of Southern Queensland

Chapter 1

Introduction

1.1 Wind Tunnel Disturbances

A wind tunnel is a device for producing an air flow to simulate atmospheric flight under controlled conditions on the ground. However, no single wind tunnel can fully simulate all aspects of hypervelocity flight [11]. Throughout the 20^{th} century, flight speeds simulated in wind tunnels have increased. In the modern era wind tunnels which are able to duplicate the high enthalpy flow associated with superorbital re-entry conditions are now available [12]. Quantification of the flow conditions produced in wind tunnels in term of both spatial and temporal uniformity is important. Without such information, it is difficult to relate wind tunnel results to flight conditions or to perform meaningful computational simulations on the tested configuration.

Disturbances present in the free stream flow of wind tunnel facilities remains a critical issue and may have a significant impact on the development of hypersonic air-breathing propulsion systems. An investigation by Watmuff [13] showed that transition on a flat plate is extremely sensitive to free-stream disturbances. The level of fluctuations in typical wind tunnels can be one or two orders of magnitude

higher than in flight due to the appearance of acoustic disturbances as they naturally occur on the test section walls [14–16].

Phenomena such as laminar-turbulent transition [16–18], turbulent flow development [6, 19–22], combustion [23, 24], and shock wave-boundary layer interaction [25–28] are likely to be impacted by such fluctuations and are important features of hypersonic design [29]. Although the boundary-layer transition phenomenon has received widespread attention, there is no single theoretical or empirical method that can be used to confidently predict the transition under all conditions that exist in flight or in ground test facilities [30]. The mechanism of transition is still not completely understood and remains an unsolved problem despite a significant amount of research that has been carried out during the past few decades [17]. Transition, for instance, plays an important role in aerodynamic drag, heat loads and shock boundary layer interactions. Heat flux rates can increase by 300% through the boundary layer transition [31]. The accuracy of determination of the transition location may lead to an uncertainty of 20% in terms of the total vehicle weight [32].

1.2 Temperature Variations

Transient compression impulse facilities such as shock tunnels and expansion tubes offer a relatively low cost solution for the generation of hypervelocity test flow. However, short duration wind tunnels such as shock tunnels and gun tunnels that rely on a transient compression process are likely to generate significant turbulent fluctuations including temperature disturbances which arise due to the large temperature differences between the hot test gas and the cold walls of the facility.

Some studies of the effect of temperature fluctuations on transition location have been done by Brinich [33] and Ross [34]. Temperature fluctuations that are

convected into the test section could also influence the results of other experiments, particularly for rate-controlled combustion experiments, for example, in certain scramjet applications. Turbulence-chemistry interaction has been studied extensively in the field of combustion [35–38] and was found to be extremely important for predicting combustion quantities, such as burning rate and ignition delay. Martin and Chandler [39], using Direct Numerical Simulation (DNS) showed that the temperature fluctuations can increase the reaction rates. As little as a 5% fluctuation in temperature can cause a 30% fluctuation in the species mass fraction. Direct measurement of the level of free stream fluctuations has rarely been achieved in short duration hypersonic facilities [40].

Many investigations have been performed to identify fluctuations in wind tunnels using non intrusive measurements [41–43] and conventional techniques [2, 44–46]. Fluctuations in certain quiet tunnels have also been identified [47, 48], however it appears that little attention has been paid to the identification of temperature fluctuations in the nozzle exit flow. Measurement of stagnation temperature fluctuations at the nozzle exit of a gun tunnel has been achieved by Buttsworth and Jones [49]. Fluctuations in stagnation temperature in that investigation were derived from heat flux fluctuation measured using transient thin film heat flux probes in Mach 6 carbon dioxide flow. RMS stagnation temperature fluctuations during a 12 ms flow period were determined to be 2.3 K for a stagnation temperature of 610 $\pm$ 10 K. This data was obtained at one location at the exit of the hypersonic nozzle. It was concluded the measured temperature fluctuations were primarily due to fluctuations in entropy. However, this experiment has no detailed information on the distribution and the origin of these temperature fluctuations.

1.3 Purpose of the Present Work

A new hypersonic wind tunnel facility based on free piston compression techniques has been established at University of Southern Queensland (TUSQ). The

facility is similar in many respects to that which was established at University of Southampton in the 1970s [50]. The University of Southampton facility was operated with an electrically heated barrel in an effort to avoid strong thermal disturbances convecting into the hypersonic nozzle during the test time. The TUSQ facility is currently being operated without any external heating on the barrel. Therefore it is important to investigate the spatial and temporal uniformity of the flow produced by the TUSQ facility.

The principal objective of this project is to investigate the thermal characteristics of the hypersonic flow produced in the TUSQ facility and to relate these characteristics to the compression and flow discharge processes within the barrel. Necessary tasks undertaken to meet the principal objective are as follows:

1. Development of a model for the temperature fluctuations at the hypersonic nozzle exit based on existing turbulent pipe flow measurements and analysis based on incompressible data applied to the compression/discharge process in the barrel.

2. Development and application of techniques for the acquisition of spatially and temporally resolved temperature data in the TUSQ facility based on thermocouple technology.

3. Analysis of thermocouple-based results in the context of thermodynamic simulations which include modelling of heat transfer from the test gas during the compression and flow discharge process.

4. Development and application of techniques for acquisition of stagnation temperature and associated fluctuations base on thin film heat flux gauge technology.

1.4 Thesis Overview

The present work focuses mainly on the investigation of the stagnation temperature at the nozzle exit of the University of Southern Queensland (USQ) hypersonic wind tunnel (TUSQ) and relates these characteristics to the compression and flow discharge processes within the barrel. Quantification of the flow conditions produced in wind tunnels is important. Without such information, it is difficult to relate wind tunnel results to flight conditions or to perform meaningful computational simulations on the tested configuration as described in the present chapter.

In Chapter 2, the relevant previous studies are briefly introduced and reviewed within the context of the experiments performed in the present work. Chapter 3 will focus on the development of a model for deduction of stagnation temperature distribution and fluctuations in transient compression wind tunnels facility based on existing boundary layer heat transfer measurements and analysis. Chapter 4 introduces the TUSQ facility and apparatus to be used in the current experiments. Chapter 5 presents and discusses preliminary efforts in measuring the flow stagnation temperature in the TUSQ facility. Details of the probe used and the method of deducing the flow stagnation temperature are described. Chapter 6 presents time-resolved stagnation temperature measurements at the hypersonic nozzle exit based on a revised probe design and a thermocouple wire thermal inertia correction method. In this chapter also, the free piston compression process has been simulated based on the measured pressure in the barrel and models for the heat loss from the test gas to the barrel wall during the test gas compression and discharge process. Chapter 7 presents measurements of spatially-resolved stagnation temperature at the nozzle exit. Chapter 8 is concerned with preliminary efforts in the measurement of stagnation temperature fluctuations using a thin film heat flux gauge. Finally, conclusions from the project are presented in Chapter 9.

Chapter 2

Literature Review

2.1 Fluctuations in Wind Tunnels

Wind tunnels can be used to simulate supersonic and hypersonic flight conditions, but different wind tunnels can give different results for the same model and nominal flow conditions. Different critical (transition) Reynolds numbers [14] and drag measurements [51] for spheres obtained in various wind tunnels can be related to the turbulence in the free stream. To reduce turbulence in conventional wind tunnels, Prandtl in 1932 suggested using devices such as screens, rectifiers and guiding vanes and such devices have become standard features in low speed wind tunnels design. The use of additional screens is reported to reduce turbulence [52]. Table of 2.1 overviews free stream fluctuations in different wind tunnels.

Turbulence in the free stream of ground test facilities is known to affect the laminar-turbulent boundary-layer transition, flow separation, shock-boundary layer interaction, and buffeting in transonic flows [53]. It is furthermore found that differences and ambiguities in ground test facility and flight data primarily arise due to a high level of acoustic fluctuations which appear and radiate into

Table 2.1: Type of fluctuations and their origin in the wind tunnels [8].

tunnel type	Mach number range	type fluctuations	source
subsonic	0 - 0.3	turbulence, acoustic	settling chamber, standing waves (organ pipe resonance)
			travelling waves (fans noise, sound generator)
transonic	1.2 - 1.5	acoustic	porous (holes) wall (edge tone discrete frequency)
			slotted wall (resonances)
supersonic-hypersonic	∼2 - ∼20	radiated sound	wall turbulent boundary layer

the nozzle with a preferred orientation [46]. Fischer & Weinstein reaffirm that acoustic disturbances spread with constant angle [54].

Wind tunnel quality can be characterized by the magnitude of the turbulent velocity (vorticity), pressure (noise), and entropy fluctuations. The starting point for analysis is typically the fluctuating energy equation. For many engineering purposes, the simplest approach is to use Reynolds decomposition in which properties in a turbulent flow could be considered as the superposition of time-averaged and fluctuating components, see figure 2.1.

Consider some scalar property g. The Reynolds decomposition of g is

$$g = \bar{g} + g' \tag{2.1}$$

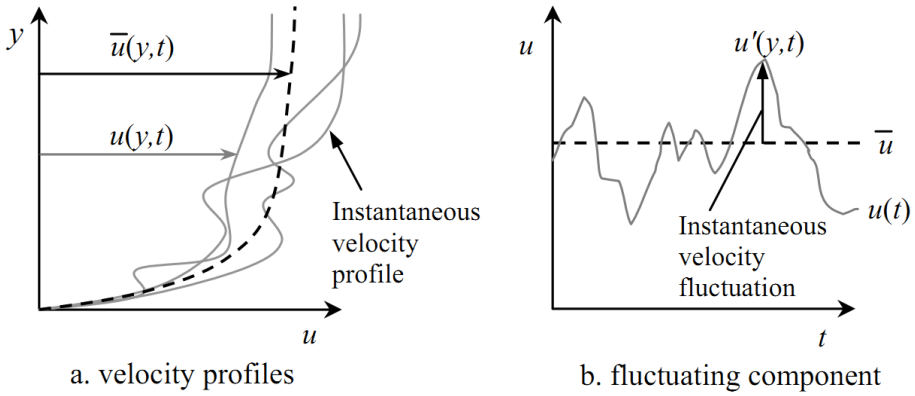

Figure 2.1: Turbulent flow near a wall. Reproduced from [1].

where the time-averaged component is determined by

$$\bar{g} = \frac{1}{\tau}\int_0^\tau g(t)\,dt \tag{2.2}$$

By definition, the time average of the fluctuating component is zero

$$\bar{g'} = \frac{1}{\tau}\int_0^\tau g'(t)\,dt = 0 \tag{2.3}$$

Turbulent flow in wind tunnels can be treated by considering the instantaneous basic flow field variables: velocity (u), pressure (p), and density (ρ). By using Reynolds decompositions, those flow field variables can be separated into mean and fluctuating components: $u = \bar{u} + u'$; $p = \bar{p} + p'$; and $\rho = \bar{\rho} + \rho'$. Furthermore, velocity fluctuations u' can be split into a rotational part $(u')_{rot}$ where $\text{curl}(u') \neq 0$ and an irrotational part $(u')_{irr}$ where $\text{curl}(u') = 0$.

Kovasznay [45] adopted a different approach for classification of free stream fluctuations in wind tunnels. In cases where the intensity of the fluctuations is small, first order perturbation theory and a linearization of the Navier-Stokes equations for a compressible, viscous and heat conductive gas can be applied. The resulting free stream fluctuations in wind tunnels can then be classified into three different modes: (i) vorticity; (ii) entropy spottiness; and (iii) sound waves. However, coupling between the modes must be considered at larger intensities.

Morkovin [55] reported that the freestream of supersonic/hypersonic flows can have three fluctuations modes with different origins. Vorticity fluctuations are known to be dominant in low speed wind tunnels whereas the acoustic mode dominates in super/hypersonic wind tunnels. These vorticity fluctuations are generated in the settling chamber where wakes and flow separation regions can occur due to components such as flow straighteners, honey combs, screens etc. Intensities of fluctuations recorded in low speed wind tunnels vary from 0.1 - 3.0 % [56, 57]. The contraction ratio of a nozzle also contributes to the vorticity fluctuations: the larger contraction ratio, the stronger the vorticity generated.

The effect of vorticity fluctuations on laminar-turbulent transition was investigated by Laufer & Marte [58]. The experiment was performed over Mach numbers from 1.7 to 4 and fluctuation levels in the settling chamber of the Jet Propulsion Laboratory (JPL) 20-inch tunnel were varied between 0.6 to 7%. The results showed that transition on a sharp cone in the test section was independent of the settling chamber fluctuations for free stream Mach numbers above 2.5. Investigation by Van Driest and Boison [59] conducted on a sharp cone at Mach numbers between 2 - 4 showed that the location of transition remained unchanged when the level of turbulence in settling chamber was varied from 0.7 to 4.6%. Subsequent research was performed by Laufer [46], Morkovin [55], Spangler & Wells [57], Donaldson & Wallace [60] with the general goal of understanding the influence of fluctuations on the transition problem. All the researchers confirmed that for Mach numbers below 2.5, certain types of experiments are strongly affected by the level of vorticity (turbulence) in the flow. However, vorticity modes can be minimized by careful design and proper selection of upstream components and in such case, fluctuations can be reduced to around 0.1 %.

Entropy fluctuations (temperature spottiness) also appear in conventional supersonic facilities at low Mach number. Kovasznay [45] identified the appearance of this type of fluctuation using a hot wire anemometer. Wagner [61] reported the existence of 0.2 % and 0.03 % RMS total temperature fluctuations in a 1.5 m

helium tunnel at Mach numbers 20 and 17.5. Morkovin [62] showed that the sources of entropy fluctuations are traceable to the settling chamber of conventional supersonic wind tunnels and farther upstream, especially when dried air is introduced to the main flow circuit and to the cooling station. Investigations by Brinich [33] on a flat plate at freestream Mach number of 3.1 and Ross [34] on a hollow cylinder at a freestream Mach number of 4.0 showed that there are no significant effects of entropy fluctuations on laminar turbulent transition when the stagnation temperature was varied in the supersonic wind tunnels flow. Entropy fluctuations can arise if there are temperature gradients in the settling chamber or the stagnation region of the nozzle. Large scale convective structures and irregularities in the temperature distribution in nozzles can appear as fluctuations in temperature at the nozzle exit. Although entropy fluctuations apparently have negligible effect on the transition, this type of fluctuations might be able to be minimized by careful design of the settling chamber and the use of heat exchangers to control mean temperature of flow. However in certain wind tunnels such as shock tunnels, arc tunnels, and combustion-type tunnels, there is a significant effect in certain applications relating to combustion processes as reported by Martin [39].

The situation for Mach numbers ≥ 2.5 is different. In this type of wind tunnel, fluctuations are dominated by acoustic waves, 'shivering Mach waves'. Although these types of fluctuations can be found in low speed wind tunnels, the values are low [57, 63]. However, in porous-wall transonic wind tunnels, the fluctuations become significant compared to well-designed solid wall subsonic wind tunnels [64]. The level of such fluctuations will be worse in higher Mach number wind tunnels since the magnitude of acoustic fluctuations increase by a factor of the fourth power of Mach number [46]. Therefore, significant acoustic fluctuations are expected for hypersonic facilities (Mach number greater than 5) compared to the disturbances in supersonic facilities at Mach numbers of around 3. Laufer [46] attempted to quantify such matters and found the level of acoustic fluctuations can be 50 times greater than fluctuations measured in low disturbance subsonic

wind tunnels.

The interaction of turbulent flow with solid boundaries promotes acoustic disturbances and the generation of fluctuations [65]. Acoustic fluctuations appear when a turbulent boundary layer exists on the nozzle wall and these fluctuations spread across the streamlines and radiate sound waves in a preferred orientation. Kendall [66] found that the freestream fluctuations were amplified by the laminar boundary layer on a flat plate by one to two orders of magnitude and a similar conclusion was reported by Beckwith [67]. The level of acoustic fluctuations will increase as the nozzle wall's boundary layer thickness increase [68]. Morkovin [2] attempted to classify the acoustic fluctuations into: (1) radiation from the wall turbulent boundary layer, (2) shivering Mach waves from wall roughness or waviness, (3) wall vibrations and (4) diffraction and scattering of otherwise steady pressure gradients. As described in [2, 46, 55], disturbances of the type described in point (1) are classified as eddy Mach waves in which disturbances are radiated across the free stream and disturbances of the type described in points of (2), (3) and (4) are classified as shivering Mach waves. Free stream fluctuation appearance, forms, and interaction as described by Morkovin in supersonic wind tunnels are illustrated in figure 2.2.

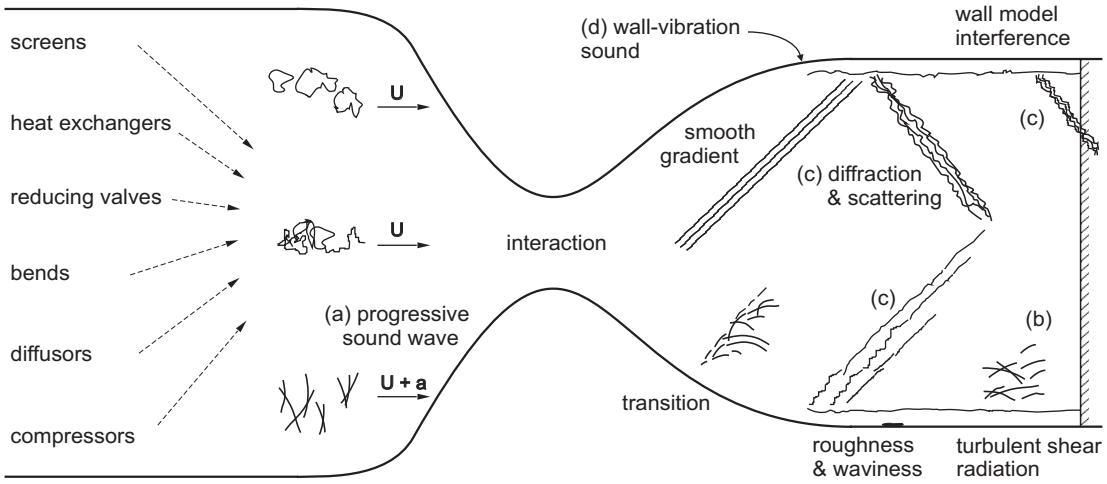

Figure 2.2: Free stream fluctuations in supersonic flow. Reproduced from [2].

2.2 Short Duration Wind Tunnel Facilities

2.2.1 Ludwieg Tube

A Ludwieg tube is a wind tunnel that produces supersonic flow for short periods. It can provide good quality of flow at a low cost. Hubert Ludwieg in 1955 proposed the concept of such a tube in response to a competition for a supersonic blow down wind tunnel which was capable of producing high Reynolds number in economical manner compared to other supersonic facilities at that time [69]. As an illustration, a small, continuous blow down facility requires power in the megawatt range [70]. In contrast, short duration wind tunnels such as Ludwieg tubes are able to use energy accumulated over a long period of time, with a relatively low input power requirement. The release of the accumulated energy occurs rapidly, but under well manage conditions. As a consequence, the flows produced by such facilities typically have limited test times of a few tens of milliseconds [71]. The operational cost of a Ludwieg tube may be reduced to up to 60% relative to that of a conventional blowdown wind tunnel [72, 73].

A Ludwieg tube consists of a long tube containing high pressure air (or another test gas) and a converging-diverging nozzle. A diaphragm, or fast opening valve, is used to initially isolate the high-pressure gas in the tube from the low-pressure region downstream of the nozzle. When the diaphragm ruptures, an expansion wave propagates upstream into the tube thereby establishing a flow of gas into the test section.

2.2.2 Free Piston Ludwieg Tube Variants

Short duration wind tunnel facilities using free piston compression for creating test flows with moderate stagnation temperatures were developed in the 1970's for turbine testing and hypersonic flow research [3, 50, 74].

The description, 'Ludwieg tube with isentropic compression heating' (LICH) was applied to the arrangement described by [74]. The principles of operation of the LICH system can be explained with reference to figure 2.3. The system of the LICH consists of a high pressure reservoir connected via a throat and a valve to the barrel that vents through nozzle into a dump tank.

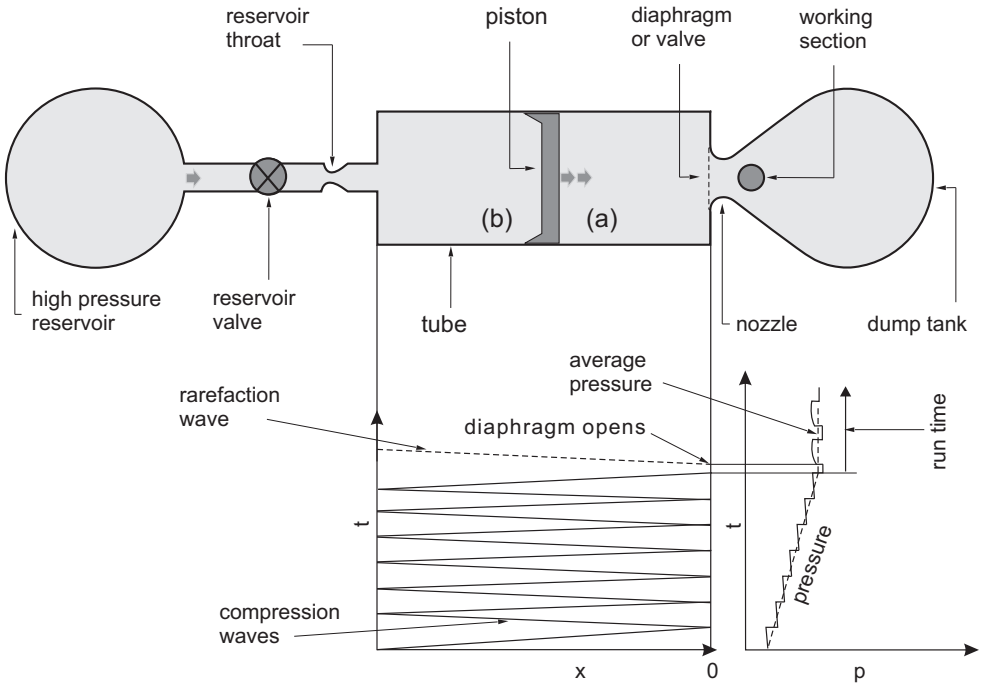

Figure 2.3: Schematic diagram of the isentropic light piston tunnel and x - t diagram, adapted from [3].

Once the reservoir valve opens, the gas from the high pressure reservoir enters the barrel, pushing the piston downstream and compressing the test gas isentropically. The x - t diagram in figure 2.3 shows the variation in the pressure within the gas that occurs due to the compression and rarefaction waves. Compression waves generated by the initial piston motion reflect repeatedly from both ends of the tube causing an increase of the pressure within the tube.

The reservoir valve not only isolates the gas between the high pressure reservoir and barrel until the required run time, but can also be used to control the volumetric flow rate that comes into the barrel. With reference to figure 2.3, the condition in which the volumetric flow rate into (b) equals the volumetric flowrate

out of region (a), is said to be a 'matched' condition. In such a case the average test gas pressure during the run time will remain constant until the piston reaches the end of the barrel.

The compression process occurring in such facilities is normally assumed to be in equilibrium and adiabatic, and the piston mass is assumed to be negligible so that the kinetic energy of the piston is zero and there is no pressure differential across it. Kinetic energy of the gas within the tube is also assumed to be negligible as velocities involved are small compare to those of the speed of sound. However, in a case where the piston has a finite mass, the piston would likely experience oscillations and the form of pressure history would follow the dotted-line as shown in figure 2.4.

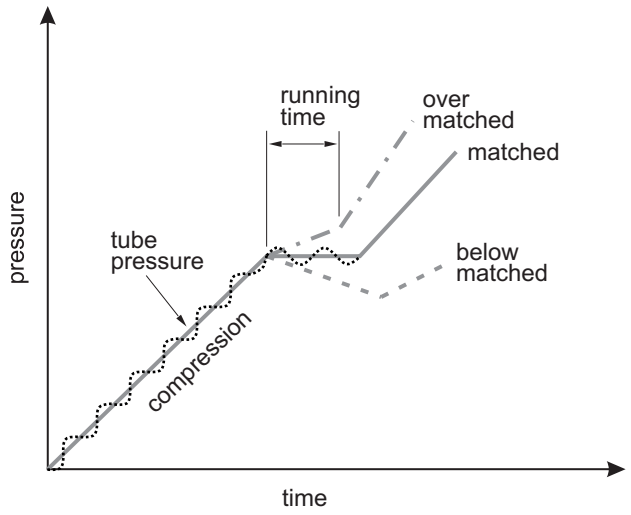

Figure 2.4: Illustrative pressure histories for an isentropic light piston tunnel.

Under these assumptions (including zero piston mass), the energy equation is used in reference [3] to demonstrate the rate of pressure increase within the barrel should be linear if the mass flow rate from the reservoir into the barrel is constant. The mass flow rate into the barrel will be maintained constant if the delivery of flow from the reservoir to the barrel is choked and the reservoir volume is infinite. Operation with a choked process at the restriction valve and infinite reservoir volume results in a linear pressure rise within the tube with constant mass flow rate.

Conditions within the facility may be explained using figure 2.4. For matched conditions, the ideal form of the pressure history in the tube is obtained as shown by the horizontal line during the test period. An over matched condition may occur if the volume flow rate from the reservoir exceeds the test gas discharge rate. Under such conditions, the running period will be shorter. A condition below matched may occur if the test gas discharge rate exceeds the rate of gas delivery from the reservoir. Under such conditions the pressure goes down with time and as consequence, the running time period is longer.

2.2.3 Temperature Variations

Determination of the stagnation temperature by direct measurement can be challenging in short duration hypersonic facilities. The difficulty of such measurements is caused by the combination of the impulsive loading of the instrumentation and the short flow duration which is often in the order of milliseconds. However, stagnation temperature is a crucial parameter in most hypersonic flow experiments and therefore stagnation temperature needs to be measured [49].

Various methods have been used to measure stagnation temperature in short duration hypersonic facilities. Measurements of transient heat flux have been made using thin film thermometers and coaxial surface junction thermocouples [9, 75, 76]. Although such methods have several advantages including fast response and durability, the signals are generally small amplitude and models for substrate heat conduction and boundary layer heat convection are required in order to deduce a flow stagnation temperature. Such techniques have been used in some experiments to good effect [77, 78], but the assumption of a convective heat transfer coefficient value at the stagnation point can lead to uncertainties.

Optical measurement techniques have also been used to deduce temperatures in hypersonic flows and a review of such techniques is presented in [79]. However, often these techniques are not well suited to routine identification of flow conditions

due to the expense and the complicated nature of the instrumentation.

In a short duration facility, East [80] estimated stagnation temperature at the start of the run of wind tunnel from the measured stagnation pressure. Platinum thin film gauges and a shell calorimeter were used by Edney [81] to identify stagnation temperature by measuring heat transfer rate at the stagnation point. Although some problems appeared in obtaining an accurate calibration, a time-resolved temperature history was produced in a single run by Edney [81]. Other relevant methods such as the used of microwave tracking to determine the speed of the piston, a sodium line reversal technique, and the use of a streak camera to measure the flow velocity in the working section have been used by Meyer, Stollery, and Merrit [82–84].

For relatively long duration hypersonic flows, measurements using exposed-junction thermocouples are possible. A thermocouple probe with a heated shield was used to measure stagnation temperature at the nozzle exit of a hypersonic facility at the University of Southampton [50]. Part of the aim of this dissertation is to explore the temporal variation of stagnation temperature at the nozzle exit of the hypersonic wind tunnel facility at the University of Southern Queensland (TUSQ). This is important because experiments in similar facilities [50] have revealed significant thermal disturbances which could degrade the quality of the test flow.

Experiments on free piston compression cold hypersonic facilities by East [50] demonstrated the existence of discrete cold fluid structures generated by the piston motion. The presence of such cold structures potentially compromise the quality of the test flow, but in the larger scale facility described by East [50], these disturbances were managed by arranging an initial axial temperature gradient within the barrel through the use of external heaters.

Previous experiments by Jones and Schultz [85] found that there are two vortices established within the barrel during compression process which responsible to the

heat loss at the end of the running time. One vortex (vortex A) exists at the entrance of the nozzle and another one (vortex B) is formed ahead the piston when the piston is moving. A further experiment by Jones *et al.* [3] was conducted to confirm these phenomena. They concluded that vortex B was responsible to the heat loss by rolling-up the boundary layer ahead the piston during compression and discharge process.

Buttsworth and Jones [49] also investigated the temperature decay in the Oxford University Gun Tunnel facility, but the experiment was focused on the fluctuation in the stagnation temperature. In the experiment, pitot probes were used to measure acoustic fluctuations and thin film heat flux probes were used measure stagnation temperature fluctuations. From the measurements, it was found that the stagnation temperature fluctuations are much greater than those due to the acoustic fluctuations alone. Hence, it was concluded that the source of the stagnation temperature fluctuations was the turbulent heat transfer from the test gas to the barrel upstream of hypersonic nozzle.

2.3 Thermocouple Probe for Wind Tunnel Measurements

2.3.1 Introduction

Various methods have been developed to identify flow temperature in wind tunnels. Some methods do not directly measure the temperature of the flow, but rely on correlation from other flow properties such as pressure or velocity which can then be related to the stagnation temperature such as in [80, 82–84]. However, measurements based on thermocouple technology offer some advantages compared to other devices.

The thermocouple is a device used for measuring temperature that consists of two dissimilar electrically conducting materials joined at one end. When the hot junction is heated to a certain temperature, an emf will be generated. If a voltage meter is put across the heated junction, a voltage can be measured that is approximately proportional to the temperature.

Thermocouples are very commonly used because they have many advantages over other devices. The advantages of thermocouples are that they are relatively inexpensive, reliable, versatile, small in size, may be used over a wide temperature range (–270 to 3000°C), have characteristics that are stable with time and repeatable in manufacture, and can have a very fast response. However, for measuring hypersonic wind tunnel flows, careful design is required.

2.3.2 Probe Designs

Some designs have been used by researchers to identify the flow temperature in hypersonic facilities in the form of bare wire thermocouple or in a shielded thermocouple to form a probe.

Bare wire thermocouple were used by Scadron and Warshawsky [86] in a subsonic wind tunnel of Mach number range 0.1 – 0.9. From these studies, they identified time constants and conduction and radiation correction methods to enable deduction of the true flow temperature. An illustration of the probe design by Scadron and Warshawsky can be seen in figure 2.5. Shielded probes consisting of thermocouples and individual bare wires were studied by Stickney [87]. Some vent configurations and various vent to entrance flow ratios were applied to the probes designs. Although no correlations were revealed clearly in that study, a recovery factor was found as a function of Mach number (in a range of Mach numbers 0.2 – 2.2 at a total temperature of 21 - 38°C) which can be used in calibration procedure.

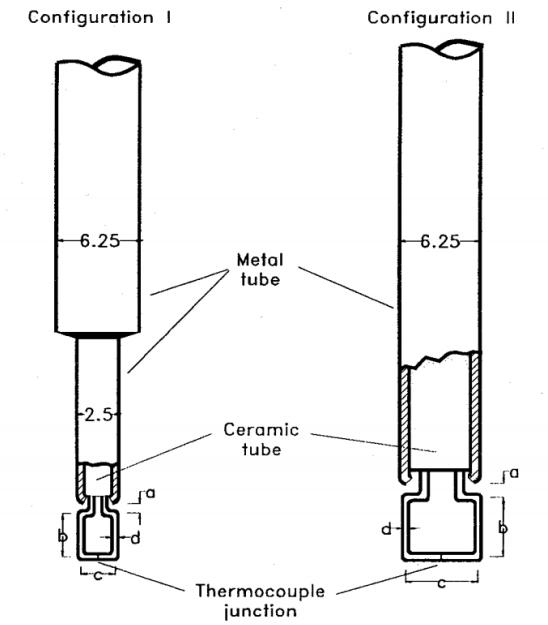

Figure 2.5: Illustration of probes used by Scadron and Warshawsky (dimension in mm). Reproduced from [4].

Albertson and Bauserman [88] designed a probe for measurement in the boundary layer of a short duration wind tunnel as illustrated in figure 2.6. The probe was shielded by a 0.125 mm thick platinum–20%–rhodium housing and used a 0.25 mm R-type thermocouple. The probe was positioned in the boundary layer for tests run over a range of Mach numbers of 5 – 6.2. A calibration factor K as a function of Nusselt number was applied in this study as suggested by Winkler [89]. As a result, a conduction correction as a function of length/diameter of the thermocouple wire, the thermophysical properties of the wire, the convective heat transfer to the wire and the probe support was found. A radiation correction was also calculated as a function of the emittance of the thermocouple, the shield, and the temperature of the radiation shield.

East and Perry [5] designed a probe with a heating element with a shield made from aluminium oxide as illustrated in figure 2.7. The probe consisted of a 0.001 inch bead-welded k-type thermocouple. Two vents were made at the downstream end of the aluminium oxide tube. The intention of the shield was to minimize

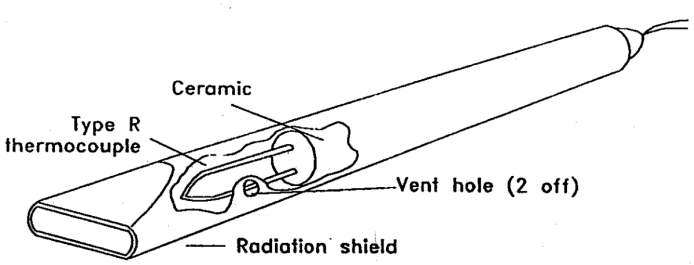

Figure 2.6: Illustration of total temperature probe designed by Albertson and Bauserman. Reproduced from [4].

radiation losses from the thermocouple. The ratio of the vent and the entrance area was set in the range of 20 – 75 %. The experiments were carried out in the freestream of a gun tunnel at nominal Mach number of 9.7 and 12.5. The results indicated that the temperature tended to decrease more rapidly during the run as the vent area was increased. The rise time obtained from this probe was around 10 milliseconds indicating that the implementation of such a probe has allowed the identification of the stagnation temperature in the hypersonic short duration wind tunnel.

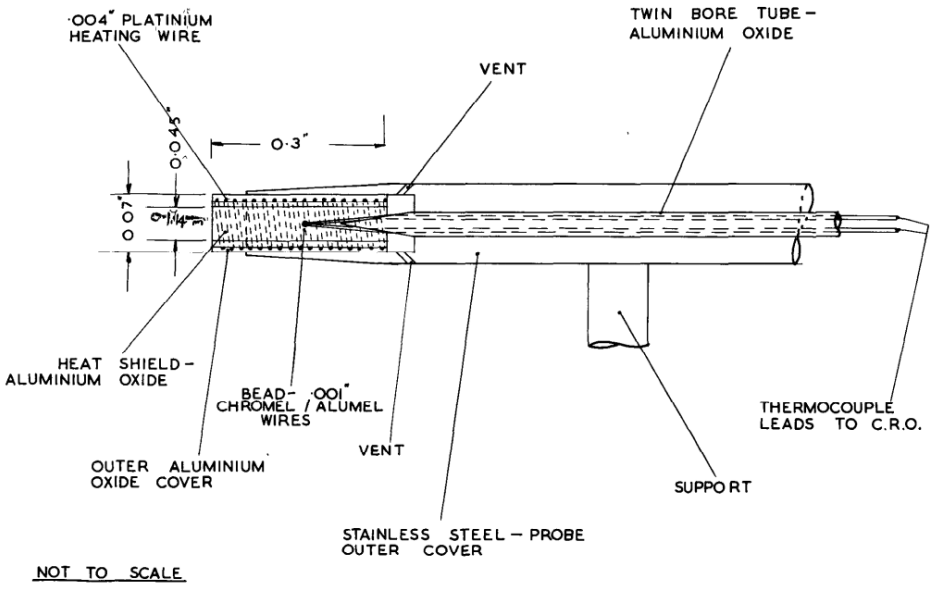

Figure 2.7: Illustration of shield probe used by East. Reproduced from [5].

2.4 Thin Film Probes for Wind Tunnel Measurements

2.4.1 Introduction

Heat flux is defined as the amount of heat transferred per unit area per unit time from or to a surface. An overview of different heat flux measurement techniques has been presented by Childs *et al.* [44] and Gülhan [90]. Determination of heat flux is most often performed by measuring a temperature difference over a piece of material with known thermal conductivity and thickness.

The thin film gauge is one of the various heat flux gauges which have been used extensively in many research applications such as in turbomachinery simulation [74, 91, 92] and in short duration wind tunnels [3, 93, 94]. In general, thin film gauges are much more sensitive than thermocouples. With capabilities to measure surface temperature changes in the order of 0.1 K and heat fluxes as small as 0.5 W/cm^2, they have many advantages over conventional gauges: capability to measure steady-state as well as transient heat fluxes, excellent transient response, minimal obstruction to fluid flow, able to be applied on surfaces with small radius of curvature, high temperature capability, and good sensitivity due to large output signal. Typical thin film heat flux gauges are even capable of producing a high bandwidth signal around 100 kHz which is useful for obtaining data that relate to transition and turbulence phenomena, and they have been used for measurements in various configurations and flows [49, 95, 96].

The thin film gauge commonly consists of a thermally or electrically insulated material (the substrate) – preferable having low thermal conductivity, listed in table 2.2 – on which a metallic film of nickel, zinc, or platinum is deposited by sputtering or hand painting. The thin metal film itself is typically in order of 0.1 μm thick so that the thin metal film is assumed to have a very low thermal inertia.

Table 2.2: Typical thermal properties of some substrates. Reproduced from [9].

Insulator	$\alpha \times 10^6$	ρ	c	k	$\sqrt{\rho c k}$
	(m^2/s)	(kg/m^3)	(kJ/kg/K)	(J/s/m/K)	($kJ/m^2/K/s^{0.5}$)
Fused Quartz	0.840	2210	0.755	1.40	1.53
Pyrex	0.791	2220	0.755	1.36	1.53
MACOR	0.733	2520	0.790	1.46	1.71

Frequency response of the film is commonly a lot higher than the frequency of the experimental effects under investigation, so the normal assumption is that the film thickness has no effect in the transient heat conduction process [93].

2.4.2 Principles of Thin Film Gauge Operation

The principle of operation of thin film gauges is based on the fact that the resistance of the thin film increases with a rise in temperature. The resistance R of the thin film as a function of surface temperature T can be approximate by

$$R(T) = R_0 \left[1 + \alpha_0 \left(T - T_0\right)\right] \tag{2.4}$$

where α_0 is the film temperature coefficient of resistance which must be determined experimentally for a particular thin film and the subscript 0 refers to the reference conditions.

According to Ohm's law, when a constant current source is applied to the thin film, the change in output voltage $V - V_0$ is related to the temperature as

$$V - V_0 = i \left(R - R_0\right) = V_0 \alpha_0 \left(T - T_0\right) \tag{2.5}$$

where i the current through the sensor and V_0 is the initial voltage across the sensor (at the reference temperature T_0). Equation 2.5 indicates that if α_0 is known by a calibration process, the voltage change is proportional to the change of the surface temperature.

Transient heat transfer measurement with thin film gauges can be achieved by utilizing a semi-infinite transient heat conduction model to convert surface temperature measurements into heat flux. Methods which have been successfully used in the determination of heat flux include the electrical analogue method [97, 98] and the numerical method. The numerical method will yield satisfactory results if the integration method follows the Cook-Felderman algorithm [97].

In modelling the one-dimensional semi-infinite transient heat conduction, the body (substrate) is assumed to have an infinite depth so that the thermal boundary layer remains far enough from the bottom of the substrate. A model for the description of the geometry of transient heat conduction in a semi-infinite body can be seen in figure 2.8.

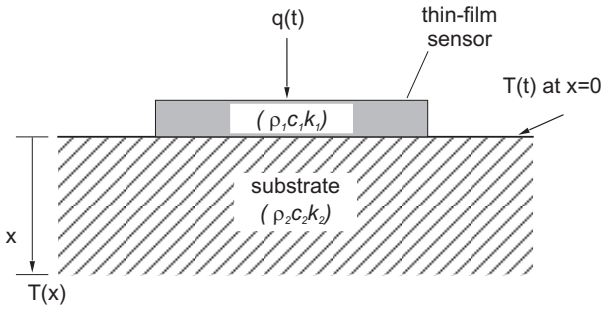

Figure 2.8: Transient heat conduction model for semi-infinite body

Carslaw and Jaeger [99] gives an expression that can be used to relate the temperature at the base of the substrate to the surface temperature for a constant heat flux into surface by

$$\frac{T(x,t)}{T(0,t)} = e^{-\frac{x^2}{4\alpha t}} - \left(\frac{\pi}{\alpha t}\right)^{\frac{1}{2}} \frac{x}{2} erfc\left(\frac{x}{2(\alpha t)^{\frac{1}{2}}}\right) \tag{2.6}$$

From such an expression, the minimum thickness of the substrate can be deduced for different test times. The one dimensional transient heat conduction approach applied to the thin film in a direction of the heat flux perpendicular to the surface sensor (see figure 2.8) and when the thermal properties of the substrate are assumed constant can be described as:

$$\frac{\partial T}{\partial t} = \frac{k}{\rho c}\frac{\partial^2 T}{\partial x^2} \tag{2.7}$$

The boundary condition at the surface is given by

$$-k\frac{\partial T}{\partial x} = \dot{q}_s \qquad \text{at} \qquad x = 0 \tag{2.8}$$

where T is the temperature, t is time, x is the distance from the surface of the substrate, $\dot{q}_s$ is surface heat flux, k is thermal conductivity, ρ is density, and c is heat capacity of the substrate.

The substrate is assumed to be sufficiently thick that heat does not penetrate to the other side of the gauge, and the properties of the film are assumed to have a very low thermal inertia and to not disrupt the properties of boundary layer on the surface substrate. Under such conditions, the temperature rise in the film is considered to be the same as the temperature at the substrate surface.

Using these assumptions and the boundary conditions as specified above, the equation 2.8 has solutions of surface temperature and heat flux as described in [93]

$$T_s = \frac{1}{\sqrt{\pi}\sqrt{\rho c k}}\int_0^t \frac{\dot{q}_s(\tau)}{(t-\tau)}d\tau \tag{2.9}$$

$$\dot{q}_s(t) = \frac{\sqrt{\rho c k}}{\sqrt{\pi}} \int_0^t \frac{\frac{dT}{d\tau}(\tau)}{(t-\tau)^{\frac{1}{2}}} d\tau \tag{2.10}$$

2.4.3 Thin Film Gauges and Probes

The application of thin film gauges for the measurement of flow in hypersonic wind tunnels was described by Schultz and Jones in the 1970's [93]. The details relating to the construction, operation, data analysis, response time, sensitivity, and possible errors are discussed comprehensively in [93].

Dunn [100] developed thin film gauges for application in a short duration shock-tube facility. The gauges consisted of a platinum film bonded to a small Pyrex insulating substrate using hand-painting techniques. With these methods it is possible to insert the small Pyrex gauges into a test model, enabling the testing of rotating components such as turbine blades. Similar to Schultz and Jones [93], the Pyrex substrate is assumed as to be a semi-infinite material and the transient heat conduction problem can be solved analytically using Laplace transforms to convert the measured surface temperature into heat flux.

Oldfield *et al.* [101] developed thin film gauges by hand-painting, but the metallic films were directly deposited onto a turbine blade made of an insulating substrate Macor. The facility used for testing was the Oxford light piston isentropic tunnel which has a test time of around 300 – 400 milliseconds, longer than used in Schultz [93] & Dunn [100]. As a consequence, Oldfield had to thicken the insulating layer in order to maintain semi-infinite assumption. However, such methods require rather complicated machining and the blades are rotating components which requires consideration of strength limitations.

Buttsworth and Jones [95, 102] developed heat flux gauges consisting of platinum thin film resistance thermometers, typically similar to the gauges of Schultz and Jones [93], but the platinum film was deposited onto 3 mm diameter quartz

substrate rod using hand-painting techniques. The platinum film had a length of 1 mm, a thickness of around 5 μm, and a resistance of around 20 Ω. The probes were used to measure total temperature in a Mach 5 conical nozzle and were operated at different initial temperatures. The intention of such a method was to obtain the flow total temperature more directly and thereby avoid relying on an empirical convective heat transfer relationship for deduction of the flow total temperature. The performance of these probes showed that the accuracy in deduction of the flow total temperature was around $\pm$ 3 K in [102] and the uncertainty in deduction of heat transfer coefficients was less than $\pm$ 2 % for the probes positioned at the centre of the jet in [95].

2.5 Conclusions

Disturbances present in the free stream flow of wind tunnel facilities remains a critical issue and may have a significant impact on the development of hypersonic air-breathing propulsion systems. However measurements of such fluctuations, including temperature fluctuations, are difficult to perform due to the combination of the impulsive loading of the instrumentation and the short flow duration which is often in the order of milliseconds.

The operation of short duration wind tunnels facilities such as Ludwieg tubes, isentropic light piston tunnels (ILPT), and Ludwieg tubes with isentropic compression heating (LICH) have been reviewed and provides a useful context for discussing the operation of TUSQ tunnel facility as a new short duration wind tunnel in the University of Southern Queensland.

A survey of existing methods for the measurement of the core flow temperature in short duration facilities has also been presented. Various designs have been developed and applied in specific facilities. Thermocouple probes for short duration facilities have been demonstrated in previous work, but improvements in

temporal resolution should be possible if response-time correction methods are applied.

Chapter 3

Estimation of Stagnation Temperature Distribution and Fluctuations

3.1 Introduction

Wind tunnels and other aero-thermal experimental facilities are likely to make a contribution to the optimisation of energy and propulsion systems for the foreseeable future. Short duration wind tunnels such as shock tunnels, gun tunnels, and the new facility at USQ rely on a transient compression process and are likely to generate significant stagnation temperature gradients and turbulent fluctuations in the nozzle reservoir region. In the present chapter, a method for deducing stagnation temperature fluctuations using incompressible turbulent flow data of other workers will be illustrated in detail for two different aero-thermal testing conditions generated by transient wind tunnel facilities: (1) the Oxford gun tunnel facility in which a piston is used to compress the test gas up to about 600 K - the test gas is carbon dioxide in this case; and (2) the T4 shock tunnel facility in which the stagnation temperature of the test gas (air) is around 6000 K. The

same approach will also be applied for conditions in the new facility at USQ.

3.2 Analysis Based on Incompressible Data

3.2.1 Brief Review of Existing Data

Many numerical and experimental investigations of temperature fluctuations in low speed boundary layers and fully developed pipe flow have been reported. Abe *et al.* [19] numerically investigated surface heat-flux fluctuations in turbulent channel flow for Re_τ = 180, 395, 640 and 1020 and with Prandtl numbers of 0.025 and 0.71. In this case, the length scale used in the Reynolds number was half the width of channel. The large scale structures were observed to affect the heat flux fluctuations and these increased with increasing Reynolds number in the expected manner. Redjem-Saad *et al.* [20] investigated the effect of Prandtl number on heat transfer of fully developed turbulent pipe flow with uniform heat-flux imposed at the wall. Redjem-Saad *et al.* performed simulations for a Reynolds number based on pipe radius, Re = 5500 (Re_τ = 186). The results showed that RMS temperature fluctuations and turbulent heat fluxes increased when the Prandtl number increased. Numerical simulations [19, 20] generally indicate that RMS values of temperature and heat flux increase when the Prandtl number increases, however for the Reynolds number Re >> 1000, [19] found that RMS values were lower for Pr = 0.71 than for Pr = 0.025 due to the increasing convective effects. Redjem-Saad *et al.* [20] observed slightly more intense temperature fluctuations in their simulated pipe flow configuration compared to that of available simulations with a channel flow configuration. Subramanian and Antonia [6] obtained temperature fluctuation measurements in a turbulent boundary layer on a slightly heated smooth plate. Zero pressure gradients were applied in this experiment. The results showed that for both momentum and thermal fields, the law of the wall does not vary with Reynolds number within the range

investigated. Spatial profiles of RMS temperature fluctuation data normalized by the friction temperature were found to vary with Reynolds number for y^+ greater than about 10.

3.2.2 Approach

To deduce stagnation temperature fluctuations in the nozzle exit flows of a gun tunnel and a shock tunnel, the experimental results of Subramanian and Antonia [6] are used, see figure 3.1. The original data of [6] was presented in terms of Reynolds numbers based on the boundary layer momentum thickness. However, for convenience, fully developed turbulent pipe flow in the gun and shock tunnel nozzle reservoir regions has been assumed. The results of [6] are assumed to apply to the fully developed turbulent pipe flows by converting the momentum thickness Reynolds number to a friction velocity Reynolds numbers (Re_τ) based on the velocity boundary layer thickness as reported in data of [6] and the conversion can be seen in Appendix E. When converted to Re_τ, the Subramanian and Antonia data corresponds to friction velocity Reynolds numbers of Re_τ = 371, 559, 1055, 1441, 1986, and 2273. The data of [6] is the applied by extrapolating their data to the appropriate pipe flow Re_τ value (based on the pipe radius) for the nozzle reservoir region. The flow within the nozzle reservoir region of each facility is assumed to be fully developed turbulent pipe flow. A constant time averaged heat flux is assumed at the pipe internal surface. Variables relating to the conservation of momentum and energy equations are normalized by friction velocity $u_\tau = (\tau_w/\rho)^{1/2}$, and the friction temperature $T_\tau = Q_w/\rho c_p u_\tau$ where Q_w is average surface heat flux.

In the present deduction of stagnation temperature fluctuations, the heat flux at the wall Q_w is obtained by using the convective heat transfer equation defined

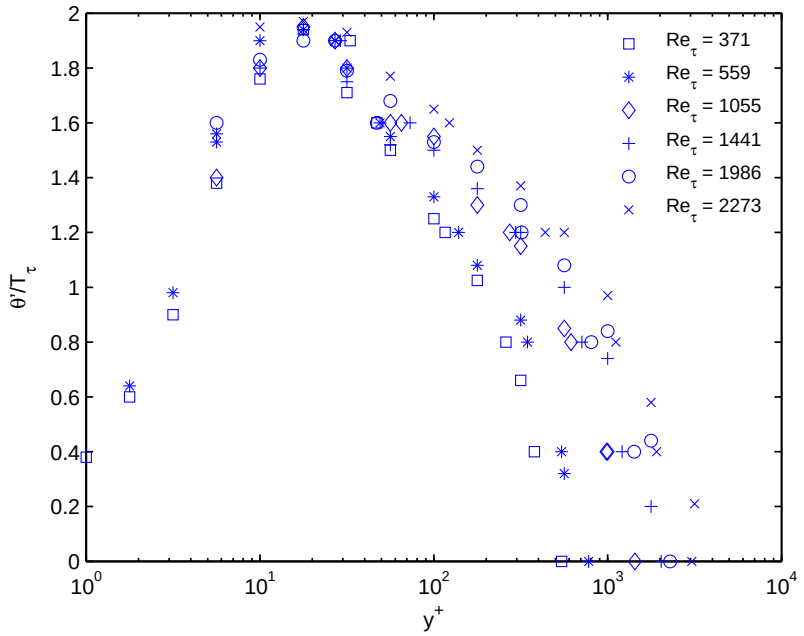

Figure 3.1: Distribution of normalized RMS temperature fluctuations for different friction velocity Reynolds numbers (Re_τ) from [6].

as:

$$Q_w = h\,(T_0 - T_w) \tag{3.1}$$

where h is convective heat transfer coefficient, T_0 is initial stagnation temperature and T_w is wall temperature. The convective heat transfer coefficient is obtained from

$$h = \frac{\mathrm{Nu}\,k}{D} \tag{3.2}$$

where Nu is the Nusselt number, k is the thermal conductivity, and D is the diameter of the barrel or shock tube. For thermally fully developed flow in a smooth tube with Prandtl number $\mathrm{Pr} > 0.5$, Gnielinski's formula is recommended

by Mills [103] for calculation of the Nusselt number

$$\mathrm{Nu} = \frac{(f/8)\,(\mathrm{Re} - 1000)\,\mathrm{Pr}}{1 + 12.7(f/8)^{\frac{1}{2}}\left(\mathrm{Pr}^{\frac{2}{3}} - 1\right)} \tag{3.3}$$

which can be applied for $3000 < \mathrm{Re} < 10^6$. This in turn, depends on the friction factor, which can be obtained from Petukhov's formula

$$f = \frac{1}{(0.790\ln(\mathrm{Re}) - 1.64)^2} \tag{3.4}$$

which applies for $10^4 < \mathrm{Re} \leq 5$ x 10^6.

The pipe flow Reynolds number required in the above correlations is based on the pipe diameter and the flow velocity which is the bulk flow velocity deduced from the stagnation conditions and the nozzle throat area.

To approximate the velocity distribution across the assumed fully developed turbulent pipe flow, a power-law velocity profile is used

$$\frac{\overline{u}}{V_c} = \left(1 - \frac{r}{R}\right)^{\frac{1}{n}} \tag{3.5}$$

where $\overline{u}$ and V_c are the local time-averaged velocity and centre line velocity of pipe flow respectively, and $n = 7$ is used as a reasonable approximation.

To approximate the temperature distribution, expressions presented by Mills [103] have been adopted.

$$T^+ = \mathrm{Pr}\ y^+ \qquad \text{if} \qquad 0 < y^+ \leq 5 \tag{3.6}$$

$$T^+ = 5\,\mathrm{Pr} + 5\ln\left[\mathrm{Pr}\left(\frac{y^+}{5} - 1\right) + 1\right] \quad y^+ \quad \text{if} \quad 5 < \mathrm{y}^+ \leq 30 \tag{3.7}$$

$$T^+ - T^+\big|_{y^+=30} = \frac{\mathrm{Pr}_t}{0.4}\left[\ln\left(\frac{\mathrm{y}^+}{30}\right) - \left(\frac{y^+ - 30}{R^+}\right)\right]^+ \quad \text{if} \quad y^+ \geq 30 \tag{3.8}$$

For the gun tunnel case, the stagnation region pressure and temperature were taken as $P_0 = 6.36$ MPa, and $T_0 = 610$ K; and for the shock tunnel case, values were taken as $P_0 = 36.5$ MPa, and $T_0 = 6187$ K. Profiles of velocity and temperature from equations 3.5 to 3.8 were used to generate the variation of ρu with radius which was in turn integrated to determine the mass flow rate through the pipe. Scaling was applied to the velocity profile because the initial velocity profile was determined without reference to the density which varied across the radius of the pipe. A factor of 1.37 was applied to the velocity profile in the case of the gun tunnel flow, and a factor of 1.31 was used in the case of the shock tunnel flow so that the mass flow rate in the pipe matched the sonic discharge values for the given stagnation pressure and temperature conditions. A similar adjustment was made to the temperature profile so that the bulk temperature calculated for the gun and shock tunnel cases matched the assumed stagnation region values. A factor of 1.05 was applied to the temperature profile in the gun tunnel case, and a factor of 1.10 was applied in the shock tunnel case.

3.3 Results and discussion

3.3.1 Result for Gun Tunnel Case

The Oxford University Gun Tunnel (OUGT) is a short duration hypersonic facility producing useful test flows with a duration of less than 100 ms for which temperature fluctuations data was available [49]. Given the similarities of the

OUGT and the TUSQ facility, the OUGT results are taken as a representative case for benchmarking the TUSQ facility. The barrel of the OUGT has a length of 9 m and an internal diameter of 96.3 mm. An illustration of the OUGT is presented in figure 3.2. The conditions in the nozzle reservoir region considered in this work are $P_0 = 6.36$ MPa, $T_0 = 610$ K, and the wall temperature of the barrel was taken as $T_w = 300$ K. The test gas considered was carbon dioxide, corresponding to the conditions in [49]. The nozzle throat diameter was 19.1 mm giving a mass flow rate of 3.57 kg/s from which the gas leaving the stagnation region of the barrel was found to be 8.89 m/s and $\mathrm{Re}_\tau = 31{,}579$.

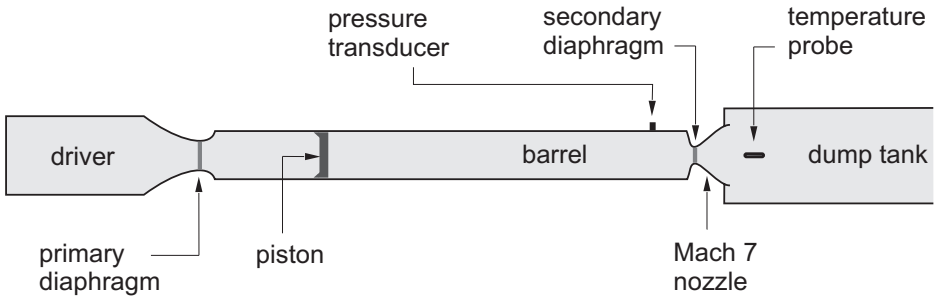

Figure 3.2: Schematic illustration of gun tunnel facility

The extrapolation of the data of [6] to the gun tunnel condition is illustrated by the broken line in figure 3.3 and this figure also presents the original data of [6]. The RMS stagnation temperature fluctuation deduced from the extrapolation is plotted versus radius of the pipe in figure 3.4. The peak of RMS stagnation temperature fluctuation is located at $r \sim 47$ mm and has a value of about 25 K. The RMS stagnation temperature fluctuations are intense near the wall and decay towards the centre line of the pipe, reaching a minimum value of about 5.3 K. The mean RMS stagnation temperature fluctuation was obtained by integrating the mass-flux-averaged mean-squared stagnation temperature fluctuation profile across the pipe. The average stagnation temperature fluctuation (RMS value) obtained in this manner was 15.3 K.

The RMS stagnation temperature fluctuations deduced in this gun tunnel case can be directly compared with the previous result obtained by Buttsworth and Jones [49] for this conditions. The experimental result of [49] gives the magnitude

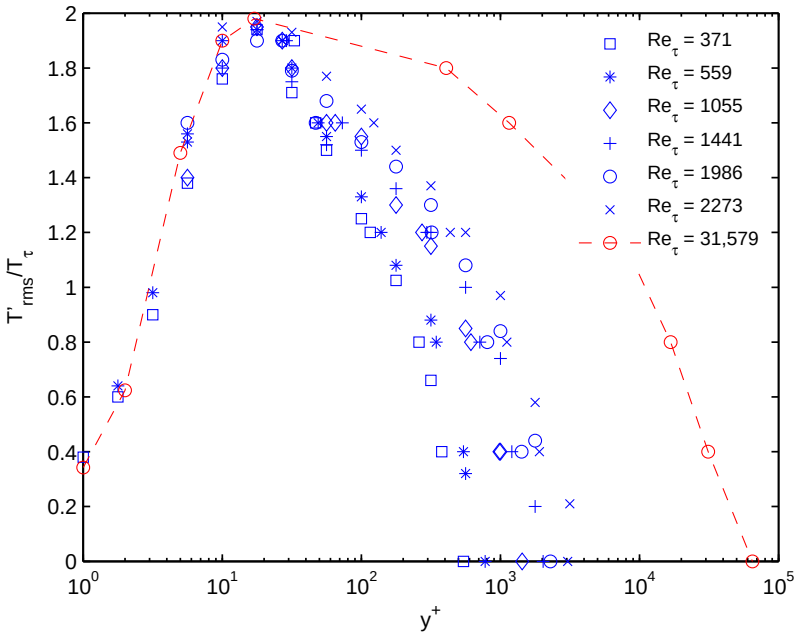

Figure 3.3: Normalised temperature fluctuation data from [6] (symbols) and extrapolated profile relevant to the gun tunnel case (symbol ∘ with a broken line).

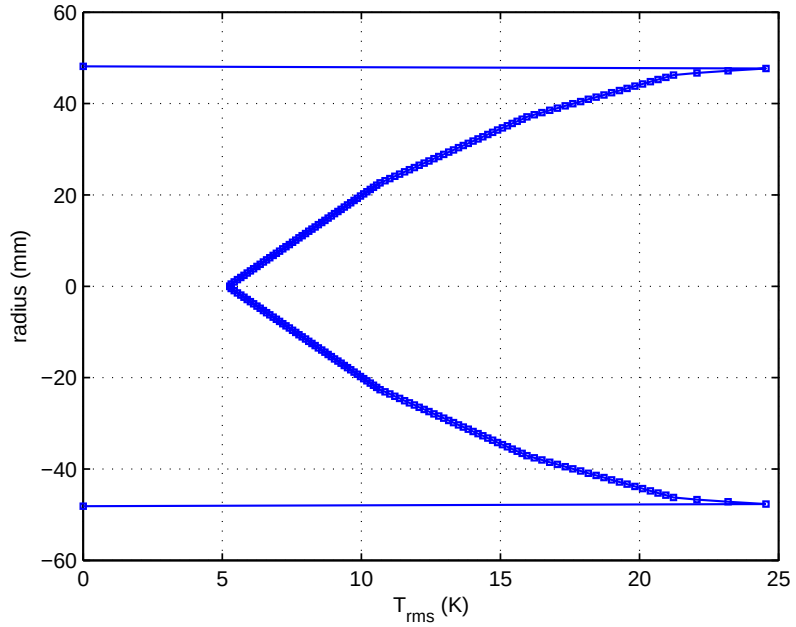

Figure 3.4: Variation of RMS stagnation temperature fluctuations with pipe radius in the gun tunnel case.

of RMS stagnation temperature fluctuation of 2.3 K at a location close to the centre line of the hypersonic nozzle exit. This is about half the magnitude of the centre line fluctuation value deduced from the data of [6] applied in the present work.

3.3.2 Results for Shock Tunnel Case

The T4 shock tunnel is a type of impulse facility, located at University of Queensland. Although the operation and the conditions generated in the T4 facility are not directly relevant to the operation of the TUSQ facility, this case is considered to illustrate the potential impact of temperature disturbances. The T4 facility is typically used to produce high enthalpy flows for high speed aerodynamic and scramjet experiments. T4 shock tunnel is capable of producing flows with total enthalpy in the range 2.5 - 15 MJ/kg. A schematic illustration of the T4 facility is presented in figure 3.5. The conditions in the nozzle reservoir region considered in this work are $P_0 = 36.5$ MPa, $T_0 = 6187$ K, and the wall temperature of the shock tube was taken as $T_w = 300$ K. The test gas considered in this work is air, and the nozzle throat diameter was 25 mm. These conditions give a mass flow rate of 9.05 kg/s from which the bulk flow velocity in the pipe was found to be 100.44 m/s and $\mathrm{Re}_\tau = 24{,}975$.

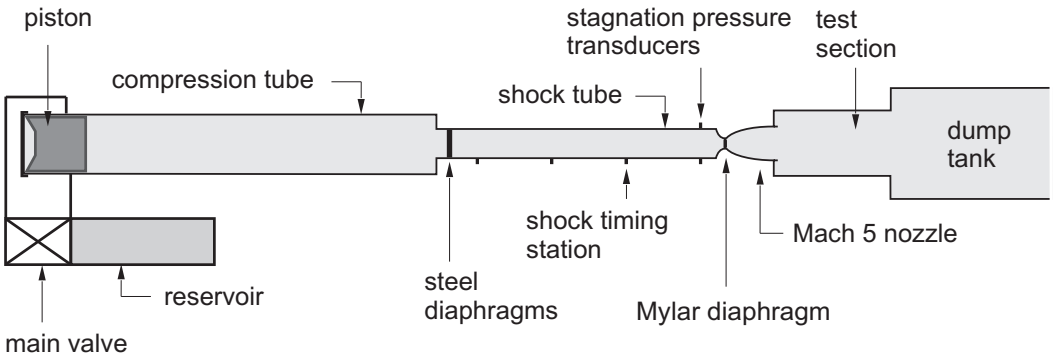

Figure 3.5: Schematic illustration of shock tunnel facility, circa 1994 [7].

The results from extrapolation of the data of [6] to the present shock tunnel condition is illustrated in figure 3.6 as the broken line. Included on this figure is

also the original data of [6]. Figure 3.7 presents the profile of the RMS stagnation temperature fluctuation deduced from the extrapolation. The peak of RMS stagnation temperature fluctuation is located at $r \sim 38$ mm and has a value of about 464 K. The RMS stagnation temperature fluctuations are intense near the wall and decay towards the centre line of the pipe, reaching a minimum value of about 100 K. The RMS of stagnation temperature fluctuation was obtained by integrating the mass-flux-averaged mean-squared stagnation temperature fluctuation profile across the pipe. The average stagnation temperature fluctuation (RMS value) obtained in this manner was 291 K. This represents a relative RMS stagnation temperature fluctuation of about 5 %.

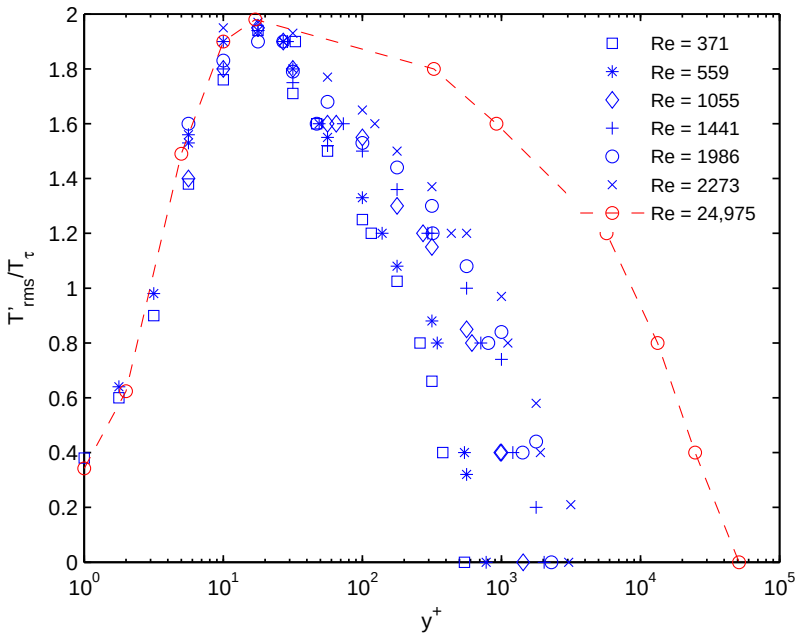

Figure 3.6: Normalised temperature fluctuation data from [6] (symbols) and extrapolated profile relevant to the shock tunnel case (symbol ∘ with a broken line).

The T4 shock tunnel is regularly used for scramjet combustion experiments. To assess the possible significance of the temperature fluctuations in the shock tunnel case, combustion characteristics of hydrogen-air mixtures are assessed using a correlation for ignition delay and reaction times. Because the residence time of fuel and air mixtures in model scramjet engines tested in T4 can be as short as several milliseconds, ignition delay and reaction times can be very important

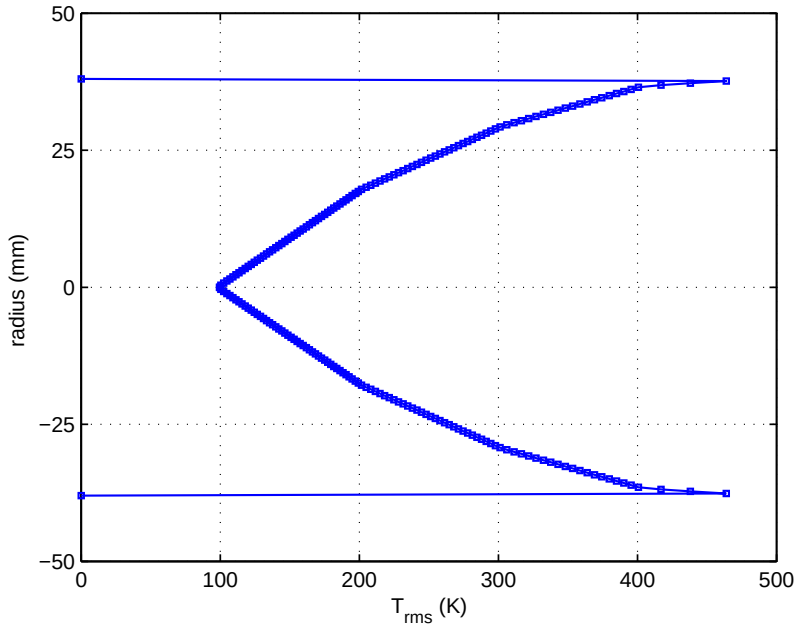

Figure 3.7: Variation of RMS stagnation temperature fluctuations with pipe radius in the shock tunnel case.

at some conditions. There are three parameters that must be within reasonable limits for self-ignition of the hydrogen-air mixture within the scramjet. These are: the static pressure, the fuel-air equivalence ratio, and the static temperature. Under the assumption that the fuel air-mixture is stoichiometric and the static pressure remains constant, the effect of different static temperatures on the ignition and reaction times can be estimated using global approximations.

Ignition is considered accomplished when the temperature rises by 5 % of the complete reaction temperature rise [104]. Ignition delay time τ_i and reaction time τ_r can be calculated by using the equations [105]

$$\tau_i = \frac{8 \times 10^{-9} e^{9600/T}}{P} \tag{3.9}$$

$$\tau_r = \frac{1.05 \times 10^{-4} e^{-1.12T/1000}}{P^{1.7}} \tag{3.10}$$

where T is the static temperature (K) and P is the static pressure (expressed in atm). This equation is reported as being valid for the range $P = 0.2$ to 1.0 atm and $T = 1000$ to 2000 K.

Static temperature at the T4 shock tunnel nozzle exit for the particular test condition of interest was obtained from [7] as 1440 K. On the assumption that the magnitude of the static temperature fluctuations at the nozzle exit scale with the magnitude of the stagnation temperature fluctuations in the nozzle reservoir region, the expected value of RMS static temperature fluctuation at the nozzle exit is 72 K (corresponding to 5 % of 1440 K).

In figure 3.8 and 3.9, the ignition delay time and the reaction time characteristics for the shock tunnel case are presented. Ignition delay and reaction times for two static pressures (20 and 100 kPa) are presented as a function of static temperature. For both pressures, two different lines are presented: the RMS static temperature fluctuation at the representative maximum temperature ($T + T_{rms}$) and the other at the representative minimum temperature ($T - T_{rms}$). At each temperature, the value of the RMS fluctuation is determined using $T_{rms} = 0.05\,T$.

Results indicate that the static temperature fluctuation can have a significant influence on the combustion process for hydrogen-air mixtures. For example, consider figure 3.8 and the pressure of 20 kPa. Over the representative peak-to-peak variation in the static temperature fluctuations (a magnitude of 2 T_{rms}), the ignition time delay will vary by around 600 μs for a mean static temperature of 1000 K. For a static pressure of 100 kPa and a mean static temperature of 1000 K, the corresponding difference in ignition delay times is somewhat shorter, at around 100 μs. The reaction time (figure 3.9) for a mean static temperature of 1000 K varies by about 70 μs at 20 kPa and 5 μs at 100 kPa for the assumed peak-to-peak fluctuation in the nozzle exit static temperature.

Scramjet combustors must be sized to accommodate mixing, ignition and reaction times for the fuel and air. The nozzle exit flow velocity was estimated at 4020

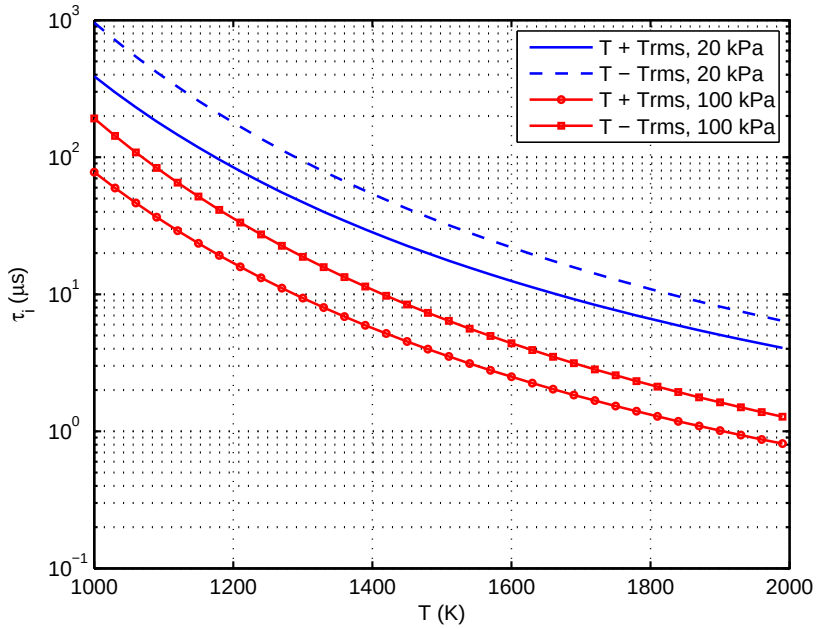

Figure 3.8: Igniton delay time characteristics for the shock tunnel case.

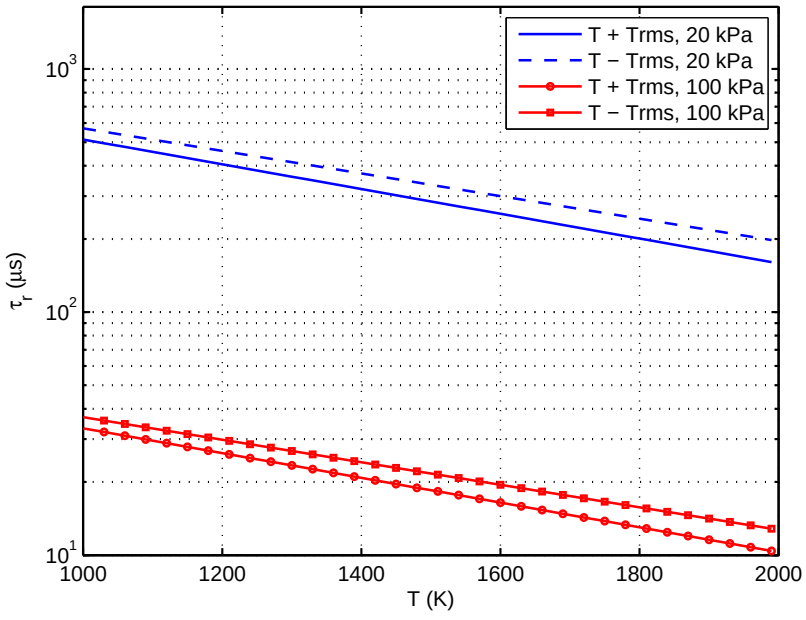

Figure 3.9: Reaction time characteristics for the shock tunnel case.

m/s for this shock tunnel condition [7]. Assuming a representative scramjet model combustor length on the order of 1 m, the residence time will only be around 250 μs. Clearly an ignition time fluctuation of 600 μs is very significant at these

conditions.

3.4 Implementation in the TUSQ Case

Estimation of stagnation temperature fluctuations has been performed in two different cases of short duration wind tunnels: the Oxford gun tunnel and T4 shock tunnel as described in previous sections. Relatively good agreement makes it possible to apply such an approach to the University of Southern Queensland wind tunnel (TUSQ). More complete details of the principal components, dimensions, and features of the TUSQ are reported in chapter 4. However for initial calculation of this work, the parameters and conditions of operation as presented in table 3.1 have been adopted.

Table 3.1: Physical characteristics and conditions as used in [10].

Parameter	Unit	Value
D_{barrel}	mm	130
D_{throat}	mm	28.8
P_0	kPa	800
T_0	K	500

The magnitude of the stagnation temperature fluctuations can be estimated using the approach as described previously. Under these conditions (table 3.1) the mass flowrate was found to be around 0.85 kg/s with the mean flow velocity in the barrel equal to 7.65 m/s and $\mathrm{Re}_\tau = 8520$. The peak of RMS stagnation temperature fluctuation was located ~ 0.64 mm from the barrel wall and had a value around 19 K. The value at the centre of the pipe was around 4.0 K because the stagnation temperature fluctuations decay from the peak value at the location adjacent to the wall barrel to the centre of the pipe. The average stagnation temperature fluctuation (RMS value) obtained using the mass-flux-averaged was 9.0 K.

3.5 Conclusions

In this chapter, the flow conditions in the hypersonic nozzle reservoir regions of transient compression facilities are assumed to be charaterised by fully developed turbulent pipe flow. The significance of temperature fluctuations in the assumed pipe flow is assessed by analysing existing temperature fluctuation data and relating it to conditions in the transient compression wind tunnel cases.

The first case considered is that of the Oxford gun tunnel in which a piston is used to compress the test gas up to about 610 K – the test gas is carbon dioxide. The second case considered is that of the T4 shock tunnel in which driver gas is used to compress the test gas up to about 6187 K – the test gas considered in this case is air. Using the suggested approach, the mean value of root-mean-square stagnation temperature fluctuations were found to be 15.3 K and 291 K for the Oxford gun tunnel and T4 shock tunnel cases respectively. The estimated RMS value in the case of the Oxford gun tunnel is significantly larger than the experimental value previously measured on the centre line of the gun tunnel nozzle of 2.3 K. The difference observed between the inferred and measured temperature fluctuations in the Oxford gun tunnel case may be related to spatial variations in the temperature fluctuations. In the case of the T4 shock tunnel, the magnitude of the fluctuations is demonstrated to be significant for supersonic combustion experiments.

The Oxford gun tunnel case is similar to that of the TUSQ facility condition considered in the subsequent chapters of this dissertation. Anticipated RMS fluctuations in stagnation temperature for the TUSQ condition are around 9 K. The calculation of the fully developed turbulent pipe flow temperature distribution illustrated in this chapter is revisited in chapter 7 where comparisons are made with spatially resolved stagnation temperature measurements.

Chapter 4

Hypersonic Facility

4.1 Introduction

This chapter presents TUSQ hardware used in the experiments that were performed in this study. The main purpose of the present experiments is to identify the freestream stagnation temperature characteristics of the new hypersonic facility built at USQ (TUSQ). The identification of stagnation temperature was performed using different probes and these will be described in subsequent chapters. This chapter will describe the facility. The facility and its operation is similar to that which was commissioned at the University of Southampton in the 1970s [80].

4.2 Facility Description

The main facility used in this experiment is University of Southern Queensland (USQ) hypersonic wind tunnel (TUSQ). TUSQ is a new short duration hypersonic wind tunnel at the University of Southern Queensland. It can be actually be used for a range of supersonic and hypersonic experiments and is illustrated in figure

4.1. The principal components and dimensions of the TUSQ facility are presented in table 4.1.

Table 4.1: Principal dimensions of the TUSQ facility

Component	**Physical Characteristic**
Air reservoir	0.350 m^3
Primary valve	ϕ = 0.0276 m ($1\frac{1}{4}$" ball valve)
Piston	0.383 kg (Nylatron)
Barrel	16.0 m, ϕ = 0.130 m
Test section	0.830 m, ϕ = 0.60 m
Mach 6 Nozzle	1.057 m, ϕ^* = 0.0288 m (throat)
(contoured)	ϕ_{exit} = 0.2175 m (exit dia.)
Diffuser	2.526 m, ϕ = 0.60 m, V = 0.714 m^3
Dump tank 1	2.900 m, ϕ = 1.40 m, V = 4.5 m^3
Inter-tank	2 m, ϕ = 0.6 m, V = 0.646 m^3
Connections	0.6 m, ϕ = 0.4 m , V = 0.075 m^3
Dump tank 2	2.700 m, ϕ = 1.7 m, V = 6.1 m^3

A 0.383 kg piston made from Nylatron is free to move inside the 16.0 m long barrel that has an internal diameter of 0.130 m. Attached to the end of the barrel is a converging-diverging nozzle that exits into a test section. The test section has optical access through four port windows (two on each side) and a test section model support base with tapped holes for model mounting.

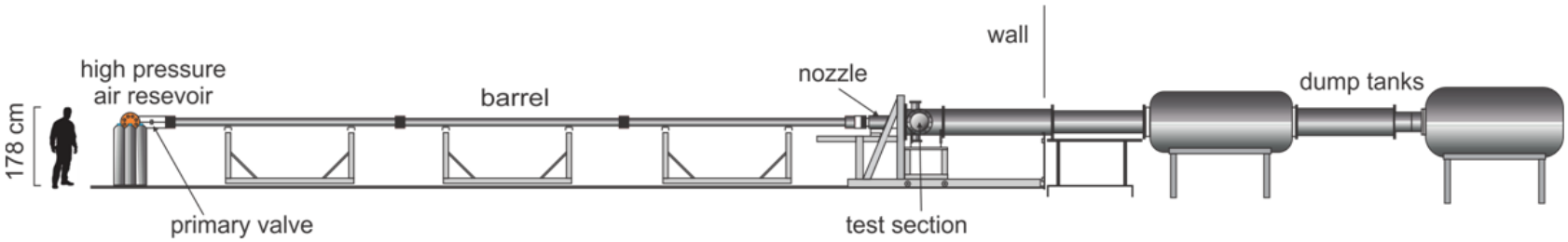

(a) Side view and main components of the TUSQ

(b) Air reservoir end

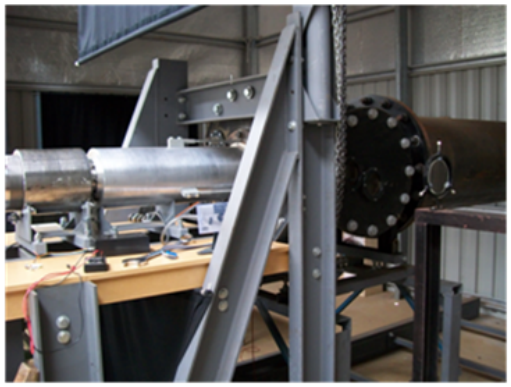

(c) Nozzle and test section

(d) Dump tanks

Figure 4.1: Illustration of the TUSQ facility: (a) Schematic representation; (b,c,d) photographs of various components.

A diaphragm made from Mylar is used at the end of the barrel. The thickness of the diaphragm is chosen according to the required pressure at which the test run is started. This diaphragm is installed at the entrance to the hypersonic nozzle in order to prevent the air in the barrel from draining into the test section before compression by the piston was completed. Table 4.2 presents Mylar diaphragm thicknesses and corresponding pressures at which the diaphragms will burst when coupled to the Mach 6 nozzle inlet.

Table 4.2: Diaphragm thicknesses and corresponding burst pressures with the Mach 6 nozzle.

Diaphragm thickness (μm)	Burst pressure (kPa)
25	230
50	420
100	860

4.3 Facility Operation

The operation of TUSQ is similar to a gun tunnel where a piston is set into motion when the primary diaphragm is ruptured. However, in the case of the TUSQ facility, the piston compression process is relatively slow and is initiated by the opening of a ball valve. The TUSQ wind tunnel can produce a relatively cold hypersonic flow – the compression process is approximately isentropic and starts from a room temperature condition. The facility also has a relatively long duration test time (around 200 ms), so enabling diverse experiments such hypersonic mixing studies, aerodynamics experiments, hypersonic boundary layer studies and scramjet start-ability experiments [10]. The TUSQ facility differs from others short duration wind tunnels such as shock tunnels in that it uses a free piston for direct compression of the test gas. An illustration of the TUSQ

arrangement can be seen in figure 4.2.

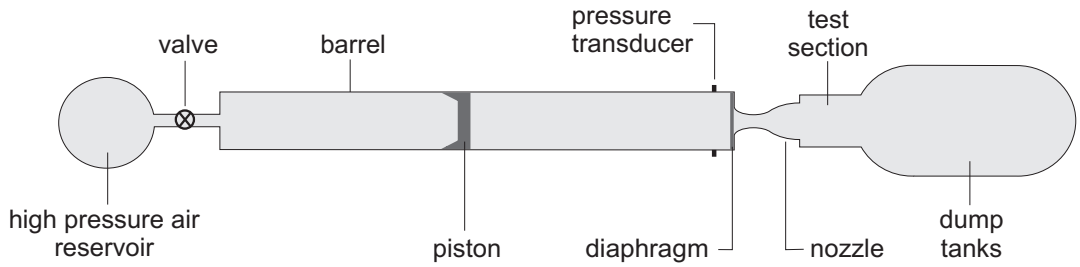

Figure 4.2: Schematic illustration of the TUSQ facility.

Facility operation is initiated by opening the primary valve which separates the high pressure air reservoir and the low pressure test gas initially residing in the barrel. The primary valve is a pneumatically driven ball valve installed in the $1\frac{1}{4}$" pipe connecting the high pressure air reservoir and the barrel. The valve opening process can be arranged to take a period of about 100 ms or longer. Moderate valve opening times are preferred to fast opening in this application in order to avoid strong compression waves during compression of the test gas. When the piston is released, it is accelerated by the compressed air to a maximum speed about 50 m/s and during this time it is subjected to a maximum acceleration of about 500 m/s^2. With a 0.383 kg piston mass, this acceleration figure implies a force of about 200 N is acting on the piston, the equivalent pressure differential being 15 kPa. This figure of 15 kPa represents less than 2% of the nozzle reservoir pressure existing during test flow. Oscillations in pressure within the barrel during compression can arise due to a piston mass effect [3] and can be large if fast primary valve opening is used [10].

Table 4.3 provides details of the main operating condition of the TUSQ with the Mach 6 nozzle and a 100 μm Mylar diaphragm. The first four parameters in table 4.3 refer to initial conditions of pressure and temperature in the facility, P_0 is the measured stagnation pressure during the run time, and T_0 is an isentropic approximation for the stagnation temperature during the run time based on the measured pressures. When the diaphragm ruptures, the test gas flows into the test section. The flowrate from the reservoir through the valve and into the

Table 4.3: Primary operating conditions of TUSQ

Parameter	Unit	Value
P_{barrel}	kPa	93.0
T_{amb}	K	300.1
$P_{reservoir}$	MPa	4.0
$P_{test\ section}$	Pa	750
P_0	kPa	860
$T_{0,isen}$	K	566

barrel can be arranged so that it compensates for the discharge of the test gas through the hypersonic nozzle, thereby maintaining the nozzle stagnation pressure approximately constant. Such a situation is referred to as a 'matched' condition [3, 50]. A sample pressure history measured in the barrel during TUSQ facility operation (at the condition in table 4.3) can be seen in figure 4.3. In this case, the valve opening time was shorter than ideal because discrete compression waves are observed during the compression time in figure 4.3.

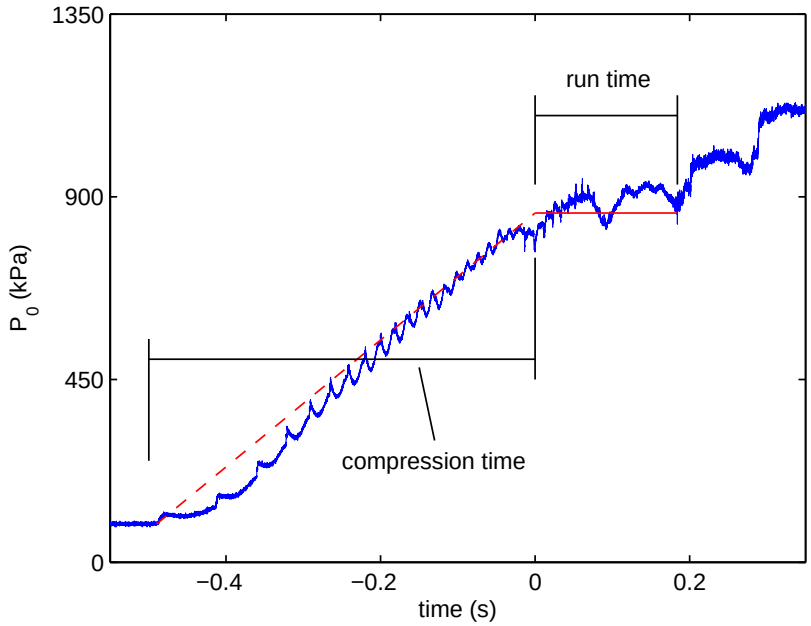

Figure 4.3: Pressure history of TUSQ for operation with a 100 μm diaphragm and initial conditions listed in table 4.3.

The compression time was around 490 ms and the run time was 190 ms for the run illustrated in figure 4.3. The maximum possible flow stagnation temperature of around 566 K can be obtained if the compression and discharge process in the TUSQ facility is actually isentropic. However, the flow stagnation temperature will generally be below that value because of heat transfer from the test gas to the barrel walls during compression and discharge proccess.

4.4 Mach 6 Nozzle

The present study employed a Mach 6 contoured nozzle as shown in figure 4.4. The total length of the nozzle is 1057 mm, the throat diameter is 28.8 mm, and the exit diameter is 217.5 mm.

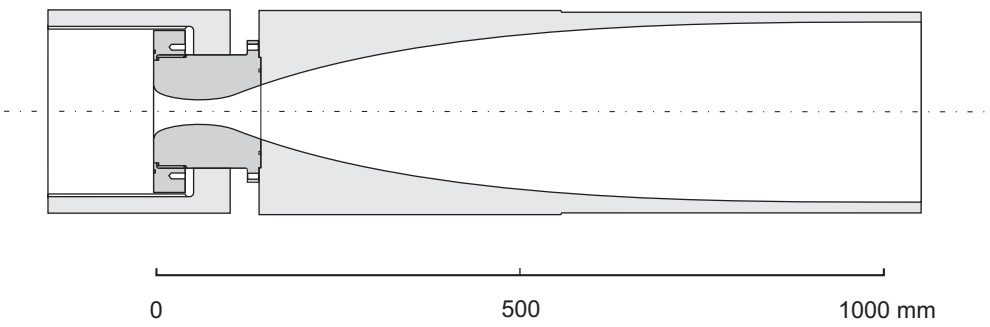

Figure 4.4: Schematic illustration of the Mach 6 contoured nozzle.

This nozzle was designed using a method of characteristics to obtain an inviscid contour and the final contour was obtained by adding a boundary layer displacement thickness correction to the inviscid contour. Contoured nozzles can produce parallel flow at the exit, but they can also can focus disturbances onto the centre line of the flow [106]. It is also possible for the flow produced by contoured nozzles to be unstable when operated at conditions far from the design point [107]. Surveys of the current nozzle exit flow presented in the following chapters have not revealed any such instabilities.

4.5 Conclusion

The present facility at USQ is similar to the hypersonic facility which was commissioned at the University of Southampton in the 1970s [80]. The presence of thermal disturbances which convected into the nozzle exit flow lead to the Southampton facility being operated with an electrically heated barrel. The USQ facility is currently operated with an unheated barrel. Therefore it is essential to identify the thermal characteristics of the nozzle exit flow produced by the TUSQ facility.

Chapter 5

Preliminary Stagnation Temperature Measurements

5.1 Introduction

For the current work, the stagnation temperature in the TUSQ facility was identified using a shielded t-type thermocouple probe with a bead junction. The flow stagnation temperature was deduced from the temperature history recorded based on the application of a time constant correction. The pressure within the barrel of the TUSQ facility was also measured to provide a theoretical value for the flow stagnation temperature based on the assumption of isentropic compression for direct comparison with the thermocouple measurements.

5.2 Condition of Operation

The Mach 6 nozzle reservoir pressure history was measured using two piezoelectric transducers located at 130 mm upstream of the end of the barrel. One transducer was PCB model 113A03 (SN14388 with a manufacturer's calibration

of -61.89 pC/MPa). This transducer was mounted on the top side of the barrel and was operated with a Kistler charge amplifier (SN1340472) giving a sensitivity of 0.5 MPa/V. The other transducer was also a PCB 113A03 (SN14387 with a manufacturer's calibration of -65.48 pC/MPa). This transducer was mounted on the bottom side of the barrel and was operated with a Kistler charge amplifier (SN1045830) also giving a sensitivity of 0.5 MPa/V. A summary of the operating conditions for measurements using the t-type thermocouple probe are listed in table 5.1.

Table 5.1: Initial condition of TUSQ for measurements using the t-type thermocouple probe

Conditions	Run		
	1	2	3
P_{amb} (kPa)	93 ± 0.5	94.45 ± 0.6	94.35 ± 0.5
T_{amb} (℃)	27.7 ± 5	27.5 ± 3	28 ± 2
P_{driver} (MPa)	4 ± 0.1	4 ± 0.1	4 ± 0.1
$P_{test\ section}$ (Pa)	750 ± 10	750 ± 12	800 ± 10
Diaphragm (μm)	100	100	100
Sensitivity of transducer (MPa/V)	0.5	0.5	0.5
Piston mass (grams)	383 ± 0.5	383 ± 0.5	383 ± 0.5

5.2.1 Thermocouple Probe

The stagnation temperature probe used in the present work was a thermocouple probe with a heated shield as illustrated in figure 5.1 and the photographs is showed in Appendix C. The stagnation temperature probe was positioned on the centre line of the TUSQ nozzle exit. The thermocouple shield was constructed using three different sizes of brass tubes. The outer tube was 42.5 mm long and

had a 2.4 mm internal diameter. The inner tube had a 0.8 mm internal diameter with a t-type thermocouple (0.003 inches diameter copper (+) and constantan (-) wires) inserted through its centre. The junction was 1.0 mm from the inner tube and was positioned at 8.0 mm from the probe tip. A 1.0 mm diameter hole acted as a vent and was located at 4.0 mm downstream from the junction.

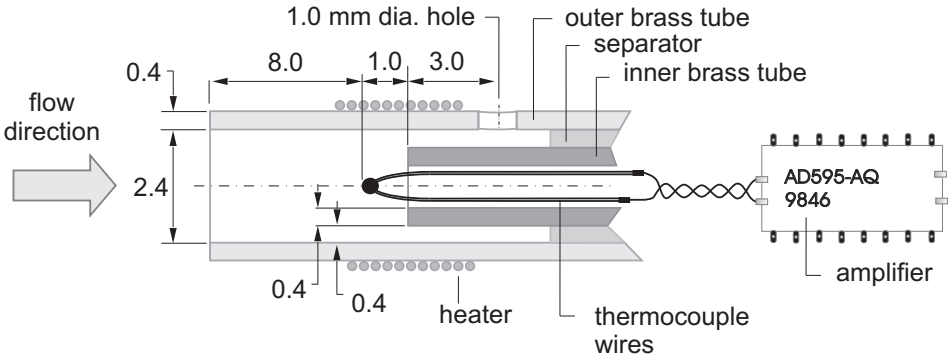

Figure 5.1: Schematic illustration of the design and the principal dimension of t-type bead-welded thermocouple probe (in mm).

An AD595-AQ (9846) chip was used to amplify the thermocouple signal. This chip provides amplification and the cold junction compensation for a k-type thermocouple, but it can be used directly with t-type thermocouple inputs due to the similarity of thermal EMFs in the 0°C to +50°C range. However, to accommodate the actual differences in the k and t-type thermocouples emf, a calibration of the thermocouple and amplifier system was performed using a furnace in order to gain coverage of the full range of temperature operation of the thermocouple in the present application. A k-type thermocouple and digital display was used as the temperature reference for the calibration of the t-type thermocouple. The two thermocouples were placed close together within the furnace during the calibration process.

Figure 5.2 provides the data and the curve fit for the temperature-voltage calibration. The results of the calibration show that 1 Kelvin temperature change produces 8.4 mV after amplification. Although this is somewhat different from

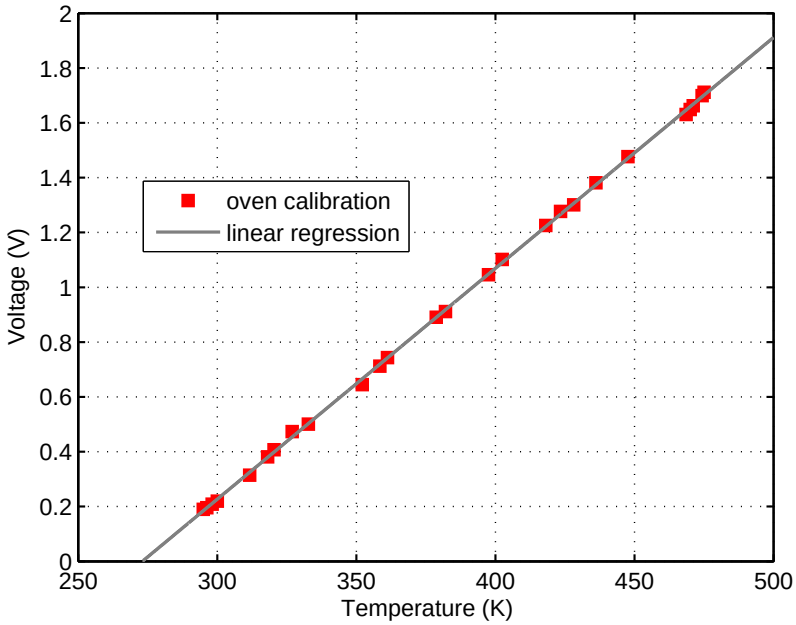

Figure 5.2: Result of calibration of the t-type thermocouple probe with amplifier.

the expected sensitivity of a t-type thermocouple amplified by the AD595, the calibration appears to be reasonable – the results show a linear correlation between temperature and voltage output over this range of temperatures, and the results are repeatable.

During TUSQ operation, a nichrome wire was used as a heater on the external surface of the outer brass tube (see figure 5.1). By increasing the initial temperature of the probe and thermocouple to a value close to the expected flow stagnation temperature, the magnitude of the response time correction can be reduced, thereby decreasing the uncertainty in the corrected stagnation temperature.

5.3 Correction for Time Constant

Thermocouple temperature measurement errors can arise if the thermocouple response time is not sufficiently fast for the flow dynamics of interest. To correct

the temperature measurement by the thermocouple, an approach using differentiation of the recorded thermocouple temperature data was applied.

The energy equation for a length of bare wire δx inserted through a containing wall into a fluid is written as [108]:

$$\rho c_v \frac{\pi d^2}{4} \delta x \frac{\partial T}{\partial t} = -\frac{\pi d^2}{4} \delta x \frac{\partial q}{\partial x} + h \pi d \delta x \left(T_f - T\right) \tag{5.1}$$

Multiplying equation 5.1 by $4/(\pi \delta x \rho c_v d^2)$ and substituting Fourier's law gives:

$$\frac{\partial T}{\partial t} = \alpha \frac{\partial^2 T}{\partial x^2} + \frac{T_f - T}{t_0} \tag{5.2}$$

where T_f is the fluid temperature, $\alpha = k/\rho c_v$ (which is the thermal diffusivity of the wire), d is the wire diameter, ρ is the density, k is the thermal conductivity, c_v is the constant volume specific heat, and h is heat transfer coefficient.

The term t_0 in equation 5.2 is defined as

$$t_0 = \frac{\rho c_v d}{4h} \tag{5.3}$$

If the hot junction position is sufficiently far from the wall, it is assumed that the heat flux along the wire is constant (meaning that $\partial^2 T/\partial x^2 = 0$), so equation 5.2 reduces to [108]:

$$T_f = T + t_0 \frac{\mathrm{dT}}{\mathrm{dt}} \tag{5.4}$$

Equation 5.4 indicates that provided a suitable time constant t_0 can be identified, the true temperature of the flow T_f can be estimated from the thermocouple

temperature measurement T and the time-derivative of the thermocouple temperature measurement, $\mathrm{d}T/\mathrm{d}t$.

The time constant of a thermocouple is normally considered the time required for a thermocouple's voltage to reach 63.2% of the value it will asymptotically approach in response to a sudden change in temperature. It takes approximately five time constants to obtain steady state readings [109].

5.4 Result and discussion

5.4.1 Pressure Measurements and Inferred Temperature History

The stagnation pressure of three runs was recorded by the barrel pressure transducers and the results are presented in figure 5.3. Based on the pressure history obtained from the transducers as presented in figure 5.3, the flow stagnation temperature for each of the three runs as deduced using the isentropic pressure-temperature relationship is presented in table 5.2. An average isentropic stagnation temperature value of about 571 K was obtained.

Table 5.2: Test gas compression time and stagnation properties during the three run time based on pressure measurements.

run	compression time (ms)	run time (ms)	P_0 (kPa)	$T_{0,isen}$ (K)
1	490 ± 10	190 ± 5	860 ± 5	566 ± 5
2	508 ± 10	188 ± 5	900 ± 5	574 ± 5
3	500 ± 10	190 ± 5	890 ± 5	572 ± 5

5.4.2 Measured and Corrected Thermocouple Results

Stagnation temperature measurements were obtained for the three different runs as presented in figure 5.4. The stagnation temperature probe readings for the runs were about 380 K, 450 K, and 500 K respectively towards the end of each run time as shown in figure 5.4. It is clear that the uncorrected temperatures indicated by the thermocouple probe in the first and second runs are not representative of the real stagnation temperature of the flow because the thermocouple temperature was still rising at the end of the run time. It appears that the thermocouple has a slow response time relative to the short duration of the present tests.

In order to directly measure a thermocouple temperature closer to the stagnation temperature of the flow, a preheating element was used in the present experiments. By increasing the initial temperature of thermocouple towards the flow stagnation temperature, it is expected to minimize the error when applying the response time correction in equation 5.4. Run 1 was performed without any preheating of the probe. For run 2, the heater was supplied with 1.15 A at 8.2 V, giving a power of 9.5 W resulting in a probe initial temperature of about 410 K. Prior to the run, the heater was turned off. The maximum temperature obtained in run 2 during the flow period was about 450 K. For run 3, the heater was left on and the initial temperature of thermocouple was about 485 K. The maximum temperature achieved in run 3 during the flow period was about 500 K.

Figure 5.5 provides a comparison between the measured thermocouple temperatures and the results corrected according to equation 5.4. The dashed lines indicate the measured (uncorrected) temperatures and corrected temperatures (referring to the stagnation temperatures) are represented by the solid line. To make the correction indicated in equation 5.4, a value for the time constant, t_0 was required. A value of $t_0 = 0.5$ s was used in this work and this value was identified by determining the stagnation temperature as defined in equation 5.4 for a range of t_0 values. The value of t_0 which minimized the difference between

the 3 corrected results during the time period indicated in figure 5.5 was selected.

5.5 Discussion

A summary of the temperature measurement results are presented in table 5.3. The results show that the uncorrected thermocouple temperatures for each of the three runs were 374.9, 447.1, and 495 K. These values were obtained as the mean values in the 100 ms time-window indicated in figure 5.5 and the values give an indication of the maximum temperature achieved by the thermocouple during the test period. After the correction was applied (equation 5.4) and using the same time-window, the stagnation temperatures for run 1, 2, and 3 were 498.2, 495.3, and 491.7 K respectively.

If the compression process within the barrel was actually isentropic, the stagnation temperature of the test gas would be about 571 K. The stagnation temperatures identified in the present work (values between about 492 and 498 K) are naturally below the isentropic temperature values because of substantial heat loss from the test gas to the barrel wall during the compression and discharge process.

Table 5.3: Mean values of the thermocouple temperature (T) and the corrected flow temperature results (T_f) for the three runs.

run	T (K)	T_f (K)
1	374.4	498.2
2	447.1	495.3
3	495.4	491.7

Based on the average temperature results obtained during the specified time-window, the corrected results for the three runs were within about 1 %. At least some of the variability in the corrected temperature results can be attributed to the run-to-run variability of the facility. For example, the isentropic temperature

values deduced from the pressure measurements differ by more than 1 % over the three runs, and there is also a similar magnitude of variability in the compression time for each run as presented in table 5.3.

5.6 Conclusions

In summary, implementation of thermocouple probe with a heated shield has allowed the identification of the stagnation temperature at a Mach 6 nozzle exit of the University of Southern Queensland hypersonic wind tunnel (TUSQ). Using a response time correction for the thermocouple measurements, it is found that the value of stagnation temperature during a 100 ms period that begins 50 ms after the start of the flow was about 495 K. This value is lower than the stagnation temperature estimated from the pressure history based on the isentropic compression assumption of about 571 K. The measured value appears feasible since the compression and discharge process is not isentropic because of heat loss from gas to the barrel, and hence measured stagnation temperature values lower than the isentropic limit are expected. The measurement of the variation of flow stagnation temperature with time has not been achieved with the probe described in this chapter. The next chapter describes an improved version of the probe that has allowed deduction of time-resolved stagnation temperature.

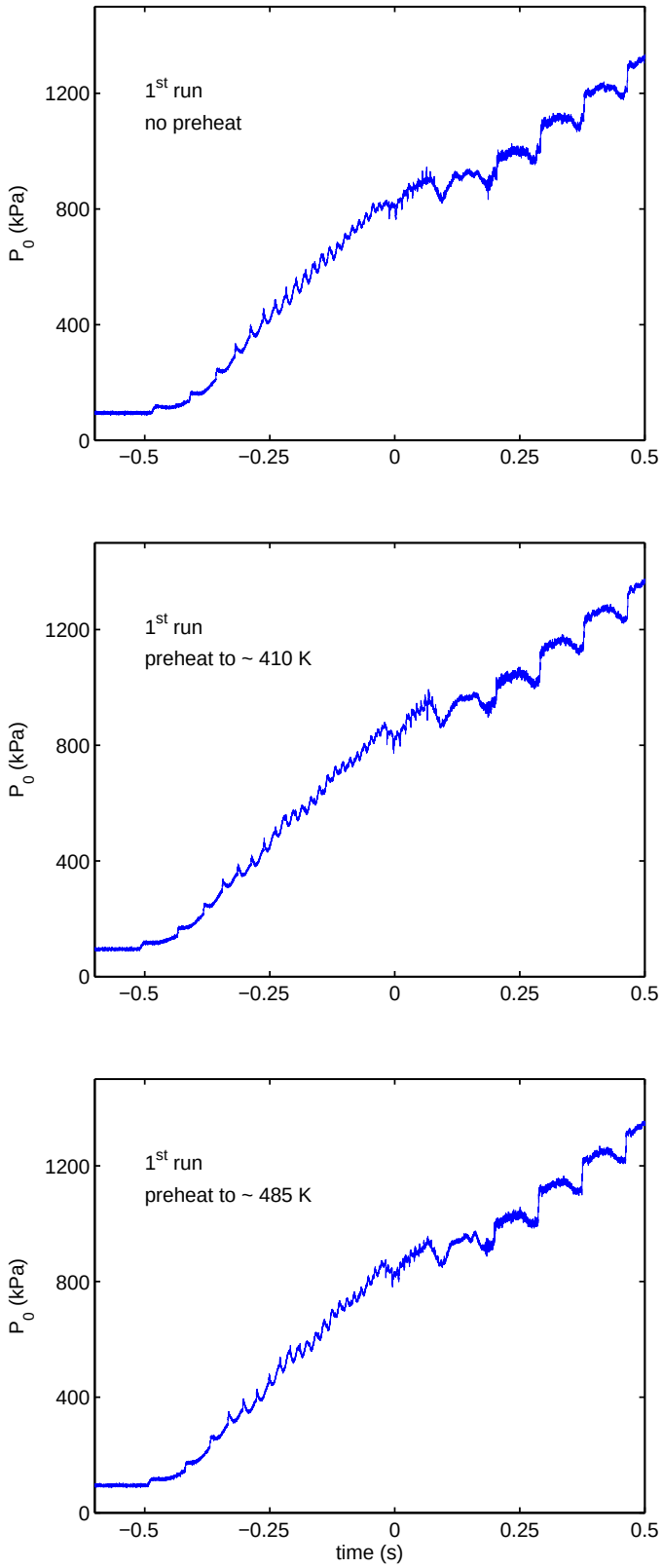

Figure 5.3: Stagnation pressure measured by the pressure transducer for the three runs of table 5.2.

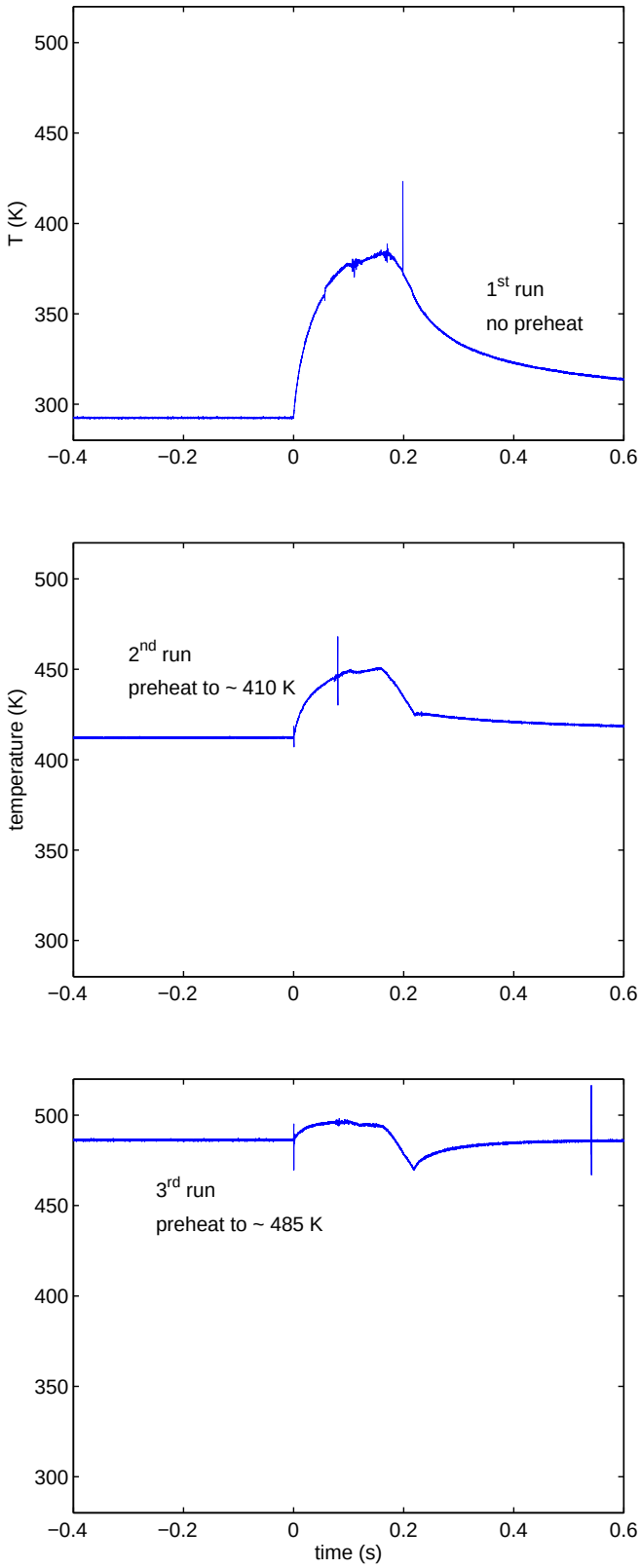

Figure 5.4: Thermocouple probe temperature measurement for the three runs of table 5.3.

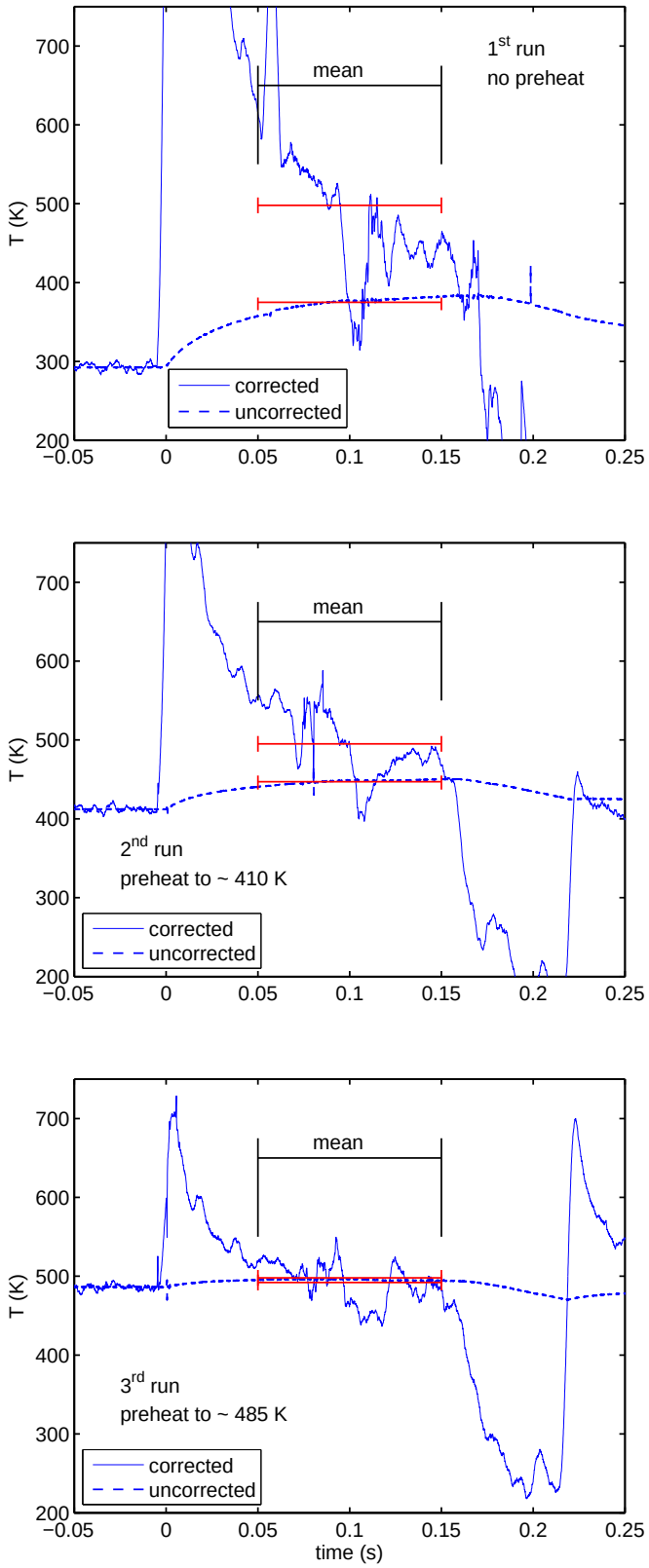

Figure 5.5: Uncorrected thermocouple temperature (T) and corrected temperature results (T_f) for the three runs of table 5.3.

Chapter 6

Time-resolved Stagnation Temperature

6.1 Introduction

In the previous chapter, stagnation temperatures at the nozzle exit of the TUSQ facility were identified using a heated shield, t-type thermocouple probe. The flow stagnation temperature was deduced from recorded temperature history based on the application of a response time correction factor. Although the results indicate feasible values with respect to the isentropic stagnation temperature estimated from the pressure history recorded by a pressure transducer, comprehensive measurements of the time-resolved stagnation temperature of the TUSQ are needed. In this chapter, the stagnation temperatures were measured using an improved aspirating tube device consisting of a k-type butt-welded thermocouple junction. A method of deducing flow stagnation temperature by using an impulse response filtering approach is introduced and uncertainness in the response time correction are assessed and minimized by operating the aspirating device over a range of different initial temperatures. Thermodynamic simulations based on an unsteady energy balance model with turbulent heat transfer from the test gas within the

barrel have also been developed in this chapter.

6.2 Operating Conditions and Probe

6.2.1 Operating Conditions

The hypersonic facility used in present work is described in Chapter 4. During the piston compression process, the pressure in the barrel was measured using two piezo-electric transducers mounted diametrically opposed and located at 130 mm upstream of the end of the barrel. The pressure transducers were manufactured by PCB (model number 113A03) and were operated in conjunction with Kistler charge amplifiers (type 5015). Figure 6.1 shows representative barrel pressure histories for experiments performed for the current work.

For the current work, experiments were performed at two different operating conditions, table 6.1. The initial pressures for the two conditions differ by a factor of 2 approximately, and the Mylar diaphragm thickness was also different by a factor of 2 so that Condition 1 and 2 maintained approximately the same compression ratio. The initial pressure in the test section for the two conditions was around 700 Pa. The variability specified in table 6.1 indicates the estimated uncertainty or the $\pm 2\sigma$ values identified from the measurements.

Table 6.1: Initial conditions for facility operation

Parameter	Unit	Condition 1	Condition 2
$P_{reservoir}$	(MPa)	4.1 ± 0.1	2.1 ± 0.1
P_{barrel}	(kPa)	94.5 ± 0.5	49.8 ± 1.0
T_{amb}	(K)	298 ± 5	295 ± 2
Diaphragm	(μm)	100	50 (2 × 25)

From nozzle exit pitot pressure surveys (reported in chapter 7) and the current stagnation pressure measurements at the end of the barrel, the flow Mach number

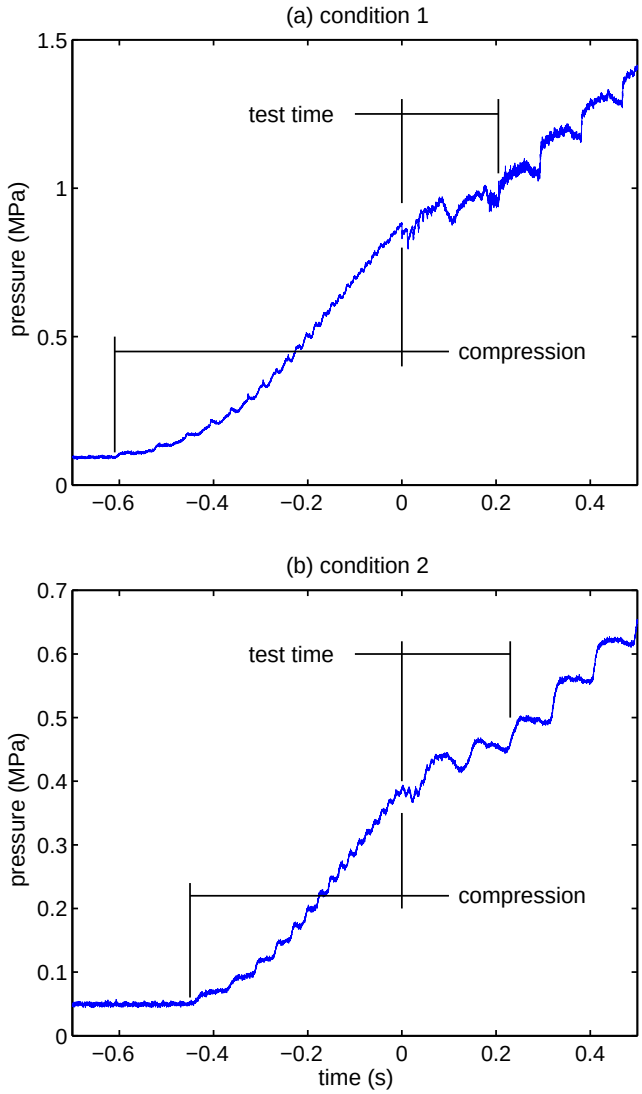

Figure 6.1: Barrel pressure measurements for Condition 1 (part a) and Condition 2 (part b).

can be deduced since the test gas was air, and to a good approximation, the ratio of specific heats can be taken as 1.4 during the nozzle expansion process. Table 6.2 provides the relevant estimates of flow properties. Stagnation pressure values for the two conditions are identified based on the barrel pressure measurement results over the the first 150 ms of the test flow duration – the mean and the $\pm 2\sigma$ values are quoted. Uncertainties in the pitot pressure to stagnation pressure ratio and the Mach number are presented based on the standard deviation ($\pm 2\,\sigma$ values) identified from the spatial distribution of the pitot pressure across the core flow

Table 6.2: Hypersonic nozzle exit flow conditions

Parameter	Unit	Condition 1	Condition 2
P_0	(MPa)	0.92 ± 0.06	0.41 ± 0.03
P_{pit}/P_0	-	0.0331 ± 0.0007	0.0345 ± 0.0009
M	-	5.84 ± 0.03	5.79 ± 0.05
$T_{0,isen}$	(K)	572 ± 14	538 ± 12

of the hypersonic nozzle. The stagnation temperature values are based on the isentropic estimate for compression from the initial barrel pressure up to the average pressure experienced by the stagnated test gas during discharge into the nozzle during the first 150 ms of flow and uncertainties in this case are based on the propagation of the pressure and initial temperature measurement uncertainties.

6.2.2 Thermocouple Probe

An aspirating tube device with a k-type butt-welded junction thermocouple was used as illustrated in figure 6.2. The probe was manufactured in-house using a ceramic tube with a 3.2 mm outer diameter and a 1.6 mm inner diameter. The butt-welded k-type thermocouple was manufactured by Omega Corporation and had a diameter of 0.075 mm (model number CHAL-003BW) and the physical properties are presented in Appendix D. A butt-welded junction thermocouple was used because it should have a faster response time and should be more rugged compared to a bead-welded junction thermocouple of the same wire diameter.

The thermocouple wire was glued to the ceramic tube using cyanoacrylate. The butt-welded junction was positioned close to the center of the tube cross-section to ensure the junction was exposed to the flow near the tube centre line, well clear of any boundary layer development at the tube wall. The probe was heated to various initial temperatures using a nichrome wire in order to obtain a range of initial thermocouple temperatures around the expected flow stagnation tem-

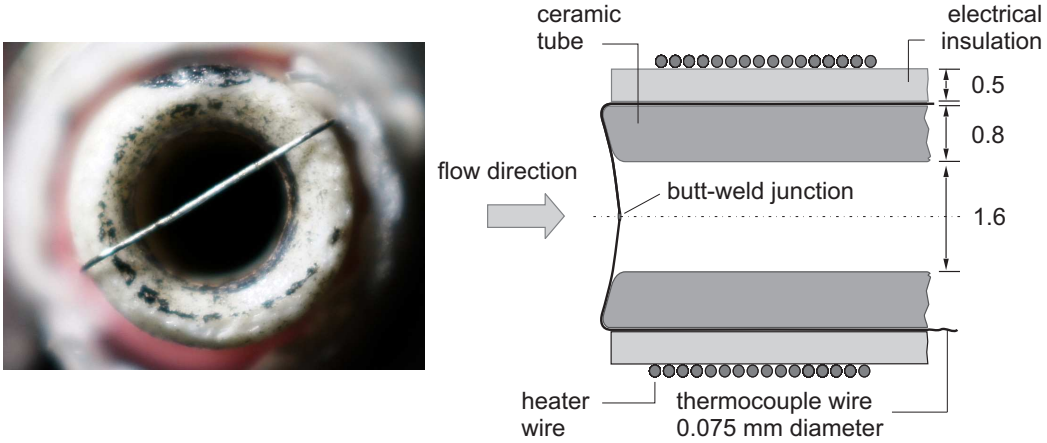

Figure 6.2: Photograph of the probe inlet (left) and schematic illustration of the probe with dimensions in mm (right).

perature. Before attaching the heating wire, a teflon tape was used to provide electrical insulation between the thermocouple wire and the heater element. The signal from the thermocouple was amplified using the AD595 chip from Analog Devices.

To confirm performance of the k-type thermocouple and amplifier (AD595) system, a calibration was performed using a furnace. This static calibration was carried out with reference to a platinum resistance temperature detector (RTD) with a nominal resistance of 100 ohm from Omega Corporation (model 2PT100KN3045). The temperature reading from the platinum RTD was obtained using a temperature monitor, also provided by Omega Corporation (model CYD211). Both the k-type thermocouple and the Platinum RTD were positioned close together within the furnace during the calibration process. Figure 6.3 illustrates the calibration results. The reference result in figure 6.3 was obtained by combining the standard emf values for a k-type thermocouple with the AD595 amplifier specifications from the manufacturer. The calibration result shows a good linear correlation between temperature and voltage with the thermocouple sensitivity of 10.2 mV/K after amplification. At the highest measured temperature of $\sim 492\,\mathrm{K}$ during calibration, the voltage difference from the reference value is only 0.8 %.

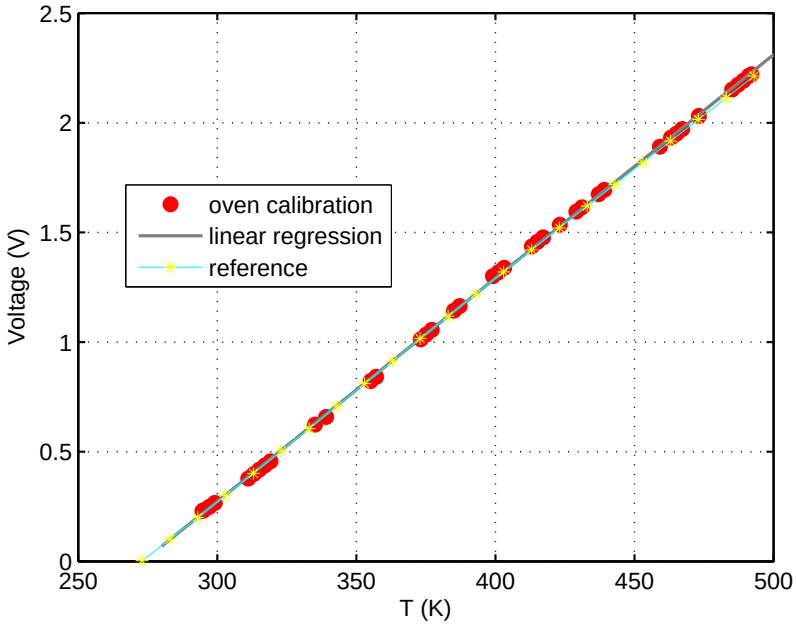

Figure 6.3: Calibration results for the k-type thermocouple and AD595 amplifier system.

6.3 Method for Deduction of Flow Stagnation Temperature

Although the smallest commercially-available butt-welded thermocouple was used in the current work, the response time in current configuration was still sufficiently long to warrant identification and application of some suitable response time compensation scheme.

6.3.1 Convective heat transfer coefficient of the wire

The heat transfer coefficient for the wire is an important variable that affects the thermocouple response time. In the present method, an effective value of the heat transfer coefficient is identified through in-situ calibrations, so the quality of the response time correction is not critically dependent on the accuracy of the

heat transfer coefficient determined from estimates of the local flow conditions at the wire. Nevertheless, it is useful to have an estimate for the wire heat transfer coefficient as a starting point for subsequent tuning. For the configuration shown in figure 6.4, the heat transfer coefficient at the thermocouple wire can be estimated using a cylinder-in-cross-flow heat transfer correlation if the local flow conditions external to the wire boundary layer can be determined.

A normal shock is present ahead of the probe, so the flow in the vicinity of the thermocouple wire will be subsonic. The flow which enters the probe is assumed to choke at the downstream end of the probe holder, which has nominally the same internal diameter as the ceramic tube. Since the stagnation conditions for the inviscid flow within the probe correspond to the post-shock stagnation conditions, the choking conditions in the inviscid core of the flow within the probe can be estimated. It is necessary to model the development of the boundary layer along the internal probe surface because the displacement thickness of the boundary layer at the downstream end will dictate the value of A/A^*, and thus all other flow properties, within the inviscid core flow of the probe, including those in the local vicinity of the thermocouple wire.

Based on the development of the displacement thickness of a laminar boundary layer in the tube which is approximated using the flat plate expression

$$\frac{\delta^*}{x} = \frac{1.721}{\sqrt{\mathrm{Re}_x}}\,, \tag{6.1}$$

the displacement thickness of the boundary layer at the downstream end of the probe ($x = L$) is estimated as 0.35 mm for Condition 1 and 0.52 mm for Condition 2 and the average velocity between $x = 0$ and $x = L$ which is used in the calculation of the the Reynolds number is 270 m/s for Condition 1 and 230 m/s for Condition 2. For the present conditions it appears likely that the boundary layer within the probe remains laminar since Re_L is calculated as 57,000 for Condition 1 and 26,000 for Condition 2. Using the flow conditions at the start of

the parallel section of the tube, where the boundary layer is assumed to have zero thickness, the thermocouple wire Reynolds number Re_D is estimated as 25 for Condition 1 and 5.2 for Condition 2. For these Reynolds numbers and a Prandtl number of 0.71, the Nusselt number of the wire was determined from [110]

$$\mathrm{Nu}_D = 0.75\,\mathrm{Re}_D{}^{0.4}\mathrm{Pr}^{0.37} \tag{6.2}$$

from which the wire heat transfer coefficients were determined as $1410\,\mathrm{W/m^2K}$ for Condition 1 and $720\,\mathrm{W/m^2K}$ for Condition 2.

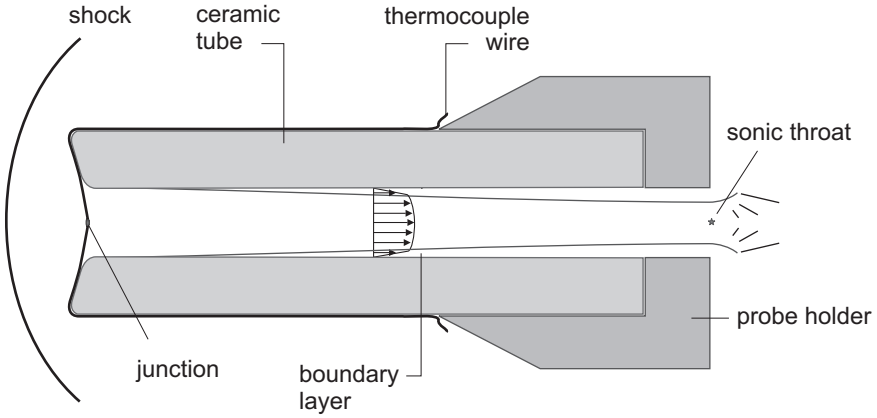

Figure 6.4: Illustration of the flow model used to estimate local flow properties at the thermocouple wire.

6.3.2 Wire response thermal model

To correct the measurements for the response time of the thermocouple wire, a model for the relationship between the flow stagnation temperature T_0 and the measured thermocouple wire temperature is useful. The analytical solution for the transient response of a homogeneous, constant cross sectional wire in a convective environment is described in Carslaw and Jaeger [99]. The unsteady

heat conduction equation in this case is written as [99]

$$\frac{\partial (T - T_0)}{\partial t} = \alpha \frac{\partial^2 (T - T_0)}{\partial x^2} - \nu (T - T_0) \tag{6.3}$$

where T is the wire temperature which is assumed to be uniform across its section, T_0 is the temperature of the environment to which the wire transfers heat, t is the time, and x is the distance along the wire from the centre. The flow stagnation temperature T_0 is the appropriate environment temperature for the convective heat exchange with the wire in this case because the flow speed in the vicinity of the wire is relatively low and thus the boundary layer recovery factor of the wire approaches unity. The thermal diffusivity of the wire α is defined as

$$\alpha = \frac{k}{\rho c} \tag{6.4}$$

where k the thermal conductivity of the wire material is, ρ is the wire density, and c is the specific heat capacity of the wire. The quantity ν is the convection parameter defined as

$$\nu = \frac{hP}{\rho c A} \tag{6.5}$$

where h is the convective heat transfer coefficient, P is the perimeter of the wire, and A is the cross-sectional area of the wire.

A number of solutions are offered by Carslaw and Jaeger [99] for different boundary and initial conditions. The wire is assumed to have a uniform initial temperature T_i such that

$$T_i - T_0 = f \tag{6.6}$$

which is a constant, and a symmetrical solution about the centre of the wire ($x = 0$) is also considered,

$$\left(\frac{\partial T}{\partial x}\right)_{x=0} = 0\,. \tag{6.7}$$

A time-invariant temperature at the wire support $(T)_{x=L} = T_L$ is also considered

$$T_L - T_0 = \phi\,. \tag{6.8}$$

Under these conditions, the solution is given by [99]

$$T = T_0 + 2\sum_{n=0}^{\infty} \frac{\cos\beta_n x}{\beta_n L}\left\{\alpha\beta_n^2(-1)^n \frac{\phi}{\alpha\beta_n^2+\nu}\left[1 - e^{-\left(\alpha\beta_n^2+\nu\right)t}\right] + f\, e^{-\left(\alpha\beta_n^2+\nu\right)t}\sin\beta_n L\right\} \tag{6.9}$$

where

$$\beta_n = \frac{(2n\ +\ 1)\,\pi}{2L} \tag{6.10}$$

and L is the half-length of the wire. For the convenience of subsequent discussions β_0 is defined as

$$\beta_0 = \frac{\pi}{2L} \tag{6.11}$$

so that $\beta_n = (2n+1)\beta_0$. If the temperature at the wire supports is taken as the initial temperature, then $\phi = f = T_i - T_0$ and the solution can be written as

$$\frac{T-T_0}{T_i-T_0} = 2\sum_{n=0}^{\infty} \frac{\cos\beta_n x}{\beta_n L} \left\{ \frac{\alpha\beta_n^2(-1)^n}{\alpha\beta_n^2+\nu} \left[1 - e^{-\left(\alpha\beta_n^2+\nu\right)t}\right] + e^{-\left(\alpha\beta_n^2+\nu\right)t} \sin\beta_n L \right\} \tag{6.12}$$

Furthermore, if only the solution at the centre of the wire ($x = 0$) is necessary, the normalised temperature can be written as a function g of the form

$$\frac{T-T_0}{T_i-T_0} = g\left(\alpha\beta_0^2, \nu, t\right) \tag{6.13}$$

since it is recognised that $\beta_n L$ is not a function of any thermal conditions or thermophysical properties of the wire.

Some results from equation (6.12) are presented in figure 6.5. For these results, parameter values listed in table 6.3 have been used as the default values for the k-type thermocouple wire properties. In the case of the density, conductivity, and specific heat, mean values of the chromel and alumel materials have been adopted. From figure 6.5 it is observed that larger values of the convective heat transfer coefficient (larger values of ν) result in a faster approach to the steady state value, and longer wires (smaller values of $\alpha\beta_0^2$) also result in a steady state temperature that more closely approximates the flow stagnation temperature.

6.3.3 Impulse Response Analysis

Impulse response processing techniques have been used successfully in the analysis of surface temperature measurements from thin film gauges [15, 111, 112] and eroding ribbon thermocouples [113] with the objective of deducing the instantaneous surface heat transfer rate. In these cases, the input which drives the system is the surface heat transfer rate associated with convective heat transfer, and the measured output is the surface temperature history. The transient

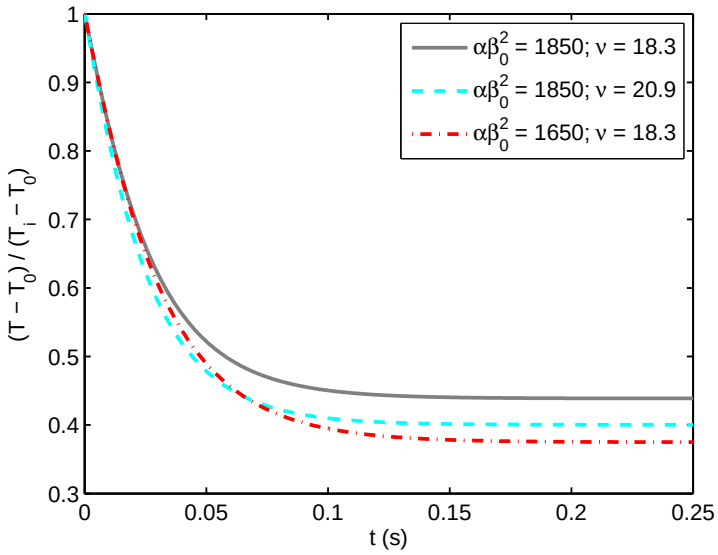

Figure 6.5: Estimated response of the thermocouple wire from equation 6.12.

heat conduction process within the substrate of the gauge is considered as a linear-time-invariant system and an appropriate impulse response filter is developed based on analytical modelling or experimental measurements. The impulse response filter is used to transfer from the surface temperature measurements (the system output) back to the instantaneous surface heat transfer (the system input).

In the present work however, the objective is to deduce the instantaneous flow stagnation temperature from measurements of the thermocouple temperature, and hence the convective heat transfer coefficient of the wire becomes part of the transfer function. For wide variations in the flow conditions experienced by the wire, heat transfer coefficient changes could compromise the linear-time-invariance assumption. Principal uncertainties in the application of the system model (step response) outlined in section 6.3.2 are:

1. The wire is not homogenous – it is a k-type thermocouple consisting of two different materials with an abrupt change of thermal properties at the butt-welded junction. The thermophysical properties of these two materials differ from the mean values, the most extreme deviation in a property value

Table 6.3: Nominal values for the thermophysical properties of the thermocouple wire.

Parameter	Symbol (Unit)	Value
density	ρ (kg/m^3)	8670
specific heat	c (J/kgK)	470
conductivity	k (W/mK)	25
diameter	d (mm)	0.075
half-length	L (mm)	0.85
$\alpha{\beta_o}^2$	(s^{-1})	1850
ν	(s^{-1})	18.3

being about $\pm 20\,\%$ in the case of the thermal conductivity [114].

2. The effective wire length and boundary conditions of the wire at the supporting ceramic tube are uncertain. A constant temperature at the support is assumed for the model, but variations in the surface temperature of the ceramic tube during the experiment will occur, and the thermal resistance of the contact between the wire and tube is likely to be moderately high in the vicinity of the face of the ceramic tube.

3. The magnitude of the heat transfer coefficient is somewhat uncertain due to the approximate and one-dimensional nature of flow model (section 6.3.1). It seems unlikely that the convective heat transfer coefficient will be constant over the entire wire length, especially in the immediate vicinity of the ceramic tube.

4. The heat transfer coefficient of the wire may not be time-invariant.

In the present work, the impact of the above uncertainties is minimized by tuning two of the model parameters based on temperature measurements obtained during operation of the probe over a range of pre-heat values. This strategy in effect provides in-situ calibration of the probe. With the current model formulation, only two parameters ($\alpha\beta_0^2$ and ν) require tuning because of the mathematical

groupings in equation (6.9) as amplified in equation (6.13).

The sensitivity of the impulse response filtering technique to errors in $\alpha\beta_n^2$ and ν is assessed with the following method.

1. Values for the magnitude of the parameters ($\alpha\beta_0^2$ and ν) as required by the model (equation 6.12) are specified in order to calculate the wire response T as a function of time. These parameter values are considered the *true* values.

2. Errors in the parameters $\alpha\beta_0^2$ and ν are introduced via scaling factors (S_L and S_h) and parameters that are only approximations of the true values are thereby defined:

$$\left(\alpha\beta_0^2\right)_a = \frac{1}{S_L^2}\alpha\beta_0^2 \tag{6.14}$$

$$\left(\nu\right)_a = S_h\nu \tag{6.15}$$

3. An impulse response is defined based on the approximate values $\left(\alpha\beta_0^2\right)_a$ and $\left(\nu\right)_a$. This impulse response $G_a(s)$ is only an approximation of the true system impulse response $G(s)$.

4. The approximate impulse response filter is designed and applied to the true wire response T in order to obtain an approximation for the stagnation temperature $T_{0,a}$.

5. The approximate stagnation temperature deduced in this manner $T_{0,a}$ is compared to the actual stagnation temperature T_0 to ascertain the significance of possible errors in the model parameters.

Note that the scaling factors defined at step (2) above (S_L and S_h) have been adopted so as to give a direct indication of the significance of errors in the effective half-length of the thermocouple wire (L) and the wire heat transfer coefficient (h) because these parameters have the highest uncertainty as described previously in

this section. Errors due to an incorrect choice of the additional wire properties ρ, c, and k and d are also related to the scaling factors S_L and S_h since these properties enter the model through the definition of $\alpha\beta_0^2$ and ν.

Results from the assessment method outlined above are presented in figure 6.6. The situation considered here is that of a step change in the convective conditions at $t = 0$. The error in the deduced stagnation temperature produced using incorrect (approximate) parameters in the model $(T_{0,a} - T_0)$ is normalised using the difference between the flow stagnation temperature and the initial wire temperature $(T_0 - T_i)$. In the case of a step change in convective conditions, errors in the stagnation temperature deduced using approximate values for the model parameters, $(T_{0,a} - T_0)$ can be minimized by using initial wire temperatures close to the flow stagnation temperature $(T_0 - T_i) \to 0$.

Results in figure 6.6 part (a) show that for short times, the error in the deduced stagnation temperature is close to zero irrespective of errors in the estimation of the effective length of the wire provided the effective heat transfer coefficient is correct – see the curves labelled $S_L = 0.7, S_h = 1.0$ and $S_L = 2.0, S_h = 1.0$ which start from $(T_{0,a} - T_0)/(T_0 - T_i) = 0$ at $t = 0$. At short times, heat conduction exchange with the wire supports (the ceramic tube) has not developed. In contrast, errors in the deduced stagnation temperature due to incorrect estimation of the heat transfer coefficient are largest at short times and will not reach zero at long times even if the effective length of the wire is correct – see the curves labelled $S_h = 0.7, S_L = 1.0$ and $S_h = 2.0, S_L = 1.0$.

An assessment of the sensitivity of errors in the deduced stagnation temperature to errors in estimation of the model parameters is provided in figure 6.6 part (b). In the case of errors in the estimation of the effective wire length, errors in the deduced stagnation temperature are assessed at a relatively long time – 0.250 s after the start of convection. In the case of errors in the estimation of the effective heat transfer coefficient, errors in the deduced stagnation temperature are assessed at a relatively short time – 2 ms after the start of convection. This

figure indicates that overestimating the model parameters by a certain ratio is preferable to underestimation by the same ratio if magnitude of the relative error in the deduced stagnation temperature is important. For example, for $S_L = 2, S_h = 1$ the relative error at 0.250 s is around -0.4 whereas for $S_L = 0.5, S_h = 1$, the relative error at 0.250 s is around 1.5.

6.4 Experimental Results

Temperatures measured using the thermocouple probe are shown in figure 6.7. A range of different initial temperatures have been used in order to assess and minimize the influence of possible incorrect estimation of system parameter values. Based on an assessment of the temporal gradient of temperature at $t = 0$ (the start of the run), the initial flow stagnation temperature in Condition 1 is expected to lie between about 540 and 560 K (run 114 and run 120 respectively). For Condition 2, the initial flow stagnation temperature is expected to lie between about 500 K and 545 K (run 124 and 121 respectively).

Flow stagnation temperatures deduced through the impulse response filtering are presented in figure 6.8 parts (a) and (b). To achieve these results, the effective heat transfer coefficient and the effective wire length have both been tuned, following an approach suggested by the sensitivity analysis of section 6.3.3. Since the initial value of flow stagnation temperature deduced by the impulse response filtering method is independent of the errors in the effective wire length, the effective heat transfer coefficient parameter is tuned first. The effective heat transfer coefficient is adjusted until the standard deviation of the stagnation temperature values deduced over the period 5 to 15 ms for the different runs is minimized. Using this tuned value of the effective heat transfer coefficient, the effective wire length is then tuned through minimization of the standard deviation of the stagnation temperature values over the period 150 to 160 ms for the different runs.

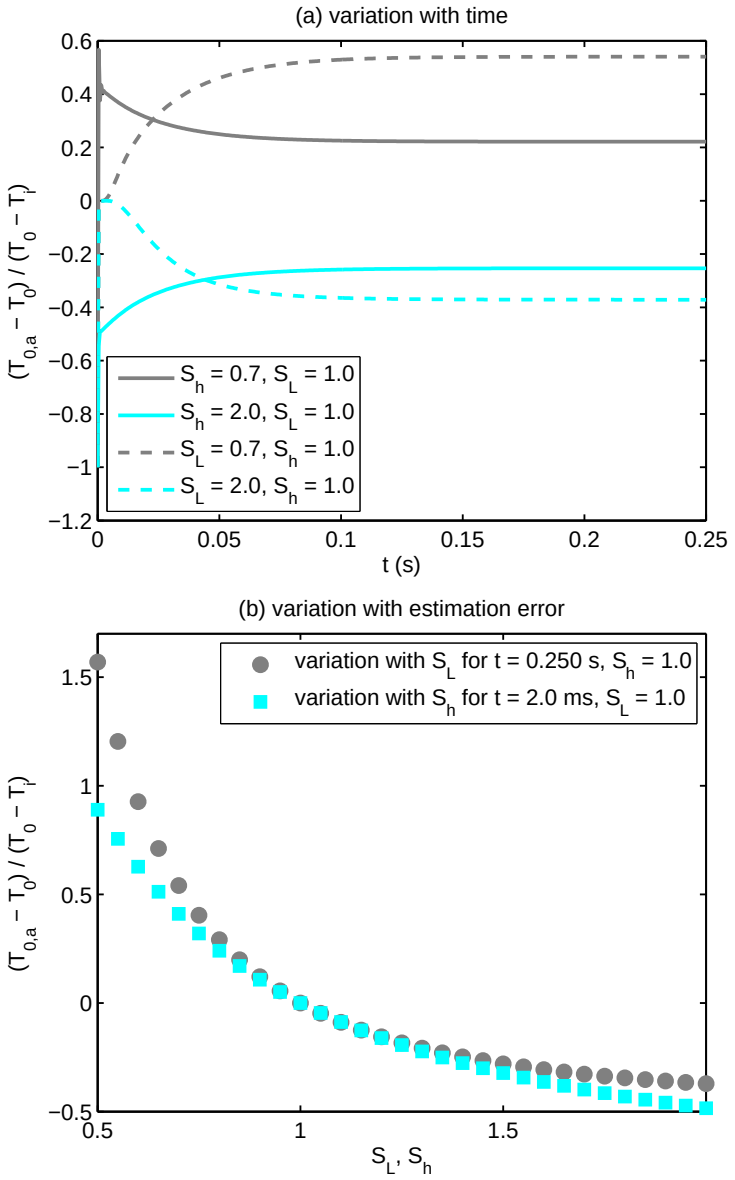

Figure 6.6: Relative error in the estimation of the flow stagnation temperature when errors are present in the parameter values of the model. A step change in the convective conditions of the wire is considered. Scaling factors S_L and S_h indicate the magnitude of the errors in effective wire length and heat transfer coefficient respectively. True model parameter values adopted: $\alpha\beta_0^2 = 1850\,\mathrm{s}^{-1}$ and $\nu = 18.3\,\mathrm{s}^{-1}$.

The tuned value of effective heat transfer coefficient for Condition 1 was $2400\,\mathrm{W/m^2K}$ (the nominal value was $1410\,\mathrm{W/m^2K}$) and for Condition 2 it was $1400\,\mathrm{W/m^2K}$ (the nominal value was $720\,\mathrm{W/m^2K}$). The tuned value of the effective half-length

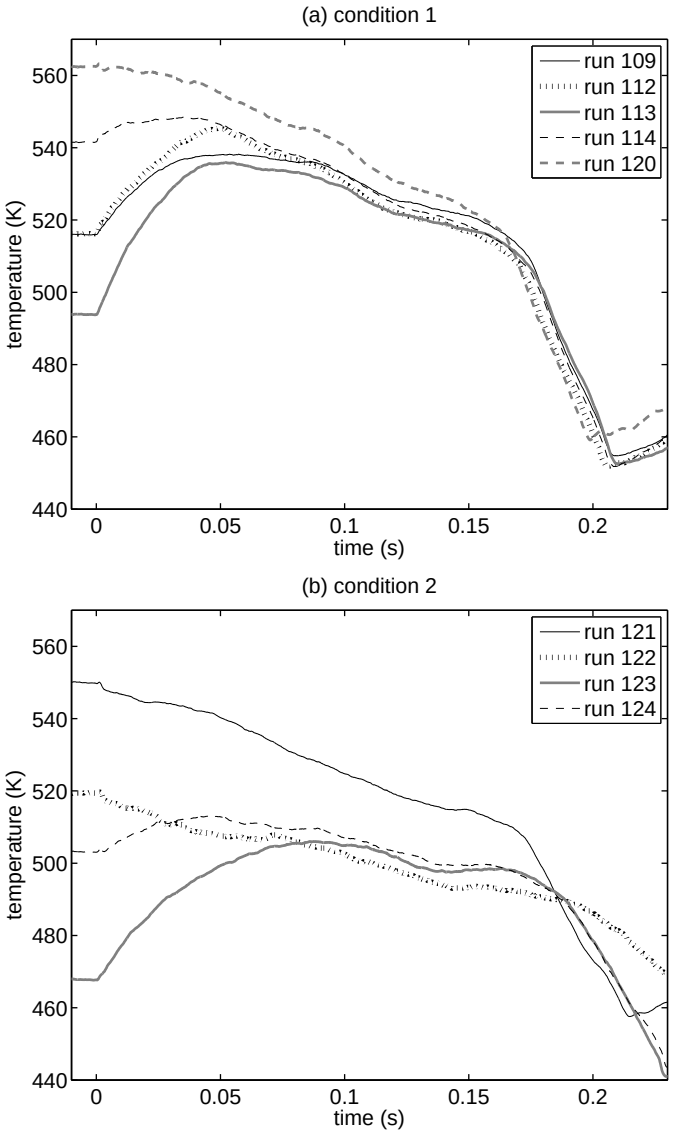

Figure 6.7: Wire temperatures measured for Condition 1 (part a) and Condition 2 (part b).

of the wire for both Condition 1 and Condition 2 was 1.5 mm (the nominal wire half-length for both conditions, based on the physical size of the probe is 0.85 mm). Given the assumptions and approximations inherent in the system model, the magnitude of such adjustments appears reasonable.

The symbol and error bars in figure 6.8 presents the isentropic estimate of flow stagnation temperature based on the measured barrel pressure during the hypersonic test flow period. It is clear that the initial stagnation temperature of the

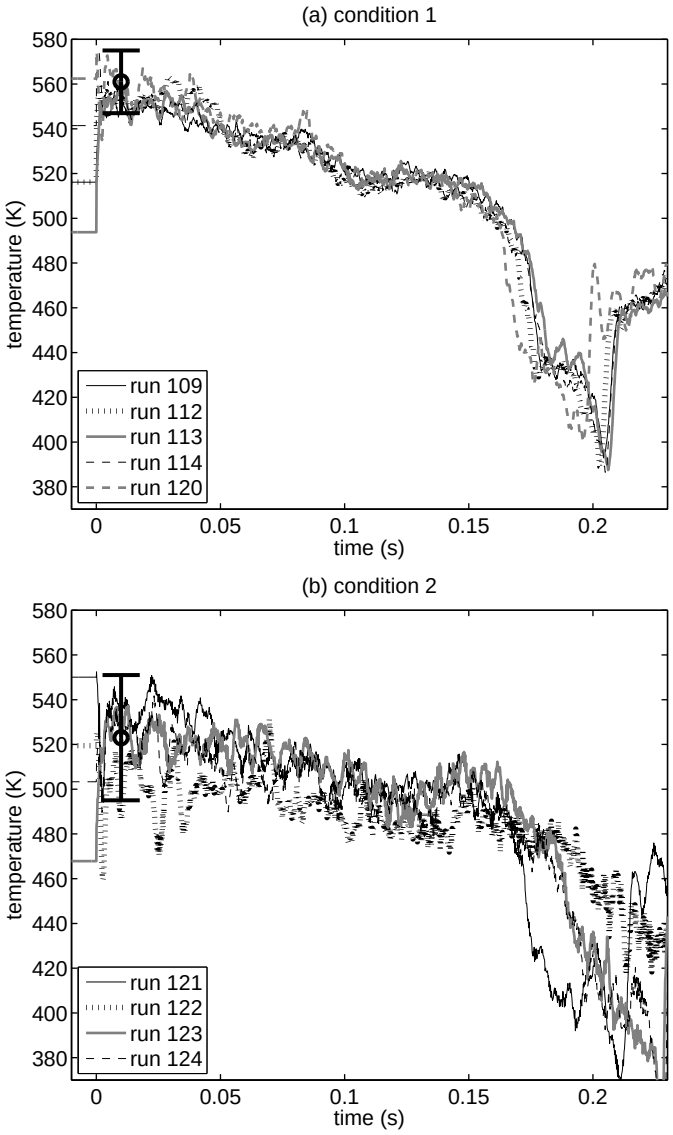

Figure 6.8: Flow stagnation temperatures deduced for Condition 1 (part a) and Condition 2 (part b). The data point and error bars positioned at $t = 10\,\text{ms}$ represents the stagnation temperature deduced from the assumption of isentropic compression from initial conditions to the stagnation pressure measured during the period from 0 to 20 ms.

flow that is discharged into the hypersonic nozzle is very close to the isentropic value for both conditions. For Condition 1, over the 5 runs considered, the initial stagnation temperature based on stagnation pressure measurements the period over the first 20 ms and an isentropic calculation is $561 \pm 14\,\text{K}$ and for Condition 2, over the 4 runs considered, $523 \pm 28\,\text{K}$. (Uncertainties quoted here are based upon

$\pm 2\sigma$ values arising from variations in the initial barrel temperature (table 7.1) and run-to-run pressure variations). These values are presented as the data point with the error bars in figure 6.8 centered at the time 10 ms and demonstrate a strong correlation with the results from the thermocouple measurements.

During the hypersonic flow discharge from the barrel, there is a gradual decrease in the flow total temperature. Over the first 150 ms of the test flow, the drop in stagnation temperature is around 40 K for both conditions. During the last 40 ms of test flow discharge, the flow stagnation temperature drops dramatically – by around 100 K. This rather sudden decrease in stagnation temperature towards the end of the test flow is attributed to the arrival of vortical flow in the vicinity of the piston [3, 50]. For two facilities with barrel aspect ratios comparable to the TUSQ facility, East and Qasrawi [50] also identified an unstable vortical structure which propagated well ahead of the piston during the compression process. Measurements of the turbulent mixing zone development are presented in [50] for a range of Reynolds numbers and compression ratios achieved in a pilot device and a larger scale facility.

Mixing zone development was also characterised for a range of Reynolds numbers using a piston in a water tube, but these results were at a comparatively low Reynolds number [50]. In an effort to correlate results, mixing zone lengths for different compression ratios were related to the zone length in an equivalent incompressible fluid column. Extrapolation of their results to the present operating conditions suggest the mixing zone length in the present cases would extend ahead of the piston by about 2 m. At the initiation of the test flow in the present work, the piston was approximately 3 m from the nozzle entrance. Therefore the existence of initial test flow with a stagnation temperature close to the isentropic value is consistent with previous observations.

6.5 Stagnation Temperature Simulation

To assist the interpretation of the stagnation temperature measurements, the free piston compression process has been simulated based on the measured pressure in the barrel and models for the heat loss from the test gas to the barrel wall during the test gas compression and discharge process. The test gas is discretized according to the scheme illustrated in figure 6.9.

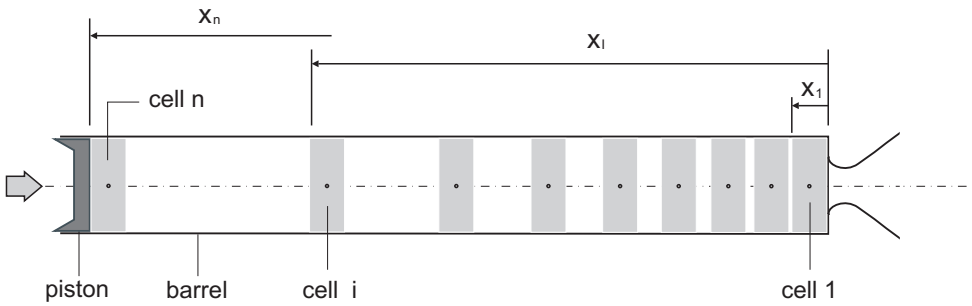

Figure 6.9: Arrangement used for thermodynamic simulation of the free piston compression process.

Considering the pressure throughout the test gas region to be uniform at any point in time, the unsteady energy equation giving the rate of change of temperature for element i is written as

$$\frac{\mathrm{d}T_i}{\mathrm{d}t}=\frac{1}{m_i c_v}\left(Q_i-P\frac{\mathrm{d}V_i}{\mathrm{d}t}\right) \tag{6.16}$$

where c_v is the constant volume specific heat, Q_i is the heat addition for element i (generally a negative quantity for the present application), and V_i is the volume of element i. The ideal gas law stated in deferential form is

$$\frac{\mathrm{d}T_i}{\mathrm{d}t}=\frac{P}{m_i R}\frac{\mathrm{d}V_i}{\mathrm{d}t}+\frac{V_i}{m_i R}\frac{\mathrm{d}P}{\mathrm{d}t} \tag{6.17}$$

where R is the gas constant for the test gas. From equation (6.16) and (6.17),

the change of volume of cell i can be written

$$\frac{\mathrm{d}V_i}{\mathrm{d}t}=\frac{\gamma-1}{\gamma}\frac{Q_i}{P}-\frac{1}{\gamma}\frac{V_i}{P}\frac{\mathrm{d}P}{\mathrm{d}t} \tag{6.18}$$

where γ is the ratio of specific heats.

The volume from the nozzle entrance to the upstream edge of element i is

$$V_I = \sum_{j=1}^{i} V_j = x_I A_b \tag{6.19}$$

where the distance x_I is as shown in figure 6.9 and A_b is the cross sectional area of the barrel. Total heat transfer to the elements from the nozzle entrance to the upstream edge of element i can also be written as

$$Q_I = \sum_{j=1}^{i} Q_j \tag{6.20}$$

Now since the velocity of the upstream face of cell i is

$$u_I = \frac{\mathrm{d}x_I}{\mathrm{d}t} = \frac{1}{A_b}\frac{\mathrm{d}V_I}{\mathrm{d}t} \tag{6.21}$$

the position of the upstream face of element i can be identified by integrating the expression

$$\frac{\mathrm{d}x_I}{\mathrm{d}t} = \frac{\gamma-1}{\gamma}\frac{1}{A_b}\frac{Q_I}{P} - \frac{1}{\gamma}\frac{x_I}{P}\frac{\mathrm{d}P}{\mathrm{d}t} \tag{6.22}$$

This integration can be achieved with the pressure and the pressure derivative on the right hand side of (6.22) obtained from experiment data and a model for the heat transfer Q_I derived from engineering correlations.

Two heat loss models have been investigated: (1) heat is transferred from the test gas to the barrel wall based on incompressible flat-plate boundary layer correlations with the Reynolds number calculated based on local flow conditions and the distance the element has moved from its initial location; and (2) heat is transferred from the test gas based on an incompressible fully developed turbulent pipe flow heat transfer correlation, again with local flow conditions being used in the Reynolds number calculation which is based on the barrel diameter. In the case of the flat plate heat transfer model, transition from a laminar to a turbulent boundary layer is assumed to take place between Reynolds numbers of 0.2×10^6 and 2×10^6. (The value of the critical Reynolds number for a incompressible flat plate may vary from 10^5 to 3×10^6, depending on the surface roughness and the turbulence level of the free stream [115].)

Results from the stagnation temperature simulations are presented in figure 6.10. Measurements of stagnation temperature are also presented in figure 6.10 and these results have been obtained by averaging the results from the five runs at Condition 1 and the four runs at Condition 2 (figure 6.8). The simulation based on the measured pressure history and the flat plate boundary layer heat transfer model provides a very good match to the temporal variation of stagnation temperature at both Conditions, except towards the end of the test flow where the fully developed turbulent pipe flow heat transfer model appears more accurate. Strong mixing and hence cooling of the gas in the vicinity of the piston has been observed in previous studies of similar facilities [3, 50], so the observed general agreement with the turbulent pipe flow simulation at the end of the test time appears reasonable. The knee in the simulated temperature history based on the flat plate heat transfer model is associated with boundary layer transition, figure 6.10.

The present thermodynamic simulations track the energy in each slug of gas without modelling temperature gradients in the radial direction – the temperature of each cell is effectively a fully-mixed temperature value. A comparison between

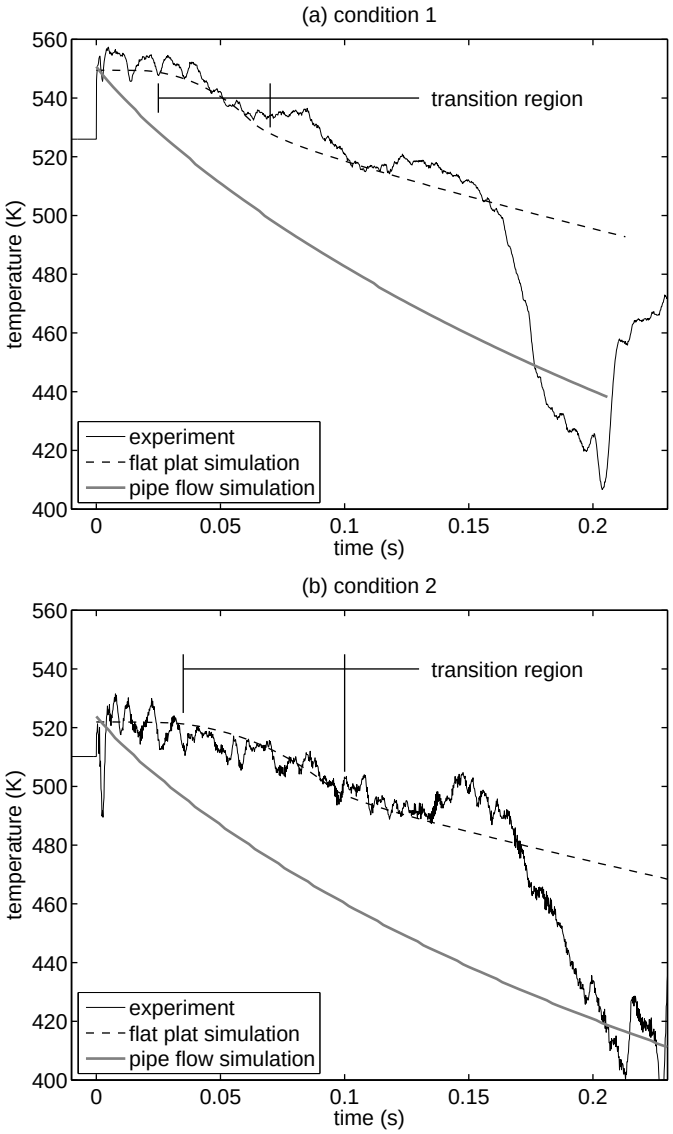

Figure 6.10: Comparison of stagnation temperature results: flat plate boundary layer model (*dashed line*), fully developed turbulent pipe flow model (*grey line*), and measurements (*solid line*) for Condition 1 (part a) and Condition 2 (part b).

the present temperature measurements and the simulations suggests that barrel heat transfer is dominated by flat plate boundary layer cooling. If this is the case, then some relatively strong mixing must have occurred between the loss of heat through flat plate boundary layer cooling and flow discharge from the nozzle because the temperature measurements were obtained at the centre of the hypersonic nozzle exit plane.

6.6 Conclusion

The temporal variation of stagnation temperature at the exit of the Mach 6 nozzle of the University of Southern Queensland's wind tunnel facility has been investigated using an aspirating tube device with a k-type butt-welded thermocouple junction. An impulse response filtering approach has been demonstrated based on a transient thermal response model for the wire and probe operation over a range of initial wire temperatures around the flow stagnation temperature value. Results demonstrate that the stagnation temperature of the flow which is initially discharged from the hypersonic nozzle is very close to the isentropic compression value. However, the flow stagnation temperature decreases with time and thermodynamic simulations accurately reflect the majority of the observed temporal variations when flat plate boundary layer cooling is used to model the heat transfer in the barrel of the wind tunnel facility.

The measured stagnation temperature in Condition 1 (which is approximately the same conditions as that used in Chapter 5) at 100 ms after the flow start is around 520 K. This temperature value is about 25 K higher than the time-constant corrected result in Chapter 5. Given the approximate nature of the correction approach adapted in Chapter 5, this is considered to be a reasonable result.

The thermodynamic simulations performed in this work are based on fully-mixed temperatures within gas slugs which span the full diameter of the barrel. Temperatures were measured on the centre line of the nozzle, but the flat plate boundary layer cooling model provides a good match to the measured temperatures for the majority of the flow duration. It is therefore concluded that significant mixing must have occurred across the diameter of barrel prior to flow discharge through the nozzle if the cooling of the gas in the barrel is dominated by boundary layer cooling effects. Strong transverse mixing within the barrel is advantageous for spatial uniformity of the test flow produced by the nozzle. Further work to quan-

tify the magnitude of the spatial gradients of temperature at the nozzle exit is described in Chapter 7.

Chapter 7

Spatial Distribution of Stagnation Temperature

7.1 Introduction

Experiments on free piston compression cold hypersonic facilities by East [50] demonstrated the existence of discrete cold fluid structures generated by the piston motion. The presence of such cold structures potentially compromise the quality of the test flow, but in the larger scale facility described by East [50], these disturbances were managed by arranging an initial axial temperature gradient within the barrel through the use of external heaters. Experiments on the similar facility at the University of Southern Queensland (the TUSQ facility) reported in chapter 6 have demonstrated that no discrete cold structures are detected on the centreline of the nozzle flow, at least for the present operating condition. An example of the East's temperature signal and temperature history signal produced by TUSQ facility can be seen in Appendix G. Nevertheless, the test flow discharged through the hypersonic nozzle decreases in temperature over the discharge period. Thermodynamic modelling suggests that heat transfer through the boundary layers on the barrel can account for the majority of the

observed temporal variations in stagnation temperature.

The possibility of spatial temperature variations at the exit of the hypersonic nozzle in the TUSQ facility is suggested because of: (1) the previous experiments in which significant thermal disturbances were observed in a similar tunnel [50]; and (2) the existence of temporal variations in flow temperature on the centre-line of the nozzle which can be explained by heat transfer in the radial direction within the barrel (chapter 6). Therefore it was considered prudent to investigate possible variations in stagnation temperature in the radial direction in an effort to understand the thermal processes within the facility, and to quantify departures from test flow uniformity which is often assumed to exist in ground-based hypersonic test flows.

The intention of the current experiments is to explore the flow stagnation temperature uniformity in the radial direction at the nozzle exit. The thermocouple probe design adopted in this chapter is similar to that used in chapter 6 except that smaller diameter thermocouple wires are used in an effort to reduce the magnitude of the necessary response time correction, thereby decreasing the uncertainty in the deduced stagnation temperature.

7.2 Operating Conditions and Probes

7.2.1 Conditions

The hypersonic facility used in present work is described in Chapter 4. Table 7.1 shows the facility operating conditions for the current experiments.

Figure 7.1 shows a representative barrel pressure history for the experiments of the current work. Once the primary valve opens, the test gas pressure within the barrel rises in an approximately linear manner due to the compression pro-

Table 7.1: Facility operating conditions.

Parameter	Unit	Value
$P_{reservoir}$	MPa	3.1 ± 0.05
P_i	kPa	93.9 ± 0.6
T_i	K	299 ± 5
P_0	MPa	0.93 ± 0.04
$T_{0,isen}$	K	575 ± 9

cess from the piston. As the pressure reaches about 950 kPa, the rupture of a Mylar diaphragm (100 μm thick) occurs, allowing the test gas to flow into the test section. The flowrate of air from the high pressure reservoir through the valve into the barrel can be arranged so that it compensates for the discharge of the test gas through the hypersonic nozzle, maintaining the nozzle stagnation pressure approximately constant. Such a situation is referred to as a 'matched' condition [3, 50].

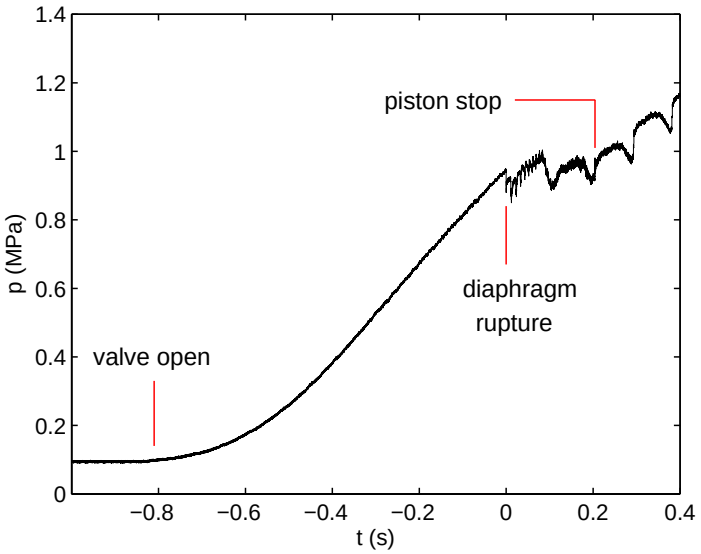

Figure 7.1: Representative barrel pressure history for the current operating condition (table 7.1).

Table 7.1 provides data on the operating conditions for the present experiments. Specified uncertainties in the initial conditions of the test gas in the barrel (P_i, T_i)

correspond to the $\pm 2\sigma$ values for the measurements. The reported stagnation pressure P_0 has been identified as the average pressure during the first 150 ms of the test flow period. Nine runs at nominally identical facility operating conditions were performed during the stagnation temperature survey work, so the stagnation pressure reported in table 7.1 is the mean results from these runs, and the quoted uncertainty is the $\pm 2\sigma$ variation for these measurements. The quoted stagnation temperature $T_{0,isen}$ is based on an isentropic calculation for compression from the initial conditions (P_i, T_i) up to the stagnation pressure (P_0) for $\gamma = 1.4$. The quoted uncertainty in this value is calculated based on the $\pm 2\sigma$ values for the measured parameters. In chapter 6 it was demonstrated that the isentropic approximation is reliable for about the first 50 ms of flow discharged from the nozzle at this operating condition.

7.2.2 Pitot Pressure Probes

A nozzle exit pitot pressure survey was performed using a pitot rake positioned 42.7 mm downstream of the Mach 6 nozzle exit. Seven piezoresistive pressure transducers (SensorTechnics BSDX2000A2R) were connected to probe bodies (figure 7.2) via short lengths of tube and these probe bodies were installed in the rake as illustrated in figure 7.3. The pitot probe locations spanned the majority of the lower radius of the Mach 6 nozzle. One probe was positioned 9.2 mm above the nozzle centreline, and then the remaining transducers were positioned at the following distances below the nozzle centreline: 10.8, 30.8, 50.8, 65.8, 80.8, 90.6 mm. Measured pitot pressures were in the vicinity of 30 kPa (absolute) so a two point, atmosphere-to-vacuum calibration of the transducers was performed.

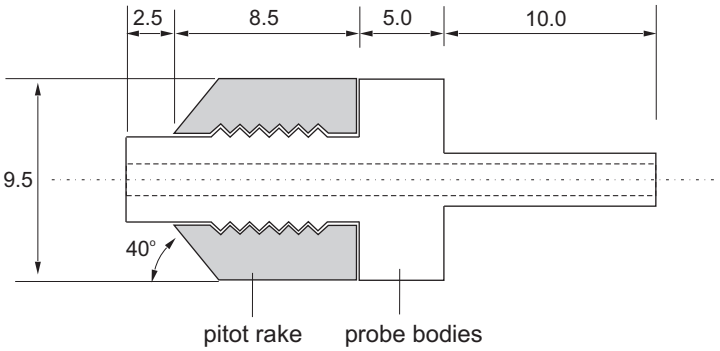

Figure 7.2: Illustration of the pitot probe arrangement with dimensions in mm.

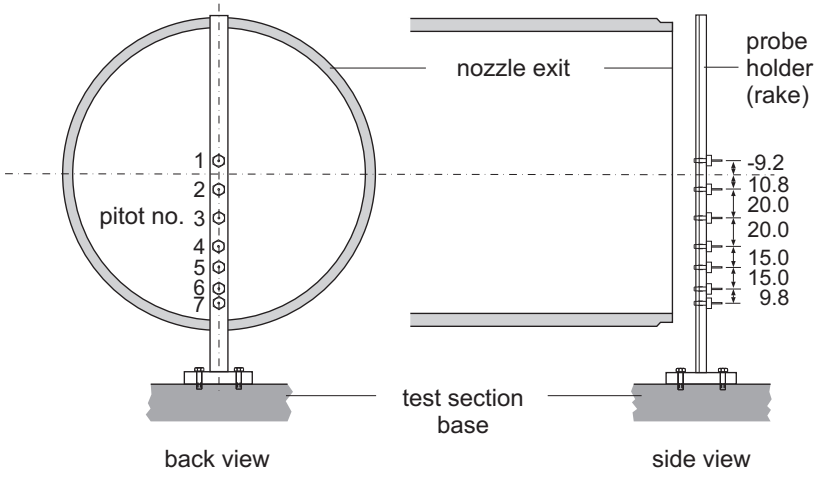

Figure 7.3: Illustration of the pitot probe rake relative to the nozzle exit with dimensions in mm.

7.2.3 Stagnation Temperature Probes

The stagnation temperature probes used in the present work were aspirating tube devices of a similar design to that used in chapter 6, except that no probe preheating was used, and a bead-welded k-type thermocouple junction with a wire diameter of 0.025 mm was used (Omega Inc.: CHAL-001). A schematic illustration of the design is presented in figure 7.4. The thermocouple used for the current work is the second-smallest bead-welded thermocouple that is commercially available from Omega Inc. Efforts were made to use the smallest diameter commercially-available bead-welded junction, 0.013 mm wire diameter (Omega Inc.: CHAL-0005), but installation and operational challenges associated with

the low wire strength were not overcome.

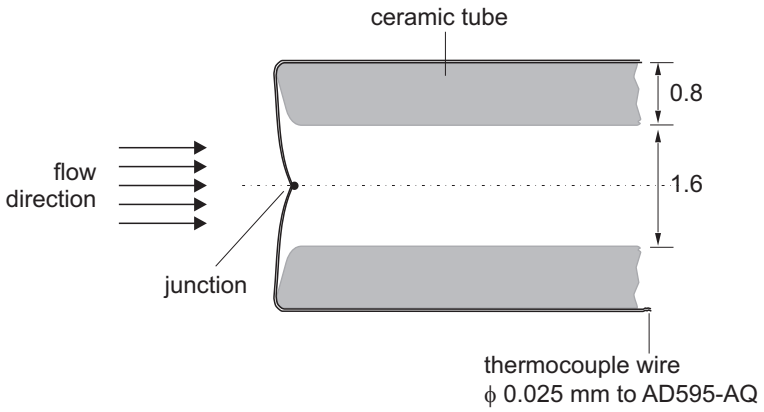

Figure 7.4: Illustration of the stagnation temperature probe arrangement with dimensions in mm.

The thermocouple wire was glued to the ceramic tube using cyanoacrylate and the junction was positioned close to the center of the tube cross-section to ensure the junction was clearly exposed to the flow, without any interference from the boundary layer development near the tube wall. For spatial resolution of nozzle exit temperature distribution, a rake consisting of 4 nominally identical probes each with the k-type bead-welded thermocouples was used, figure 7.5. Photographs of the probe rake can also be seen in Appendix C. To obtain a higher effective spatial resolution than allowed by the separation of the probes, a number of runs were performed with the rake displaced radially by around 5 mm (typically) between the runs. An AD595-AQ (9846) chip was used to amplify the thermocouple signal in each case. Calibration of the thermocouples was achieved as in chapter 6.

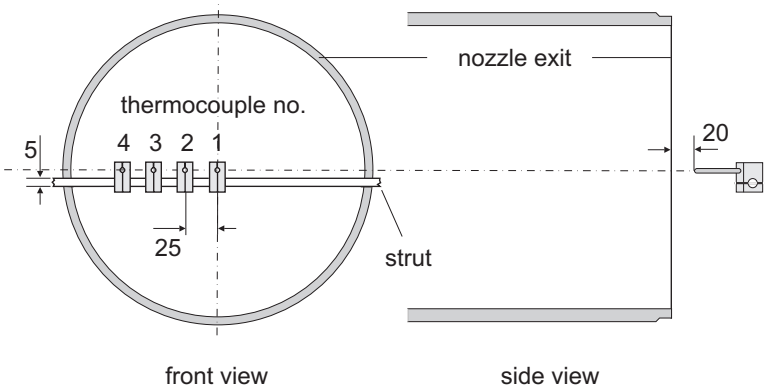

Figure 7.5: Illustration of the stagnation temperature probe rake relative to the nozzle exit with dimensions in mm.

7.3 Result and Discussion

7.3.1 Pitot Pressure Results

Representative pitot pressure results – the average of measurements obtained from the 6 probes within the nozzle core flow (up to a radius of approximately 80 mm) – are presented in figure 7.6. For a given Mach number and ratio of specific heats, the pitot pressure scales with flow total pressure under steady conditions, so the pitot pressure results of figure 7.6 have been normalised by the flow stagnation pressure (figure 7.1) and presented in figure 7.7. Pitot pressure and normalised pitot pressure history outside the core also can be seen in Appendix F. During the nominally steady test flow period, there are fluctuations in the stagnation pressure associated with diaphragm-opening waves and piston oscillations so it is appropriate to normalize the pitot pressure measurements in this manner in order to deduce the Mach number.

Mach number results have been deduced from the normalized form of the nozzle exit pitot pressure using $\gamma = 1.4$ and results are summarized in table 7.2 for each transducer location at different times after the start of the nozzle flow. Spatial distributions of normalized pitot pressure and Mach number at various times

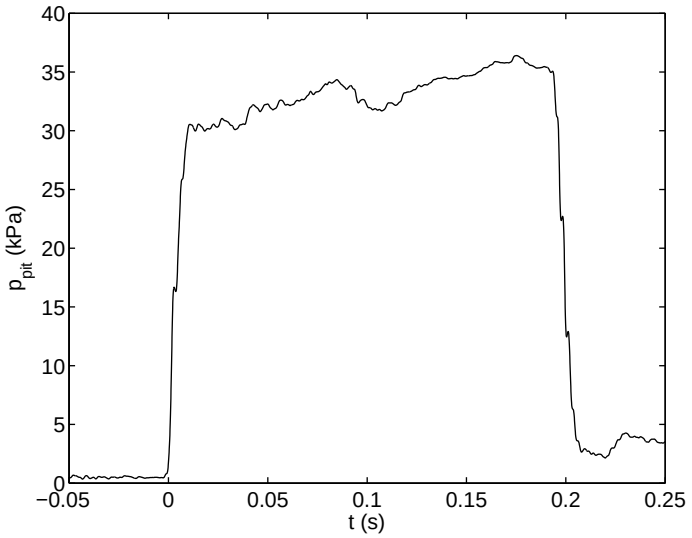

Figure 7.6: Pitot pressure history from the transducers within the nozzle core flow.

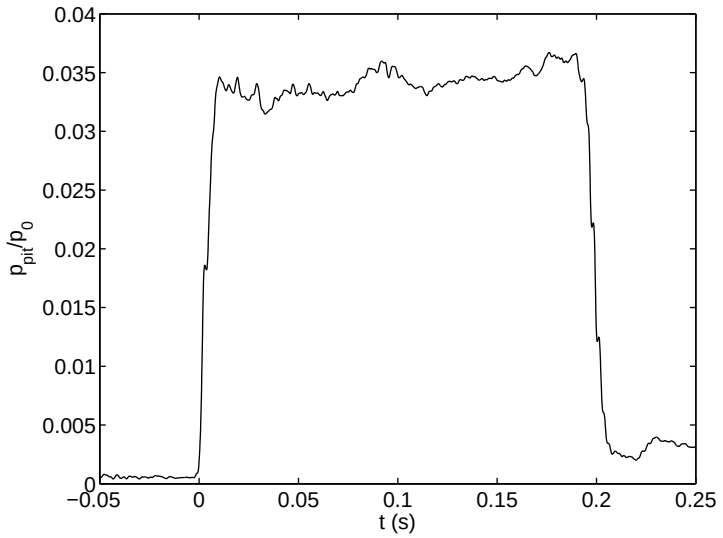

Figure 7.7: Normalized pitot pressure (p_{pit}/p_0) histories.

relative to the start of the nozzle flow are also presented in figures 7.8 and 7.9.

Results at 50 ms after flow starting demonstrate the Mach 6 nozzle has a uniform core flow with a spatial variation in normalized pitot pressure (p_{pit}/p_0) of less that $\pm 2\,\%$ over an 80.8 mm radius, with a corresponding variation in the spatial distribution of the Mach number of less than $\pm 0.5\,\%$. The change of normalized pitot pressure observed beyond the radius of 80.8 mm is attributed to the presence of the nozzle boundary layer and/or wave effects from the nozzle lip which

Table 7.2: Normalized pitot pressure measurements and calculated Mach numbers results at 50, 100 and 150 ms after flow start, each result averaged over a period of 20 ms.

		$t = 50$ ms		$t = 100$ ms		$t = 150$ ms	
	y (mm)	p_{pit}/p_0	M	p_{pit}/p_0	M	p_{pit}/p_0	M
1	-9.2	0.0332	5.8373	0.0345	5.7828	0.0338	5.8131
2	10.8	0.0331	5.8415	0.0349	5.7672	0.0338	5.8122
3	30.8	0.0327	5.8610	0.0348	5.7731	0.0339	5.8091
4	50.8	0.0337	5.8175	0.0358	5.7345	0.0353	5.7534
5	65.8	0.0330	5.8458	0.0350	5.7662	0.0346	5.7800
6	80.8	0.0329	5.8526	0.0355	5.7445	0.0349	5.7670
7	90.6	0.0253	6.2352	0.0280	6.0810	0.0334	5.8287
mean_{1-6}		0.0331	5.84	0.0351	5.76	0.0344	5.79
$\max_{1-6}$		+1.8 %	+0.32 %	+1.9 %	+0.37 %	+2.6 %	+0.41 %
$\min_{1-6}$		–1.3 %	–0.43 %	–1.5 %	–0.46 %	–1.7 %	–0.62 %

can arise due to a difference in the static pressure between that of the hypersonic nozzle flow and that of the test section surrounding the hypersonic free jet. Throughout the period of the test flow, the normalized pitot pressures tend to increase slightly with time and hence Mach numbers tend to decrease slightly with time. Spatial variations in the pitot pressure distribution increase slightly with time, and consequently, spatial variations in the Mach number distribution likewise increase slightly with time.

7.3.2 Stagnation Temperature Results

The intention of using the relatively small bead-welded junction thermocouple was to obtain a sufficiently short response time so as to avoid having to implement a response time correction in deducing flow stagnation temperature. A comparison of the flow stagnation temperature obtained from the response-time corrected, butt-welded thermocouple results described in chapter 6 and the temperature obtained directly from a bead-welded junction thermocouple in this work is illus-

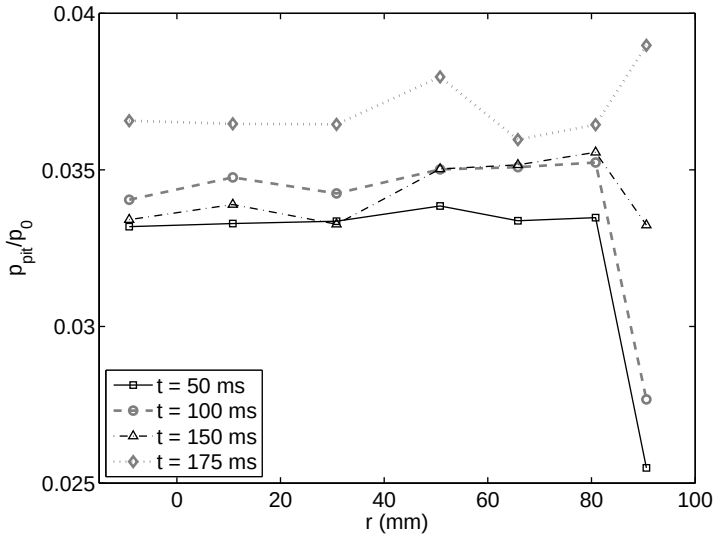

Figure 7.8: Radial distribution of the normalized pitot pressure for t = 50, 100, 150, and 175 ms.

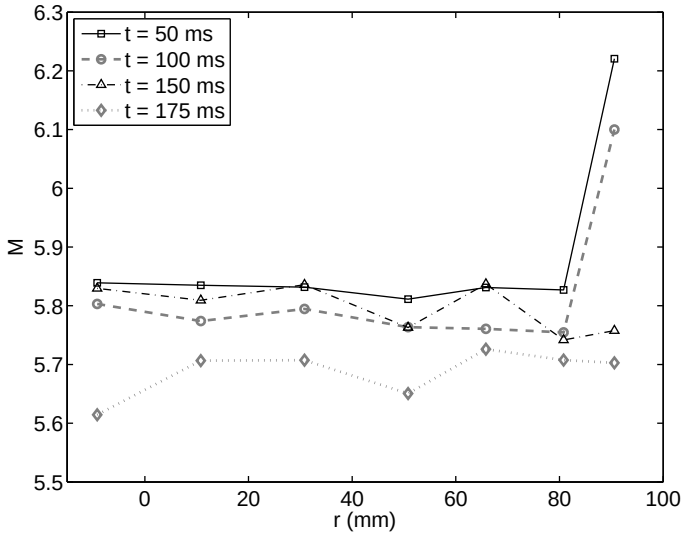

Figure 7.9: Radial distribution of the Mach number for t = 50, 100, 150, and 175 ms.

trated in figure 7.10. The bead-welded junction result presented in figure 7.10 was obtained from the probe design as described in section 7.2.3 and demonstrates a 10-90 % rise time of less than 20 ms. Between 2 and 4 of the thermocouple probes successfully generated data within each of the 9 facility runs performed for the stagnation temperature survey in this work. Over this campaign, 2 thermocouple wire breakages occurred.

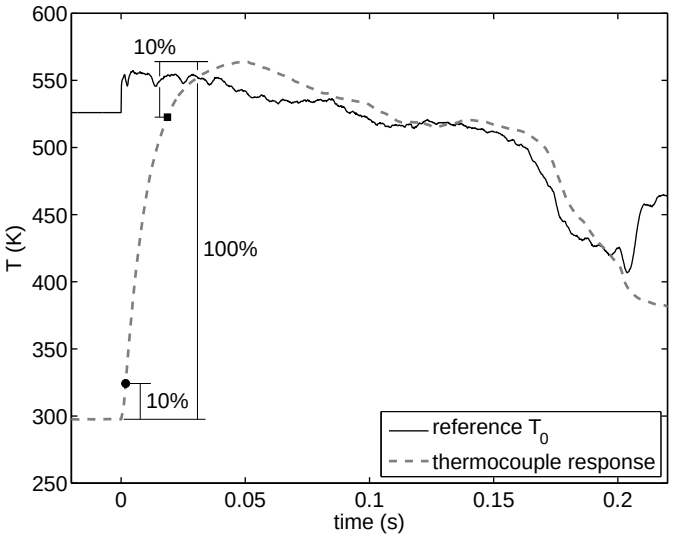

Figure 7.10: Comparison of the stagnation temperature deduced via response-time correction of a butt-welded thermocouple (solid line labelled 'reference T_0') from chapter 6 and a signal from a representative bead-welded junction thermocouple used in the present work (broken line labelled 'thermocouple response').

Results from the thermocouple probes at the different radial locations were compiled and selected results at times after the start of flow of 50, 100, 150, and 175 ms have been presented in figure 7.11. For nozzle radii $r \leq 80$ mm, variations of stagnation temperature of ± 20 K are indicated. For nozzle radii $r > 80$ mm, the stagnation temperature decreased rapidly, indicative of the presence of the nozzle boundary layer in this region, and consistent with the pitot pressure survey results of figure 7.8.

7.3.3 Turbulent Pipe Flow Model

Thermodynamic simulations reported in chapter 6 suggest that rapid mixing of the test gas occurs within the barrel after the compression process. A fully-developed turbulent pipe flow heat transfer correlation used in the simulations demonstrated a reasonable level of agreement with stagnation temperature measured on the centre line of the nozzle exit but only towards the end of the test

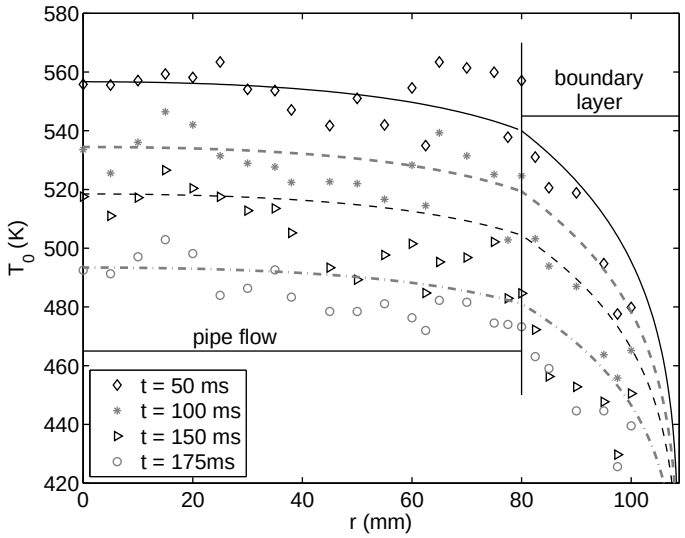

Figure 7.11: Variation of flow stagnation temperature measurements with radius across the nozzle exit for $t = 50\,\text{ms}$ ($\diamond$), $100\,\text{ms}$ ($*$), $150\,\text{ms}$ ($\triangleright$), and $175\,\text{ms}$ ($\circ$) relative to the flow start. Lines within the region $r < 80\,\text{mm}$ represent the stagnation temperature distribution associated with a supposed fully developed turbulent pipe flow within the barrel. Lines for the region $r > 80\,\text{mm}$ represent the stagnation temperature variations within the Mach 6 nozzle flow boundary layer based on an assumed 1/7th power-law velocity profile and a temperature variation according to the Crocco-Busemann relation.

time. If mixing within the barrel approaches something like fully-developed turbulent pipe flow during some parts of the compression and discharge processes, then a spatial variation in flow stagnation temperature at the nozzle exit might be modelled reasonably well using the temperature distributions observed in fully-developed turbulent pipe flow experiments. This is because the temperature distribution which is present in the incompressible barrel flow region close to the nozzle inlet will effectively be 'frozen' into the flow since there is insufficient time during the flow transit through the hypersonic nozzle for further mixing to occur.

In the present case, the flow transit time from the nozzle inlet to the nozzle exit is approximately 2 ms. The turbulent thermal conductivity k_t in the nozzle inlet region within the barrel is estimated on the assumption of fully-developed turbulent pipe flow in this region as $13.4\,\text{W/mK}$. This value is obtained by equations

suggested by Mills [103]

$$k_t = \varepsilon_M \rho c_p \mathrm{Pr}_t \tag{7.1}$$

where ε_M is eddy diffusivity of momentum which can be obtained from an expression for the core proposed by Hinze [116] as

$$\frac{\varepsilon_M}{\nu} = 0.035\sqrt{\frac{f}{8}}\mathrm{Re}_D \tag{7.2}$$

where ν is the kinematic viscosity. Hence an effective (turbulent) diffusivity can be estimated using

$$\alpha_t = \frac{k_t}{\rho c_p} \tag{7.3}$$

The estimated value for stagnation conditions is $\alpha_t = 2.3$ x $10^{-3}\,\mathrm{m}^2/\mathrm{s}$ and hence the transverse thermal penetration distance during the nozzle transit time is estimated to be around 2.2 mm – a small fraction of the radius of the nozzle.

A model base on the temperature law of the wall (TLW) for a fully-developed turbulent pipe flow as presented by Mills [103] has been used to assess the observed stagnation temperature gradients at the nozzle exit. Quantities necessary for the adopted version of TLW include the heat flux at the wall Q_w which is obtained according to

$$Q_w = h\,(T_0 - T_w) \tag{7.4}$$

where h is the convective heat transfer coefficient, T_0 is the initial stagnation temperature and T_w is the wall temperature. The convective heat transfer coefficient

is obtained from the pipe-flow correlation

$$h = \frac{\mathrm{Nu}\, k}{D} \tag{7.5}$$

where Nu is the Nusselt number, k is the thermal conductivity, and D is diameter of the pipe. For thermally fully developed flow in a smooth tube with Prandtl number $\mathrm{Pr} > 0.5$, Gnielinski's formula is recommended by Mills [103] for calculation of the Nusselt number

$$\mathrm{Nu} = \frac{(f/8)(\mathrm{Re} - 1000)\mathrm{Pr}}{1 + 12.7(f/8)^{1/2}(\mathrm{Pr}^{2/3} - 1)} \tag{7.6}$$

which can be applied for $3000 < \mathrm{Re} < 10^6$. This in turn, depends on the friction factor, which can be obtained from Petukhov's formula

$$f = \frac{1}{(0.790 \ln(\mathrm{Re}) - 1.64)^2} \tag{7.7}$$

which applies for $10^4 < \mathrm{Re} \leq 5 \times 10^6$.

The pipe flow Reynolds number used in the friction factor equation is defined as

$$\mathrm{Re} = \frac{\rho u D}{\mu} \tag{7.8}$$

where ρ is density, u is flow velocity, μ is dynamic viscosity of the gas. The flow velocity used in this definition is the bulk flow velocity within the barrel during the test flow discharge from the hypersonic nozzle.

The TLW can then be expressed in non-dimensional form as

$$T^+ = \mathrm{Pr}\, y^+ \quad \text{if} \quad 0 < y^+ \leq 5 \tag{7.9}$$

$$T^+ = 5\,\mathrm{Pr} + 5\ln\left[\mathrm{Pr}\left(\frac{y^+}{5} - 1\right) + 1\right] \quad \text{if} \quad 5 < y^+ \leq 30 \tag{7.10}$$

$$T^+ - T^+\big|_{y^+=30} = \frac{\mathrm{Pr}_t}{0.4}\left[\ln\left(\frac{y^+}{30}\right) - \left(\frac{y^+ - 30}{R^+}\right)\right] \quad \text{if} \quad y^+ > 30 \tag{7.11}$$

The turbulent Prandtl number is taken as $\mathrm{Pr}_t = 0.9$ in the present work, and the dimensionless variables R^+, y^+, and T^+ are defined as

$$R^+ = \frac{u_\tau R}{\nu} \tag{7.12}$$

$$y^+ = \frac{y u_\tau}{\nu} \tag{7.13}$$

$$T^+ = \frac{(T_w - T)\rho c_p u_\tau}{Q_w} \tag{7.14}$$

where R is radius of the pipe (the barrel in this case), and y distance from the wall. The friction velocity u_τ appears in each of the dimensionless variables used in the TLW (Equations 7.12, 7.13 to 7.14) and is defined as

$$u_\tau = \sqrt{\frac{\tau_s}{\rho}} \tag{7.15}$$

where τ_s is wall shear stress which can be obtained from equation

$$\tau_s = \frac{f}{8}\frac{1}{\rho u^2} \tag{7.16}$$

Results from the fully developed turbulent pipe flow model described above are included in figure 7.11 at the four different times specified relative to the start of

the flow. The model was applied by taking the stagnation temperature measured on the nozzle centre line as the bulk temperature of the flow upstream of the nozzle throat, and the measured stagnation pressure of 0.93 MPa (table 7.1) was also applied. These conditions were combined with the nozzle throat diameter to give the mass flow rate from the barrel, which in turn yielded the bulk flow velocity within the barrel, from which deduction of Reynolds numbers and the other necessary parameters is then a trivial exercise. For the pipe flow stagnation temperature model results in figure 7.11, the radial distances have been scaled up by the ratio of the nozzle exit radius to the barrel radius, reflecting the assumption that spatial distributions of stagnation temperature do not alter during the flow transit through the nozzle.

The measured stagnation temperature results presented in figure 7.11 for $r \leq 80\,\text{mm}$ demonstrate an overall decrease in stagnation temperature with distance from the nozzle centre line, although local variations are also present. The origin of the overall decreasing stagnation temperature effect for $r \leq 80\,\text{mm}$ is almost certainly the heat transfer from the test gas while it is residing in the barrel. The fully-developed turbulent pipe flow model seemingly offers a degree of explanation here – the model certainly simulates a decrease in the stagnation temperature with distance from the nozzle centre line. However, the coefficient of determination (R^2) values for the pipe flow model results presented in figure 7.11 are around -0.2, which suggests that the overall fit to the experimental data is worse than simply taking the average of all the data within the region $r \leq 80\,\text{mm}$.

7.3.4 Nozzle Boundary Layer Model

In figure 7.11 for the region $r > 80\,\text{mm}$, the fully-developed turbulent pipe flow model is not shown. Instead, a stagnation temperature distribution based on the Crocco-Busemann approximation is presented since in this region, the presence of the nozzle boundary layer is detected. The Crocco-Busemann approximation

[117] relates the boundary layer temperature distribution to the velocity profile according to

$$T_0 \;=\; T_w + (T_{aw} - T_w)\,\frac{u}{u_\infty} \;+\; (1 \;-\; r)\,\frac{u^2}{2c_p} \tag{7.17}$$

where T_0 is stagnation temperature within the boundary layer, T_w is the wall temperature, and T_{aw} is the adiabatic wall temperature given by

$$T_{aw} = T_s + r\frac{u_\infty^2}{2c_p} \tag{7.18}$$

where T_s is the static temperature at the edge of the boundary layer, r is the recovery factor, and u_∞ is the velocity at the edge of the boundary layer. In the present work the recovery factor is taken as $r = \mathrm{Pr}_t^{1/3} \approx 0.88$ since a turbulent boundary layer is considered. The velocity profile within the turbulent boundary layer u is assumed to follow a 1/7th power law,

$$\frac{u}{u_\infty} = \left(\frac{y}{\delta}\right)^{\frac{1}{7}} \tag{7.19}$$

where y is the distance from the wall, and δ is the boundary layer thickness.

Results from the present model for the stagnation temperature within the nozzle boundary layer are presented in figure 7.11 as the solid and broken lines in the region $r > 80\,\mathrm{mm}$. The model uses the TLW value for stagnation temperature at the location $r = 80\,\mathrm{mm}$ and this location is specified as the edge of the boundary layer and u_∞ at this point is determined on the assumption that the Mach number here is 5.8, consistent with the value identified from the pitot pressure measurements. The Crocco-Busemann profile is observed to over-estimate the stagnation temperature values, but it does provide a closer approximation of the distribution in the boundary layer region than the TLW model.

7.3.5 Temperature Gradients and Core Flow Identification

Deficiencies in the fully-developed turbulent pipe flow model and in the Crocco-Busemann approximation with the 1/7th power-law velocity profile have been noted in sections 7.3.3 and 7.3.4. Therefore in this section, a linear, least-squares error model has been adopted for the distribution of stagnation temperature in the core flow and in the boundary layer region respectively, as illustrated in figure 7.12. Two straight-line fit regions have been identified: the first for locations $r \leq 80\,\text{mm}$, and the second for locations $r \geq 80\,\text{mm}$. The intersection of the two lines is designated as the edge of the nozzle core flow, the edge of the nozzle boundary layer.

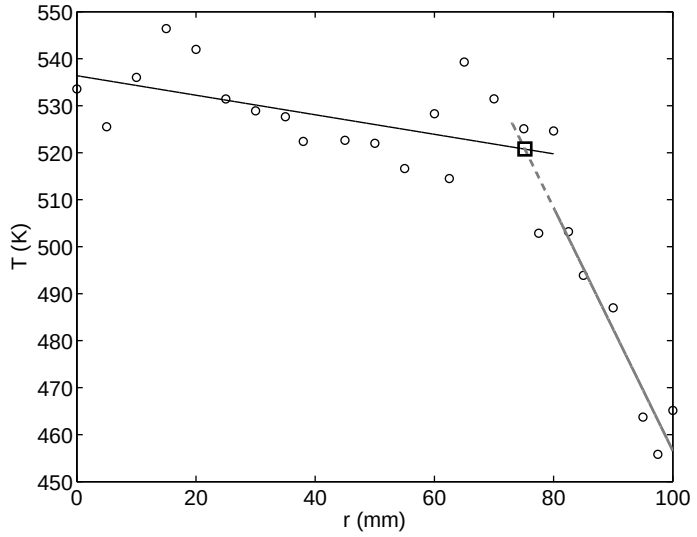

Figure 7.12: Illustration of the linear regression analysis for the spatial distribution of stagnation temperatures for the case of $t = 100\,\text{ms}$ from the flow start. Two lines are used: one for $r \leq 80\,\text{mm}$; the other for $r > 80\,\text{mm}$. The point of intersection of these two lines (□) is taken to indicate the extent of the nozzle core flow.

Results from the analysis of the spatial distribution of stagnation temperature for the identification of the nozzle core flow are presented as the solid line in figure 7.13 as a function of time relative to the start of the test flow. The extent of the nozzle core flow as identified from the pitot pressure survey are also shown

in figure 7.13 – in this case, symbols are presented with error bars indicating that the pitot pressure survey revealed the core flow to be essentially uniform up to at least $r = 80\,\text{mm}$, but that the next measurement location at $r = 90\,\text{mm}$ was within the nozzle boundary layer region. Core flow radii deduced from the pitot pressure survey are slightly larger than those deduced using the stagnation temperature survey – the two sets of results are generally within about 10 mm using the different methods, except for the flow period between about 0.11 and 0.17 s.

Nozzle core flow results from the analysis of the nozzle exit Mach number history are also presented in figure 7.13. The Mach number history was itself derived from the pitot pressure, but for the present analysis, the geometric area ratio of the nozzle was used in combination with the Mach number deduced from the pitot pressure in order to determine the displacement thickness of the nozzle boundary layers at the exit plane. To deduce the core flow radius, the full boundary layer thickness is needed. This value was deduced from the displacement thickness on the assumption that the density variation within the compressible turbulent boundary layer at the nozzle exit was related to the local velocity within the boundary layer according to the Crocco-Busemann relationship (Section 7.3.4), and a 1/7th power-law velocity profile was again assumed in this case. The size of the core flow deduced in this manner is consistent with the pitot pressure survey results but is somewhat larger than the size of the core flow deduced from the stagnation temperature measurements.

Figure 7.14 presents the variation of the average gradient of stagnation temperature within the core flow as a function of time as deduced from the linear least-squares error model. Also shown on this figure is the stagnation temperature gradient deduced from the fully-developed turbulent pipe flow model discussed in section 7.3.3. In this case the temperature gradient within the core flow is approximated as the difference in temperature between the location $r = 80\,\text{mm}$ and $r = 0\,\text{mm}$ divided by the distance 80 mm. While the fully-developed turbu-

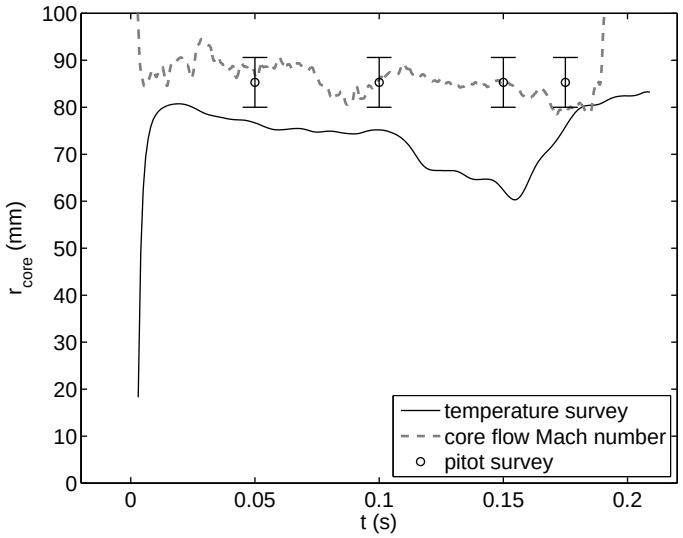

Figure 7.13: Core flow radius deduced from stagnation temperature survey, from the Mach number history, and from the pitot pressure survey.

lent pipe flow model provides a reasonable order-of-magnitude estimate for the temperature gradients observed in the experiments, it is unable to simulate the observed temporal variation of the temperature gradient with any fidelity.

The spatial gradient of stagnation temperature determined from the experimental data remains close to zero for about the first 20 to 30 ms, figure 7.14. This result is consistent with previous observations presented in chapter 6 which have demonstrated that during this period of time, the nozzle exit stagnation temperature is in close agreement with the isentropic value deduced from the measured pressure ratio. The magnitude of the spatial gradient of stagnation temperature then increases with time, reaching a value of around $-0.45\,\mathrm{K/mm}$ at a time of about 150 ms from the start of the flow discharge. For times after 160 ms, the flow stagnation temperature decreases rapidly (see figure 7.10) and the magnitude of the spatial gradient for stagnation temperature also decreases rapidly during this period, figure 7.14.

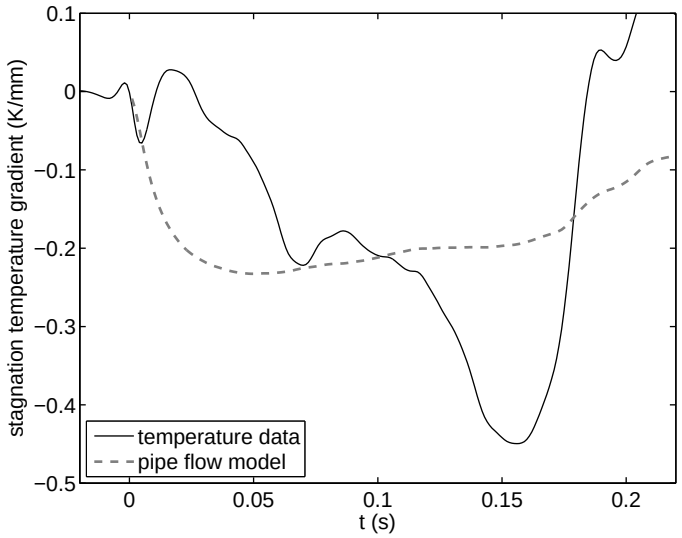

Figure 7.14: Spatial gradient of stagnation temperature across the core flow based on linear least-squares error for the stagnation temperature data (solid line). Results from the fully developed turbulent pipe flow model are also presented (broken line) for comparison.

7.4 Conclusion

Previous measurements of stagnation temperature at the centre line of the nozzle exit plane in the present facility demonstrated the presence of a cooling effect which was successfully modelled using engineering correlations for the heat transfer from the test gas to the barrel during the free piston compression and test gas discharge processes (chapter 6). Test gas cooling within the barrel implies the presence of temperature gradients in the radial direction. The present work was undertaken to investigate the magnitude of the non-uniformity in the stagnation temperature and other flow parameters near the exit plane of the hypersonic nozzle.

For the present facility operating conditions, pitot pressure measurements at the exit of the Mach 6 nozzle indicate core flow uniformity to within 2 % and a core flow radius of at least 80 mm for the majority of the test flow duration of around 200 ms. Mach number profiles deduced from the pitot pressure measurements are

likewise uniform with a Mach number of 5.81 ± 0.05 for the majority of the test flow duration.

Stagnation temperature probes consisting of 0.025 mm diameter bead-welded k-type thermocouples located near the inlet of a ceramic tubes have been used to measure the stagnation temperature distribution at the nozzle exit. Profiles of stagnation temperature measured at the nozzle exit have a peak temperature near the nozzle centreline, reflecting the heat transfer from the test gas to the barrel which occurs during the piston compression and discharge process. The hypersonic nozzle boundary layer is also distinguished by the the stagnation temperature measurements.

The stagnation temperature measurements indicated a core flow region of almost 80 mm radius near the start of the test flow, consistent with that derived from the pitot pressure measurements. A decrease in the available core flow radius was registered throughout the majority of the test flow according to the stagnation temperature measurements. The average spatial gradient of stagnation temperature within the core flow region was essentially zero for the first 30 ms of the test flow and this result in consistent with those of chapter 6 in which it was found that the initial flow discharge from the nozzle had a stagnation temperature very close to the isentropic compression value. The maximum average spatial gradient of stagnation temperature was registered at about 150 ms after the start of the test flow and had a value of approximately $-0.45\,\mathrm{K/mm}$, indicating an average drop in stagnation temperature of about 20 K over the core flow region at this time.

Similar measurements in other facilities indicated the existence of a discrete, large-scale thermal disturbances which propagated ahead of the piston and potentially compromised the test flow quality [50], but no such disturbances were identified in chapter 6 at the centre line of the nozzle exit, and such discrete disturbances have not been detected at any radial location explored in the present work.

Chapter 8

Thin Film Heat Flux Probe

8.1 Introduction

Transient thin film heat flux gauges have been used in various hypersonic flow wind tunnels for many decades. A comprehensive outline of the use of such gauges was presented by Schultz and Jones [93], and other experiments relating to the use of thin film heat flux gauges have been described in section 2.4. Thin film gauges have advantages over hot wire devices and thermocouples in that they are rugged and have a fast response. A typical thin film heat flux gauge can provide a high bandwidth signal of around 100 kHz [49, 96].

The intention of the current work is to identify stagnation point heat flux, stagnation temperature, and ideally stagnation temperature fluctuations at the nozzle exit of the TUSQ facility through the implementation of the thin film heat flux gauge technique. Buttsworth and Jones [49] have identified stagnation temperature fluctuations in the Oxford University Gun Tunnel (OUGT) at a particular operating condition with carbon dioxide as the test gas. The results from the OUGT facility indicated stagnation temperature fluctuations of about 2.3 K (RMS) and it was concluded that such fluctuations are primarily due to fluctu-

ations in entropy, based on comparison with pitot pressure fluctuation measurements. The OUGT facility is similar to the TUSQ facility, however, it would be useful to have actual temperature fluctuation data for the TUSQ facility because of the differences in facility size and operation.

8.2 Operating Conditions and Probes

8.2.1 Operating Condition

The facility operating condition used in the current work is the same as that described in chapter 7, section 7.2. A typical barrel pressure history representative of the current experiment is also presented in that section. Measurements with the heat flux probe and the aspirating thermocouple probes of chapter 7 were obtained simultaneously: the thin film heat flux probe was attached on the same support rod as the thermocouple probes.

8.2.2 Thin Film Gauges

For the current experiments, a thin film heat flux probe was used to obtain the surface temperature history near its stagnation point. The probe consisted of platinum film painted onto the rounded end of 3 mm diameter fused quartz rod. The length of the active film was around 1 mm. For electrical connection to the film, gold leads were also painted onto either side of the quartz to obtain low resistance electrical leads. The probe was placed at around 20 mm downstream from the nozzle exit on the centre line of the nozzle flow. An illustration of the probe and its arrangement is presented in figure 8.1.

A constant current mode of operation was used with the thin film in order to obtain electrical resistance as a function of temperature. In such a mode, the

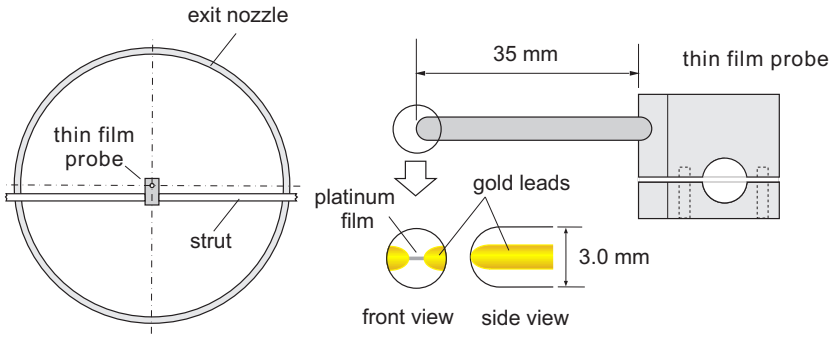

Figure 8.1: Illustration of the thin film probe and its arrangement, dimensions in mm.

change of measured voltage E - E_0 is related to the temperature as

$$E - E_0 = i(R - R_0) = E_0\alpha_0(T - T_0) \tag{8.1}$$

where i is the constant current through the film, R is the film resistance, α is the film temperature coefficient of resistance, E is the film voltage and T is the temperature. The subscript 0 refers to the reference condition. In the experiments, the thin film was operated in conjunction with an 8-pin monolithic differential amplifier INA105 to obtain amplification and precision output. The circuit diagram of the thin film gauge power supply and amplifier used in the current experiment is presented in Appendix A.

8.2.3 Calibrations

To obtain the temperature-resistance characteristics of the sensor, a calibration over the operating temperature range of the experiment was performed. Calibrations were performed in a temperature controlled water bath within the range of 23 to 70 °C, and also in a thermos in which water initially at around 90 °C was allowed to slowly cool towards ambient temperature. In the case of the thermos calibration, a Matlab script was used to automatically record the output signal of

the film as the hot water in the thermos cooled over a period of about 12 hours. In both cases calibrations were carried out with a reference to a platinum resistance temperature detector (RTD) with a nominal resistance of 100 Ohm from Omega Corporation (model 2PT100KN3045). The temperature reading from the Platinum RTD was obtained using a temperature monitor, also provided by Omega Corporation (model CYD211). Both the thin film probe and the Platinum RTD were positioned close together within the thermos during the calibration process. The outputs of both calibrations were in the form of film voltage as a function of temperature.

To convert the calibration output into a temperature-resistance relation which can be useful in tracking permanent resistance changes of the film at ambient temperature, it is necessary to identify the resistance-voltage characteristics of the amplifier circuit. So, the second step of calibrations involved a characterisation of the amplifier by utilizing a digital multimeter Protex 608 and a Vishay Spectrol Precision Potentiometer 1047 MEX model 535 to provide a variable resistance input. The resistance-voltage characteristics of the amplifier used for current experiments is presented in figure 8.2.

Figure 8.3 provides the data and the curve fit for the calibration presented in terms of normalised resistance as a function of temperature. A line following an equation of the form

$$\frac{R_{film}}{R_{0,film}} = a.T_{film} + b \tag{8.2}$$

was fitted to the calibration data. The terms T_{film} and R_{film} are the film temperature and resistance respectively, $R_{0,film}$ is the resistance of the film at the reference temperature of 20 °C. The line fit parameters identified from a least-squares analysis were $a = 25{\times}10^{-4}\,{}^{\circ}\mathrm{C}^{-1}$ and $b = 0.95$. The thin film resistance without any extension leads was measured and it was deduced that the resistance of the extension leads, R_{lead}, was equal to 1.66 Ohm during the calibrations.

A summary of the conditions of the thin film during the sequence of runs is listed

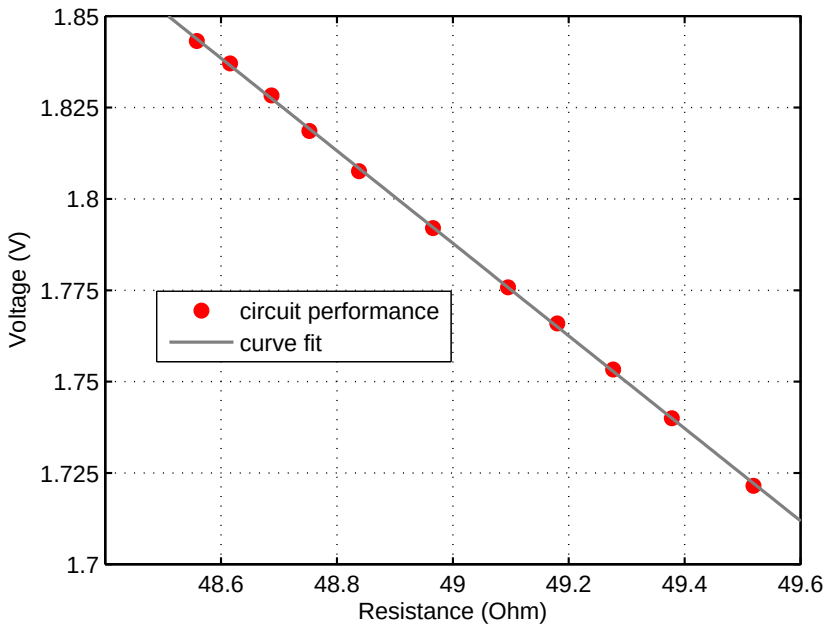

Figure 8.2: Voltage-resistance characteristics of the thin-film supply and amplifier used in the current experiment.

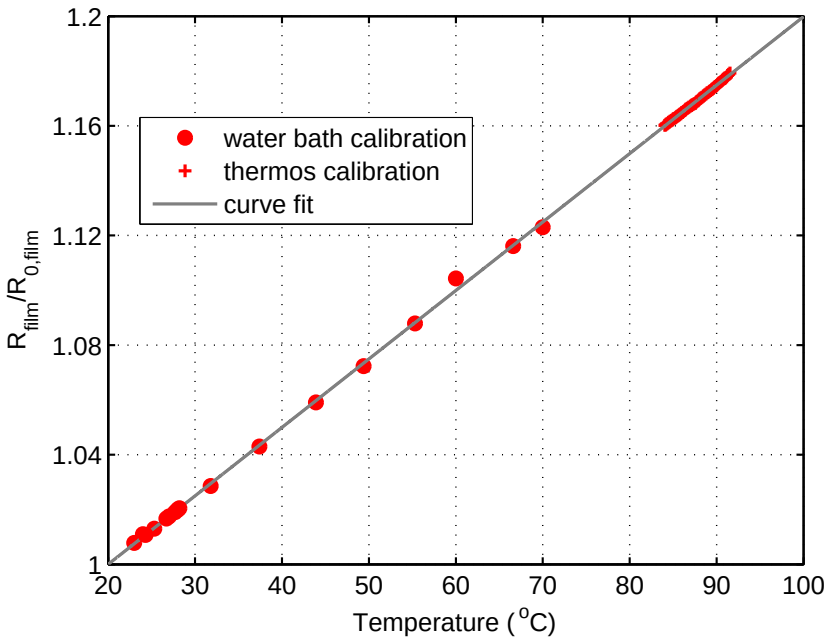

Figure 8.3: Temperature-resistance calibration for thin film.

in table 8.1. The film resistance tended to increase with time, over the successive runs (consider the R_0 values presented in table 8.1). This may be attributed to

wear on the film due to suspended particles in the flow [118].

Table 8.1: Thin film conditions over seven runs

run	T_{fi} [a]	V_i [b]	R_i [c]	T_{amb}	$R_{f,amb}$ [d]	$\frac{R_{f,amb}}{R_0}$	R_0
171	27.0	3.02	39.28	26 ± 2	37.62	1.02	36.97
172	26.7	2.68	41.99	26.7	40.33	1.02	39.67
173	28.0	2.69	41.86	28.0	40.20	1.02	39.41
174	28.0	2.59	42.68	28 ± 0.5	41.02	1.02	40.22
175	28.2	2.45	43.78	28.2	42.12	1.02	41.27
176	28.0	2.14	46.22	28 ± 0.5	42.43	1.02	41.60
177	24.3	2.42	43.99	24.3	42.33	1.01	41.88

[a] initial temperature of film in each run
[b] initial voltage of film in each run
[c] initial resistance in film each run
[d] resistance of film at ambient temperature, $R_i - R_{lead}$

8.3 Heat Transfer Coefficient Correlation

The heat flux at the stagnation point of the thin film heat flux gauge can be determined using an equation of

$$q = h\,(T_0 - T_w) \tag{8.3}$$

where q is the heat flux, h is the heat transfer coefficient, T_0 is the flow stagnation temperature, and T_w is the wall temperature which in this case is considered as being the surface temperature measured by the film.

The parameter h in equation 8.3 is a property of stagnation point boundary layer that has to be estimated in order to identify the heat flux for given flow and probe conditions. The total temperature of the flow remains constant even though a normal shock wave is formed ahead of the probe, whereas pitot measurements in the supersonic flow is significantly lower than the flow total pressure in such situations.

In the case of a spherical-tipped probe, the stagnation point heat transfer co-

efficient can be expressed in the form of Nusselt number as described in White [117]

$$\mathrm{Nu} = 0.763\mathrm{Pr}^{0.4}\mathrm{Re}^{0.5}C^{0.1}\left(\frac{KD}{u_\infty}\right)^{0.5} \tag{8.4}$$

where,

$$\mathrm{Nu} = \frac{hD}{k_e} \tag{8.5}$$

$$\mathrm{Pr} = \frac{c_p\mu_e}{k_e} \tag{8.6}$$

$$\mathrm{Re} = \frac{\rho_e\mu_\infty D}{\mu_e} \tag{8.7}$$

$$K = \frac{\mathrm{d}u_e}{\mathrm{d}x} \tag{8.8}$$

$$C = \frac{\rho_w\mu_w}{\rho_e\mu_e}. \tag{8.9}$$

Pitot pressure measurements can be related to equation 8.4 by the application of the sequence of equations below,

$$\rho_e = \frac{p_e}{RT_e} = \frac{p_{pit}}{RT_0}. \tag{8.10}$$

with the Mach number of the freestream flow defined as

$$M_\infty = \frac{u_\infty}{(\gamma RT_\infty)^{0.5}} \tag{8.11}$$

and

$$R = \frac{\gamma - 1}{\gamma} c_p. \tag{8.12}$$

Following Buttsworth and Jones [95], with use of the equations (8.10), (8.11), and (8.12), the heat transfer coefficient in equations (8.4) can be rearranged into the form

$$h = 0.763 D^{-0.5} f\left(M_\infty, \gamma\right) f\left(\text{thermophysical properties}\right) p_{pit}^{0.5} \tag{8.13}$$

where

$$f\left(M_\infty, \gamma\right) = \gamma^{0.5} \left(\gamma - 1\right)^{-0.25} \left(M\right)^{0.5} \left(\frac{T_\infty}{T_0}\right)^{0.25} \left(\frac{KD}{u_\infty}\right)^{0.5} \tag{8.14}$$

and

$$f\left(\text{thermophysical properties}\right) = c_p^{0.15} k_e^{0.6} \mu_e^{-0.1} C^{0.1} T_0^{-0.25} \tag{8.15}$$

8.4 Temperature fluctuations analysis

As shown by Buttsworth and Jones [49], equation 8.3 can be expanded in terms of time-averaged and small fluctuating components to give the expression

$$\frac{q'}{q} = \frac{h'}{h} + \frac{T_0'}{T_0 - T_w} - \frac{T_w'}{T_0 - T_w} + \frac{h'(T_0' - T_w')}{h(T_0 - T_w)} \tag{8.16}$$

where the prime ($'$) denotes fluctuating components and the other (non-prime) symbols indicate time averaged values. The magnitude of temperature fluctua-

tions in surface temperature and heat flux are related in the frequency domain and can be described as

$$\frac{|T'_w|}{|q'|} = \frac{1}{\sqrt{\omega}\sqrt{\rho c k}} \tag{8.17}$$

where ω is the angular frequency and ρ, c, k are the density, specific heat, and conductivity of the thin film respectively. Buttsworth and Jones [49] stated that for conditions where the second term on he right side of equation 8.16 has a contribution of less than 2 %, it is reasonable to neglect the third term and as the last term of equation 8.16 is second order, it is can also be neglected. So the equation 8.16 reduces to

$$\frac{q'}{q} = \frac{h'}{h} + \frac{T'_0}{T_0 - T_w} \tag{8.18}$$

From equation 8.18 and 8.3, it can be seen that when $T_w \approx T_0$, the fluctuations in heat flux are primarily due to stagnation temperature fluctuations and the two fluctuating quantities are related through the time averaged heat transfer coefficient according to

$$T'_0 = q'/h \tag{8.19}$$

8.5 Results and discussion

8.5.1 Heat Flux and Stagnation Temperature

A typical surface temperature history from the probe in the TUSQ test flow is shown in figure 8.4. The temperature is observed to increase in an approximately parabolic manner at the start of the flow, and to reach a maximum temperature

of about 365.5 K at approximately 170 ms after the flow start.

The heat flux result in figure 8.5 was obtained by treating the surface temperature of the probe using the semi-infinite substrate impulse response filtering techniques as described in [111]. To apply the impulse response filtering method, a value for the thermal product of the quartz substrate is needed. The probe substrate was quartz so its density was taken as 2200 kg/m^3. The specific heat and thermal conductivity of the quartz were calculated using data in Toulokian [119]. The thermal product ($\sqrt{\rho ck}$) obtained from this calculation was around 1500 kJ/m^2/K/s$^{0.5}$. Representative stagnation point heat flux results obtained in this manner are presented in figure 8.5. The maximum heat flux recorded for the current operating condition was around 300 kW/m^2.

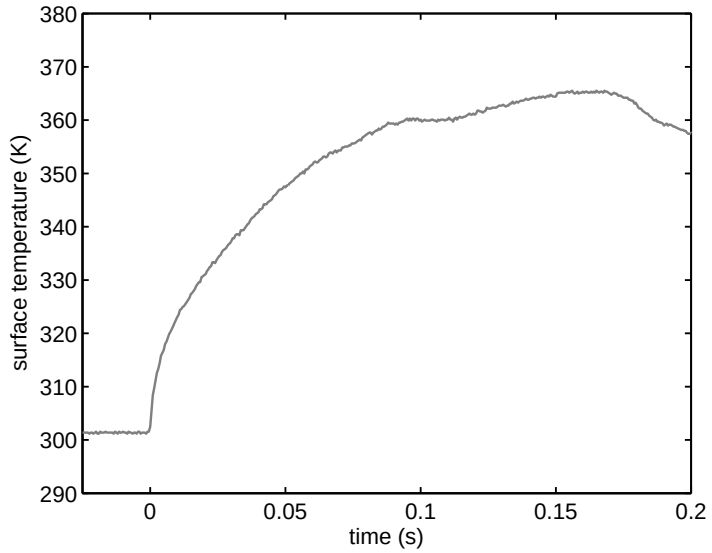

Figure 8.4: Representative film temperature history from the thin film probe. Result actually from run 175.

In the present work, the stagnation temperature data derived from thin film heat flux gauge measurements relies on the accuracy of the heat transfer coefficient calculation. The heat transfer coefficient calculation itself depends on the free stream flow properties, the radius of curvature at the stagnation point, and is weak function of the probe temperature and the flow stagnation temperature (see equations 8.13, 8.14, and 8.15). For the current experiment, the heat transfer

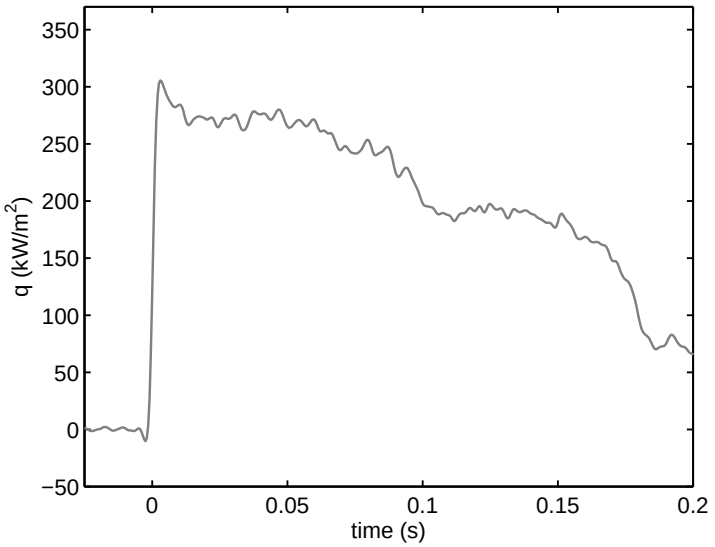

Figure 8.5: Representative heat flux derived from the surface temperature of the thin film probe as presented in figure 8.4.

coefficient was calculated using function scripts in matlab with the procedure as described in section 8.3. All values for the parameters such as the time-resolved pitot pressure and Mach number used in this calculated were obtained from the results of the previous chapter (chapter 7) and the flow stagnation temperature (for the purpose of calculating h) was taken from the result from chapter 6.

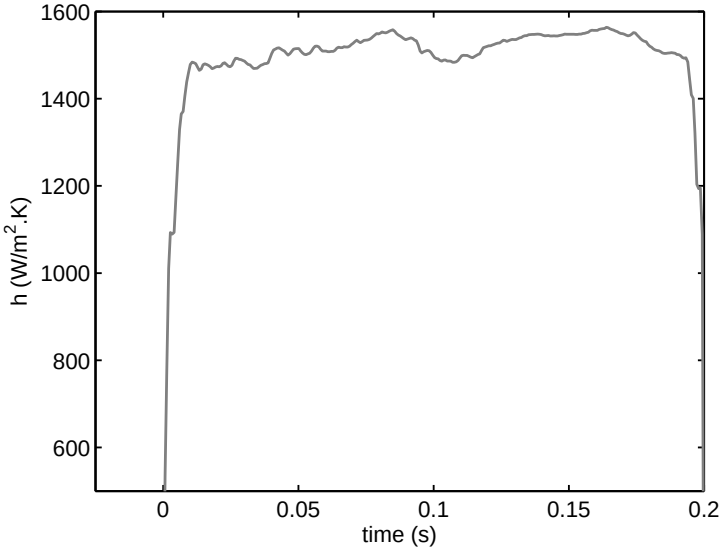

Figure 8.6: Heat transfer coefficient result calculated for the probe.

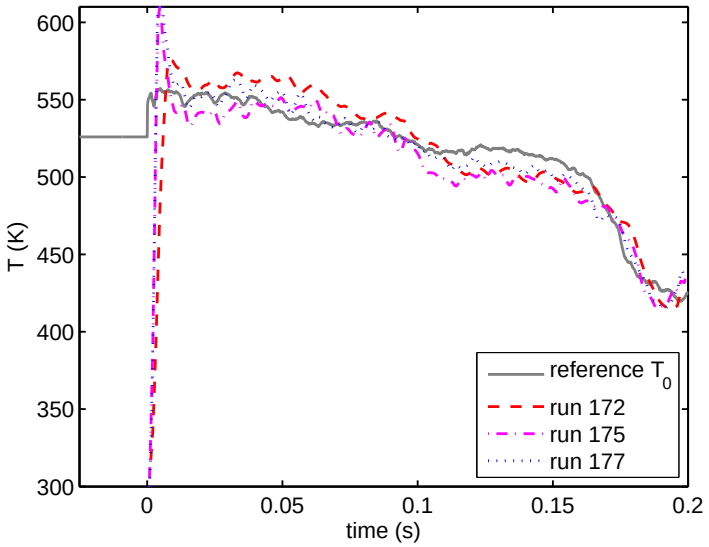

Figure 8.7: Stagnation temperature derived from the heat flux probe using results in figures 8.4, 8.5 and 8.6. A scaling factor of 0.85 was applied to the heat transfer coefficient of figure 8.6. The reference T_0 result was obtained from the thermocouple work of chapter 6.

Figure 8.6 present the time-resolved heat transfer coefficient calculated in this manner. The stagnation temperature was then calculated using equation 8.3 based on the results presented in figure 8.4, 8.5, and 8.6. The calculated stagnation temperature result is shown in figure 8.7 with a comparison to the thermocouple result of chapter 6. The calculated thin film result in figure 8.7 was obtained by the application of scaling factor of 0.85 to the heat transfer coefficient, otherwise the calculated stagnation temperature would be lower than the reference stagnation temperature obtained in chapter 6. Although the factor of 0.85 is somewhat arbitrary, it is justified on the grounds of uncertainties in the heat transfer coefficient correlation. Evidence of the overall success of the method is drawn from the agreement with the thermocouple results in terms of the temporal distribution of stagnation temperature. For example, both methods indicate essentially the same drop of stagnation temperature between 0.16 and 0.19 s of around 80 K.

8.5.2 Heat flux fluctuations

If fluctuations in stagnation temperature are isentropically related to fluctuations in stagnation pressure, then the relationship

$$\frac{T_0'}{T_0} = \frac{\gamma - 1}{\gamma} \frac{p_0'}{p_0} \tag{8.20}$$

will be valid provide the magnitude of the fluctuations is small.

The heat transfer coefficient varies with the pitot pressure according to (equation 8.13)

$$h \sim p_{pit}^{0.5} \tag{8.21}$$

and on the assumption that fluctuations in Mach number or other thermophysical properties of the flow or the probe are very small and do not impact the probe heat transfer coefficient,

$$\frac{h'}{h} = 0.5 \frac{p_{pit}'}{p_{pit}} \tag{8.22}$$

and with the assumption of M_∞ = constant,

$$\frac{p_{pit}'}{p_{pit}} = \frac{p_0'}{p_0} \tag{8.23}$$

Combining equations 8.20, 8.22, and 8.23 with equation 8.18 gives the expression

$$\frac{q'}{\bar{q}} = \frac{p_0'}{p_0} \left\{ 0.5 + \frac{(\gamma - 1)/\gamma}{1 - T_w/T_0} \right\} \tag{8.24}$$

Figure 8.8 (parts a and b) shows stagnation pressure and heat flux result during the period of 30 - 50 ms after diaphragm rupture. There is substantial noise on the heat flux result. The magnitude of this noise is comparable to that observed prior to diaphragm rupture as illustrated in figure 8.8 part c. Therefore a centered, moving average filter having a time window of 0.2 ms was applied, giving the results shown as the dark line in figure 8.8 part b.

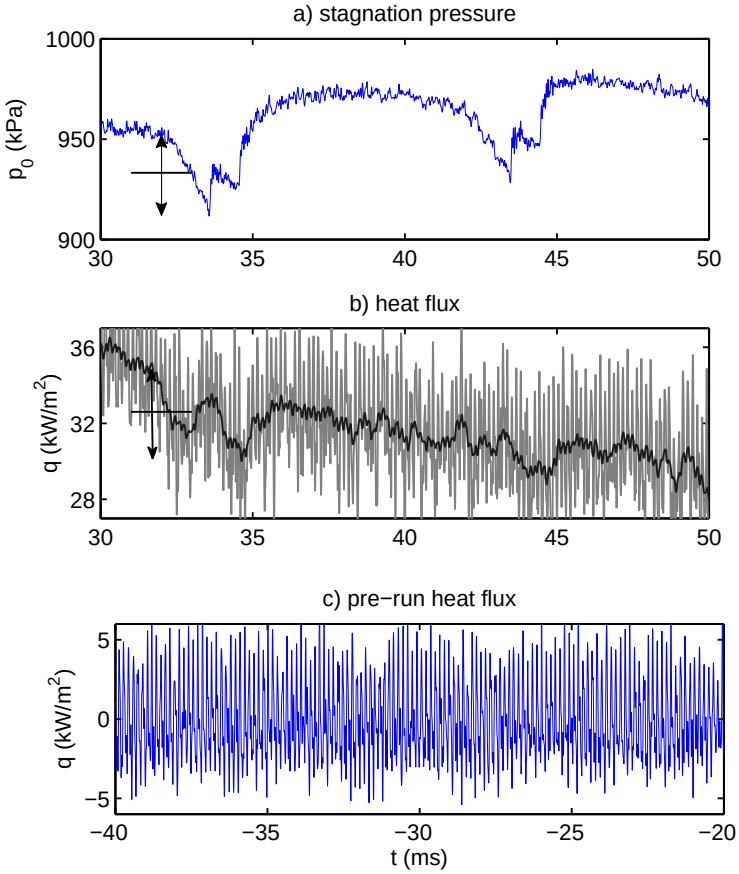

Figure 8.8: Sample fluctuations observed in the barrel pressure history (part a); in the corresponding heat flux signal (part b); and in a pre-run portion of the heat flux result (part c).

Referring to again figure 8.8 parts a and b, the largest fluctuations of the stagnation pressure and the heat flux are around 43 kPa and 3.95 kW/m^2 respectively (*see the arrow lines*), and the corresponding average stagnation pressure and heat flux are around 933 K and 33 kW/m^2 respectively (*see the horizontal lines*). Through the implementation of equation 8.24 and the use of the thin film stagnation temperature of run 175 (as presented in figure 8.7) of around 562 K and

the thin film wall temperature (figure 8.4) of around 339 K at 32 ms from start of the flow, it was found that relative magnitude of the measured the heat flux fluctuation (figure 8.8 b) corresponds to only 50 % of the value derived from the stagnation pressure fluctuations. The difference is likely to be related to the relatively poor effective signal bandwidth obtained in the case of the direct measurements (as presented as the dark line in figure 8.8 b) because of the relatively high signal to noise ratio.

8.6 Conclusion

Stagnation temperature at the exit of the Mach 6 nozzle of the University Southern Queensland has been investigated using thin film heat flux gauge techniques. The form and magnitude of the stagnation temperature variations derived from thin film results was consistent with the results obtained from the thermocouple probe used in chapter 6.

Fluctuation in the heat flux were related to the stagnation pressure fluctuations via an analytical expression on the assumption of an isentropic relationship between the pressure and temperature. It was found that the expected heat flux fluctuations based on the stagnation pressure measurements at a particular point in time were about twice as large as the measured values at the corresponding time. It is expected that the fluctuations in the probe heat flux should be at least as large as those attributable to isentropic variations in the nozzle reservoir region. The discrepancy is likely to be related the noise and effective bandwidth of the current thin film heat flux measurements. Future efforts should target the reduction of noise in the thin film power supply and amplifier arrangement.

Chapter 9

Conclusions

9.1 Motivation

A new hypersonic short duration wind tunnel facility has been developed at the University of Southern Queensland and the facility is designated as TUSQ. The TUSQ can be operated as a Ludwieg tube with free piston compression heating and is capable of producing a cold flow for a relatively long test flow duration of more than 100 milliseconds, so diverse experiments can be accommodated in this tunnel. However, because the facility is relatively new and because strong thermal disturbances have previously been observed in a similar facility, a study has been performed to investigate the thermal characteristics of the hypersonic flow generated by TUSQ and relate these characteristics to the compression and discharge processes within the barrel.

9.2 Temperature Probe Development

Three different versions of an aspirating thermocouple probe were developed for this work, and a thin film transient heat flux gauge was also tested. The first aspirating thermocouple probe consisted of bead-welded t-type junction with a

heated shield and this allowed the identification of a stagnation temperature value at the Mach 6 nozzle exit. A response time correction method was developed and the value of stagnation temperature was found to be 495 K at 100 ms after the flow start.

For the second thermocouple probe, an improved version of the heated aspirating probe was developed based on a k-type butt-welded thermocouple junction. This probe allowed the measurement of the temporal variation of stagnation temperature at the nozzle exit. A thermocouple response time correction technique was also developed in this case. A transient thermal response model for the wire was used and the probe was operated over a range of initial wire temperature around the flow stagnation temperature value. The measured stagnation temperature at 100 ms after the flow start was around 520 K for the same flow conditions tested with the t-type probe. Given the very approximate nature of the correction approach adopted for the t-type probe, this level of agreement was be reasonable. The first probe did not facilitate temporal resolution of the stagnation temperature history. The second probe is considered for superior because not only did it enable acquisition of time-resolved data, the response time correction methodology is more rigorous, apparently yielding more reliable data.

The third probe arrangement for the aspirating stagnation temperature probe used 0.025 mm diameter bead-welded junction k-type thermocouple located near the inlet of the ceramic tube which was unheated in this case. Unheated probes are considerably more convenient and this arrangement was developed in an effort to obtain spatially-resolved stagnation temperature data. Although the response time of measurement with this third probe is longer than the corrected result from the second probe, it is still considered sufficiently fast for the spatially-resolved temperature measurement work.

The last probe that was tested was a stagnation point thin film heat flux gauge. The primary objective of this work was the measurement of stagnation temperature fluctuations at the nozzle exit. Stagnation temperature results from the

thin film probe were lower than those obtained with the aspirating thermocouple probes and the difference was attributed to an error of around 15 % in the calculation of the stagnation point heat transfer coefficient of the thin film probe.

9.3 Temperature Variations

9.3.1 Temporal

The stagnation temperature of the flow which is initially discharged from the hypersonic nozzle is very close to the isentropic compression value. However, the flow stagnation temperature decreases with time and thermodynamic simulations accurately reflect the majority of the observed temporal variations when a flat plate boundary layer cooling is used to model the heat transfer in the barrel of the wind tunnel facility. Because the flat plate boundary layer cooling model provides a good match to the measured temperature on the nozzle centre line for the majority of the flow duration, it is concluded that significant mixing must have occurred across the diameter of barrel prior to flow discharge through the nozzle. Measurements in other facilities have indicated the existence of discrete, large scale thermal disturbance with propagated ahead of the piston and potentially compromised the test flow quality, but no such disturbance were detected at the centre line of the nozzle exit.

9.3.2 Spatial

The stagnation temperature measurements indicated a core flow region of almost 80 mm radius near the start of the test flow, consistent with that derived from separate pitot pressure measurements. A decrease in the available core flow radius was registered throughout the majority of the test flow according to the stagnation temperature measurements. The average spatial gradient of stagna-

tion temperature within the core flow region was essentially zero for the first 30 ms of the test flow and this result is consistent with the temporally-resolved results in which it was found that the initial flow discharge from the nozzle had a stagnation temperature very close to the isentropic compression value. The maximum average spatial gradient of stagnation temperature was registered at about 150 ms after the start of the test flow and had a value of approximately -0.45 K/mm within the core flow region, indicating an average drop in stagnation temperature of about 20 K over the core flow region at this time.

Substantially better flow uniformity was registered by the pitot pressure measurements. At the exit of the Mach 6 nozzle, pitot pressure data indicate core flow uniformity to within 2 % and a core flow radius of at least 80 mm for the majority of the test flow duration of around 200 ms. Mach number profiles deduced from the pitot pressure measurements are likewise uniform with a Mach number of 5.81 ± 0.05 for the majority of the test flow duration.

9.4 Temperature Fluctuations

A model for the temperature fluctuations in transient compression hypersonic facilities was developed base on existing incompressible turbulent pipe flow results. Using the suggested approach, the mean value of the root-mean-square stagnation temperature fluctuations was estimated to be around 9 K in the case of the TUSQ facility. Comparison with previous experiments in a gun tunnel facility suggest the turbulent pipe flow model over-estimates the magnitude of the temperature fluctuations. Nevertheless, this value is consistent with the magnitude of the spatial variation in stagnation temperature within the core region of the nozzle exit flow. Given the magnitude of these estimates of temperature fluctuations, it was anticipated that measurements could be successfully made using a thin film probe. Attempts were made to relate the observed fluctuations in heat flux to the pressure fluctuations in the barrel by using the isentropic relationship.

9.5 Future Directions

Direct measurements of temperature in transient wind tunnels are often difficult to perform due to the short duration test period. However, the result obtained in the current work present some interesting possibilities for future researchers. Some recommendations for future work are presented here:

The use of a thermocouple probe with a smaller diameter wire should be revisited with a view to overcoming the installation and operational challenge experienced in this work. If it is possible to overcome these challenges, additional fast-response data can be obtained and this would provide a good comparison to the present measurements of the stagnation temperature.

Relatively low bandwidth fluctuations in the stagnation point heat flux were observed and these appeared to correlate with the stagnation pressure fluctuations to some degree, but further effort in this area is required in order to resolve stagnation temperature fluctuations due to the turbulent mixing in the barrel.

References

[1] L. M. Jiji, *Heat Convection*, 2nd ed. Springer, 2009.

[2] M. V. Morkovin, "On supersonic wind tunnels with low free stream disturbances," *J. Appl. Mech.*, vol. 26, pp. 319–323, 1959.

[3] T. V. Jones, D. L. Schultz, and A. Hendley, "On the flow in an isentropic light piston tunnel," Aeronautical Research Council, Report and Memoranda, R&M No. 3731, 1973.

[4] R. C. Warren, *Design of Thermocouple Probes for Measurement of Rocket Exhaust Plume Temperatures.* DSTO Aeronautical and Maritime Research Laboratory, Melbourne, Vic., 1994.

[5] R. A. East and J. H. Perry, "A short time response stagnation temperature probe," C.P. No. 909, British Aeronautical Research Council, 1967.

[6] C. S. Subramanian and R. A. Antonia, "Effect of Reynolds number on a slightly heated turbulent boundary layer," *Int. J. Heat Mass Transfer*, vol. 24, no. 11, pp. 1833–1846, 1981.

[7] D. R. Buttsworth, "Shock induced mixing and combustion in scramjets," Ph.D. dissertation, University of Queensland, 1994.

[8] S. R. Pate, "Effect of wind tunnel disturbances on boundary-layer transition with emphasis on radiated noise: A review," *11th Aerodynamic Testing Conference, Colorado Springs, Colorado, March 18-20*, 1980.

[9] K. M. Kinnear and F. K. Lu, "Design, calibration and testing of transient thin film heat transfer gauges," *AIAA Paper 1998-2504*, 1998.

[10] D. R. Buttsworth and M. K. Smart, "Ludwieg tunnel facility with free piston compression heating for supersonic and hypersonic scramjet inlet starting experiments," AIAA 2010-588, pp. 1-6, 48^{th} AIAA Aerospace Sciences Meeting Including the New Horizons Forum and Aerospace Exposition, Orlando - Florida, USA, 4 - 7 Jan. 2010.

[11] S. P. Schneider, "Flight data for boundary-layer transition at hypersonic and supersonic speeds," *Journal of Spacecraft and Rocket*, vol. 1, no. 36, pp. 8–13, January-February 1999.

[12] R. G. Morgan, "A review of the use of expansion tubes for creating superorbital flows," in *Aerospace Sciences Meeting and Exhibit, AIAA Paper 97-0279*, Reno, NV., 6 - 10 January 1997.

[13] J. H. Watmuff, "Detrimental effects of almost immeasurably small freestream nonuniformities generated by wind-tunnel screens," *AIAA Journal*, vol. 36, no. 3, pp. 379–386, Mar. 1998.

[14] D. L. Bacon and E. G. Reid, "The resistance of spheres in wind tunnels and in air," NACA Report No. 185, Ninth Annual Report of the National Advisory Committee for Aeronautics - 1923, Government Printing Office, Washington DC, 1924.

[15] R. J. Anthony, M. L. G. Oldfeld, T. V. Jones, and J. E. LaGraff, "Development of high-density arrays of thin film heat transfer gauges," 1999, Proceedings 5th ASME/JSME Thermal Engineering Joint Conference, San Diego, CA.

[16] S. P. Schneider, "Development of hypersonic quiet tunnels," *Journal of Spacecraft and Rockets*, vol. 45, no. 4, pp. 641–664, Jul/Aug 2008.

[17] E. Reshotko, "Boundary-layer instability, transition, and control," *AIAA Paper 94-0001*, 1994.

[18] S. P. Schneider, "Hypersonic laminar-turbulent transition on circular cones and scramjet forebodies," *Progress in Aerospace Sciences*, vol. 40, no. 1-2, pp. 1–50, 2004.

[19] Y. Abe, H. Kawamura, and Y. Matsuo, "Surface heat-flux fluctuations in a turbulent channel flow up to $\mathrm{Re}_\tau = 1020$ with $\mathrm{Pr} = 0.025$ and 0.71," *International Journal of Heat and Fluid Flow*, vol. 25, pp. 404–419, 2004.

[20] L. Redjem-Saad, M. Ould-Rouiss, and G. Lauriat, "Direct numerical simulation of turbulent heat transfer in pipe flows: effect of Prandtl number," *Int. J. Heat Fluid Flow*, vol. 28, no. 5, pp. 847–861, 2007.

[21] D. R. Chapman and G. D. Kuhn, "The limiting behaviour of turbulence near a wall," *J. Fluid Mech.*, vol. 170, pp. 265–292, 1986.

[22] J. G. M. Eggels, F. Unger, M. H. Weiss, J. Westerweel, R. J. Adrian, R. Friedriech, and F. T. M. Nieuwstatdt, "Fully developed turbulent pipe flow : a comparison between direct numerical simulation and experiment," *J. Fluid Mech.*, vol. 268, pp. 175–209, 1994.

[23] P. E. Dimotakis, "Turbulent free shear layer mixing and combustion," GALCIT Report FM91-2, 1991.

[24] M. Haibel and F. Mayinger, "The effect of turbulent structures on the development of mixing and combustion processes in sub- and supersonic H2 flames," *International Journal of Heat and Mass Transfer*, vol. 37, no. Supplement 1, pp. 241–253, 1994.

[25] S. J. Baresh, N. T. Clemens, and D. S. Dolling, "Relationship between upstream turbulent boundary-layer velocity fuctuations and separation shock unsteadiness," *AIAA Journal*, vol. 40, no. 12, pp. 2412–2422, 2002.

[26] J. Délery and G. Degrez, "Shock-wave boundary layer interactions," AGARDograph No. 280, ISBN 92-835-159-6, 1996.

[27] D. Knight and G. Degrez, "Shock wave boundary layer interactions in high Mach number flows - a critical survey of current cfd prediction capabilities," AGARD-AR-319, Vol. 2, 1998.

[28] J. Müller, R. Mümmler, and W. Staudacher, "Comparison of some measurements techniques for shock-induced boundary layer separation," *Aerosp. Sci. Technol.*, vol. 5, no. 6, pp. 383–395, 2001.

[29] S. Wagner, R. Wirtz, and R. Losch, "A methodology for the conceptual aerodynamic design of transatmospheric flight vehicles," in *2nd International Conference on Aerospace Science and Technology, 6th Australian Aeronautical Conference*, vol. I, Melbourne, Australia, pp. 405-412, 1995.

[30] A. M. O. Smith, "Review of the M and M tapes, an AIAA recorded lecture series review : High speed boundary layer stability and transition," *Astronautics and Aeronautics*, April 1972.

[31] H. Consigny and B. E. Richards, "Short duration measurement of heat transfer rate to a gas turbine motor blade," *Journal of Engineering Power*, vol. 104, pp. 542–551, 1982.

[32] J. F. Wendt, "External hypersonic aerodynamics: State-of-the-art and future perspective," in Future Aerospace Technology in the Service of the Alliance CP-600. NATO AGARD, vol. 3, pp. C10.1-C10.7, 1997.

[33] P. F. Brinich, "Effect of leading edge geometry on boundary-layer transition at $M_\infty = 3.1$," NACA TN 3659, 1956.

[34] R. Ross, "Influence of total temperature on transition in supersonic flow," *AIAA Journal*, vol. 11, no. 4, pp. 363–565, Apr. 1973.

[35] R. A. Baurle and S. S. Girimaji, "Assumed pdf turbulence-chemistry closure with temperature-composition correlations," *Combustion and Flames*, vol. 134, pp. 131–148, 2003.

[36] B. J. Delarue and S. B. Pope, "Shock-wave boundary layer interactions," *Physics of Fluids*, vol. 10, no. 2, pp. 487–498, 1998.

[37] R. L. Gaffney, J. A. White, S. S. Girimaji, and J. P. Drummond, "Modeling temperature and species fluctuations in turbulent reacting flow," *Computing Systems in Engineering*, vol. 5, no. 2, pp. 117–133, 1994.

[38] T. J. Mcintyre, P. A. B. Rabbat, and A. F. P. Houwing, "Imaging of combustion processes in a supersonic combustion ramjet," *Proceedings of the 12th International Symposium on Air-breathing Engines, Melbourne, Australia, September 10-15 (1995), (Billig, F.S., ed.), ISBN: 1563471779, AIAA*, p. 1163, 1995.

[39] M. P. Martin and G. V. Candler, "Temperature-fluctuation scaling in reacting boundary layers," *American Physical Society, 54th Annual Meeting of the Division of Fluid Dynamics, San Diego, California Meeting, November 18 - 20*, 2001.

[40] S. P. Schneider, "Effects of high speed tunnel noise on laminar-turbulent transition," *Journal of Spacecraft and Rocket*, vol. 38, no. 3, pp. 323–333, May - Jun. 2001.

[41] J. P. Bonnet, D. Grésillon, and J. P. Taran, "Nonintrusive measurements for high-speed, supersonic, and hypersonic flows," *Ann. Rev. Fluid Mech*, vol. 30, pp. 231–273, 1998.

[42] C. Tyler and F. E. Eastep, "Analysis of a Rayleigh scattering measurement system in a hypersonic wind tunnel," AIAA Paper 1997-772, 35th Aerospace Sciences Meeting and Exhibit, Reno, NV, Jan. 1997.

[43] P. V. Vukoslavcevic and J. M. Wallace., "The simultaneous measurement of velocity and temperature in heated turbulent air flow using thermal anemometry," *Measurement Science and Technology*, vol. 13, pp. 1615 – 1624, 2002.

[44] C. S. K. Cho, G. C. Fralick, and H. D. Bhatt, "Heat flux measurement techniques," *Proceedings of the Institution of Mechanical Engineers, Part C: Journal of Mechanical Engineering Science*, vol. 213, pp. 655–677, 1999.

[45] L. S. G. Kovasznay, "Turbulence in supersonic flow," *Journal of The Aeronautical Sciences*, vol. 20, no. 10, pp. 657–674, 1953.

[46] J. Laufer, "Aerodynamic noise in supersonic wind tunnels," *Journal of The Aeronautical Sciences*, vol. 28, no. 9, pp. 685–692, 1961.

[47] S. P. Schneider and E. Haven, "Mean flow and noise measurements in the Purdue quiet-flow Ludwieg tube," *AIAA 94-0546*, 1994.

[48] M. Borg and J. M. Smith, "Effect of disturbances on quiet flow in the Mach 4 Ludwieg tube," AAE 520 Experimental Aerodynamics Final Report, 2004.

[49] D. R. Buttsworth and T. V. Jones, "High bandwidth stagnation temperature measurements in a mach 6 gun tunnel flow," *Experimental Thermal and Fluid Science*, vol. 27, no. 2, pp. 177–186, 2003.

[50] R. A. East and A. M. S. Qasrawi, "A long stroke free isentropic free piston hypersonic wind tunnel," Aeronautical Research Council, Report and Memoranda, R&M No. 3844, 1978.

[51] C. Wieselsberger, "Der luftwidersland von kugelh," *Z.F.M.*, vol. 5, pp. 140–144, 1914.

[52] G. Taylor and G. K. Batchelor, "The effect of wire gauze on small disturbances in a uniform stream," *Quart J. Mech. Appl. Math. Cambridge*, vol. 2, no. 1-29, 1947.

[53] J. P. Hartzuiker, P. G. Pugh, W. Lorenz-Meyer, and G. E. Fasso, "On the flow quality necessary for the large European high Reynolds number transonic wind tunnel LEHRT," AGARD-R-644, 1975.

[54] M. Fischer and L. Weinstein, "Cone transitional boundary-layer structure at Me = 14," *AIAA Journal*, vol. 10, no. 5, pp. 699–701, 1972.

[55] M. V. Morkovin, "On transition experiments at moderate supersonic speeds," *Journal of the Aeronautical Sciences*, vol. 24, no. 7, pp. 480–486, 1957.

[56] H. L. Dryden, "Air flow in the boundary layer near a plate," NACA report No. 562, 1936.

[57] J. G. Spangler and C. S. Wells, "Effects of free-stream disturbances on boundary layer transition," *AIAA Journal*, vol. 6, pp. 543–545, 1968.

[58] J. Laufer and J. E. Marte, "Results and a critical discussion of transition-Reynolds numbers measurement on insulated cones and flat plates in supersonic wind tunnels," rep. No. 20-96 (Contract No. DA-04-495-Ord 18), Jet Propulsion Lab., C.I.T., Nov. 30, 1955.

[59] E. R. Van Driest and J. C. Boison, "Experiments on boundary layer transition at supersonic speeds," *J. Aero. Sci.*, vol. 24, pp. 885–889, 1957.

[60] J. C. Donaldson and J. P. Wallace, "Flow fluctuation measurements at Mach number 4 in the test section of the 12-inch supersonic tunnel D," AEDC-TR-143 (AD723630), August 1971.

[61] R. D. Wagner, "Hot wire measurements of free stream and shock layer disturbances," *AIAA Journal*, vol. 9, no. 12, pp. 2468–2470, 1970.

[62] M. V. Morkovin, "Fluctuations and hot-wire anemometry in compressible flows," AGARDograph 24, 1956.

[63] G. Schubauer and H. K. Skramstad, "Laminar boundary layer oscillations and stability of laminar flow," *J. Aeronaut. Sci.*, vol. 14, no. 2, pp. 69–78, 1947.

[64] J. Dougherty, N. S. and D. F. Fisher, "Boundary-layer transition on a 10-degree cone: Wind tunnels/flight data correlations," *AIAA Paper No. 80-0154, AIAA 18th Aerospace Sciences Meeting*, Jan. 1979.

[65] P. O. A. L. J. Davies, "Structure of turbulence," *Journal of Sound and Vibration*, vol. 28, no. 3, pp. 513–526, 1973.

[66] J. M. Kendall, "Wind tunnel experiments relating to supersonic and hypersonic boundary-layer transition," *AIAA Journal*, vol. 13, no. 3, pp. 290–299, 1975.

[67] I. E. Beckwith, "Development of high Reynolds number quiet tunnel for transition research," *AIAA Journal*, vol. 13, no. 3, pp. 300–306, 1975.

[68] T. Vrebalovich, "Discussion on supersonic wind tunnels with low free stream disturbances," *Journal of Applied Mechanics*, pp. 362–364., Jun 1960.

[69] H. Ludwieg, "Tube wind tunnel: A special type of blowdown tunnel," AGARD Report No 143, 1957.

[70] F. L. Lu and D. R. Wilson, "Survey of short duration, hypersonic and hypervelocity facilities," in *18th AIAA Aerospace Ground Testing Conference, American Institute of Aeronautics and Astronautics*, Colorado Springs, CO, 1994.

[71] R. J. Stalker, "Modern developments in hypersonic wind tunnels," *Aeronautical Journal*, vol. 110, no. 1103, pp. 21–39, 2006.

[72] S. P. Schneider, "Facilities and instrumentation for hypersonic measurement of transition mechanisms at Purdue university," Summary of Facilities as of February 2006, Purdue University, School of AAE, 765-494-3343, 2009.

[73] T. Wolf, M. Estorf, and R. Radespiel, "Investigation of the starting process in a Ludweig tube," *Theoretical and Computational Fluid Dynamics*, vol. 21, no. 2, pp. 81–98, Mar. 2007.

[74] M. L. G. Oldfield, T. V. Jones, and D. L. Schultz, "On-line computer for transient turbine cascade instrumentation," *IEEE Trans. Aerosp. Electron. Syst.*, vol. 14, no. 5, pp. 738–749, 1978.

[75] C. S. K. Cho, G. C. Fralick, and H. D. Bhatt, "An experimental study of a radially arranged thin-film heat-flux gauge," *Meas. Sci. Tech.*, vol. 8, pp. 721–727, 1997.

[76] A. Fiala, R. Hillier, S. G. Mallinson, and H. S. Wijesinghe, "Heat transfer measurement of turbulent spots in a hypersonic blunt-body boundary layer," *J. Fluid Mech.*, vol. 555, pp. 81–111, 2006.

[77] B. E. Edney, "Temperature measurement in a hypersonic gun tunnel," *J. Fluid Mech.*, vol. 27, pp. 503–512, 1967.

[78] H. Oliver, "An improved method to determine freestream conditions in hypersonic facilities," *Shock Waves*, vol. 3, pp. 129–139, 1993.

[79] D. Estruch, N. J. Lawson, and K. P. Garry, "Application of optical measurement techniques to supersonic and hypersonic aerospace flows," *J. Aerosp. Eng.*, vol. 22, p. 383, 2009.

[80] R. A. East, "The performance and operation of the University of Southampton hypersonic gun tunnel," U.S.A.A. Report No. 135, August 1960.

[81] B. E. Edney, "The correlation of measured and predicted temperatures in the FFA hypersonic gun tunnel," F.F.A. Report AU-209:2, 1965.

[82] R. F. Meyer, W. F. Campbell, and K. P. Jackson, "The NAE hypersonic gun tunnel part i: the compression heater," N.R.C. Aeronautical Report LR-432, August 1965.

[83] J. L. Stollery, "Stagnation temperature measurements in a hypersonic wind tunnel using the sodium line reversal method," *Nature*, vol. 190, no. 4778, pp. 778–781, 1961.

[84] G. E. Merritt, "Velocity measurements in the University of Southampton hypersonic gun tunnel," ARC 22 873. April 1961.

[85] T. V. Jones and D. L. Schultz, "A study of film cooling related to gas turbines using transient techniques," ARC 32 420, 1970.

[86] M. D. Scadron and I. Warshawsky, "Experimental determination of time constants and nusselt numbers for bare-wire thermocouples in highvelocity air streams and analytic approximation of conduction and radiation errors," NACA TN-2599, 1952.

[87] T. M. Stickney, "Recovery and time response characteristics of six thermocouple probes in subsonic and supersonic flow," NACA Technical Note 3455, 1955.

[88] C. W. Albertson and W. A. Bauserman Jr., "Total temperature probe for high-temperature hypersonic boundary-layer measurements," NASA Technical Memorandum 4407, 1993.

[89] E. M. Winkler, "Stagnation temperature probe for use at high supersonic speed and elevated temperatures," NAVORD Rep 3834, US Navy, 1954.

[90] A. Gülhan, "Heat flux measurements in high enthalpy flows," RTO EN-8, AC/323(AVT)TP/23, 2000.

[91] M. G. Dunn, "Measurement of heat flux and pressure in a turbine stage," *ASME J. Eng. Gas Turbines Power*, vol. 107, pp. 76–83, 1985.

[92] J. E. Doorly and M. L. G. Oldfield, "New heat transfer gauges for use on multi-layered substrates," *ASME J. Turbomach.*, vol. 108, pp. 153–160, 1986.

[93] D. L. Schultz and T. V. Jones, "Heat-transfer measurements in short-duration hypersonic facilities," AGARDograph No. 165, 1965.

[94] R. Vidal, "Model instrumentation techniques for heat transfer and force measurement in a hypersonic shock tunnel," Cornell Aeronautical Laboratory Buffalo New York, Rept AD-917-A-1, 1956.

[95] D. R. Buttsworth and T. V. Jones, "Transient temperature probe measurements in a mach 4 nitrogen jet," *Experimental in Fluid*, vol. 37, pp. 137–145, 2004.

[96] A. H. Epstein, G. R. Guenette, R. G. Norton, and C. A. Yuzhang, "High frequency response heat-flux gage," *Review of Scientific Instruments,*, vol. 57, pp. 639–649, 1986.

[97] W. J. Cook and E. J. Felderman, "Reduction of data from thin-film heat transfer gauges: A concise numerical technique," *AIAA Journal*, vol. 4, no. 3, pp. 561–562, 1966.

[98] M. G. Dunn, W. K. George, W. J. Rae, S. H. Woodward, J. C. Moiler, and P. J. Seymour, "Heat flux measurements for the rotor of a full-stage turbine. part ii. description of analysis techniques and typical time resolved measurements," *ASME Journal of Engineering for Power*, vol. Int. Gas Turbine Conf., Dusseldorf, West Germany, 8-12 June, 1986.

[99] H. S. Carslaw and J. C. Jaeger, *Conduction of Heat in Solids*, 2nd ed. Clarendon Press, 1989.

[100] M. G. Dunn, "The thin-film gage, von karman institute for fluid dynamics," Von Karman Institute for Fluid Dynamic, Lecture Series 1995-01, 1995.

[101] M. L. G. Oldfield, R. Kiock, A. T. Holmes, and C. G. Graham, "Boundary layer studies on highly loaded cascades using heated thin films and traversing probe," *ASME Journal of Engineering for Power*, vol. 103, pp. 237–246, 1981.

[102] D. R. Buttsworth and T. V. Jones, "A fast-response total temperature probe for unsteady compresible flows," *J. Eng. Gas Turbines Power*, vol. 120, no. 4, pp. 694–702, 1998.

[103] A. F. Mills, *Heat and Mass Transfer*, 2nd ed. Richard D. Irwin, 1995.

[104] P. Huber, J. Charles, J. Schexnayder, and C. R. McClinton, "Criteria for self-ignition of supersonic hydrogen-air mixtures," NASA Technical Paper 1457, August 1979.

[105] H. S. Pergament, "A theoritical analyssis of non-equilibrium hydrogen-air reactions in flow systems," *American Inst. Aeronaut. & Astronaut.*, vol. 11, April 1963.

[106] K. Hannemann, R. Krek, and G. Eitelberg, "Latest calibration results of HEG contoured nozzle," *in 20th International Symposium on Shock Waves', World Scientic*, pp. 1575–1580, 1996.

[107] A. F. Burke and K. D. Bird, "The use of conical and contoured expansion nozzles in hypervelocity facilities," in Advances in Hypervelocity Techniques', Second Symposium on Hypervelocity Techniques, Plenum Press, University of Denver, pp. 373-424, 1962.

[108] B. Lawton and G. Klingenberg, *Transient Temperature in Engineering and Science*. Oxford University Press, Oxford, 1996.

[109] ASTM, *Manual on the Use of Thermocouples in Temperature Measurement, Fourth Edition*. Revision of ASTM Special Publication 470B, Philadelphia, PA., 1993.

[110] A. A. Zukauskas, *Heat Transfer from Tubes in Cross Flow, Advances in Heat Transfer*. Academic Press, 1972.

[111] M. L. G. Oldfield, "Impulse response processing of transient heat transfer gauge signals," *Journal of Turbomachinery-Transactions of the ASME*, vol. 130, no. 2, 2008.

[112] S. M. Guo, C. C. Lai, T. V. Jones, and M. L. G. Oldfield, "Influence of surface roughness on heat transfer and effectiveness for a fully film cooled nozzle guide vane measured by wide band liquid crystals and direct heat flux gages," *ASME J. Turbomach.*, vol. 122, no. 4, Oct. 2000.

[113] D. R. Buttsworth, "Transient response of an erodable heat flux gauge using finite element analysis," *Proceedings of the Institution of Mechanical Engineers Part D (Journal of Automobile Engineering)*, vol. 216, pp. 701–706, 2002.

[114] D. R. Buttsworth, "Assessment of effective thermal product of surface junction thermocouples on millisecond and microsecond time scales," *Experimental Thermal and Fluid Science*, vol. 25, no. 6, pp. 409–420, 2001.

[115] Y. A. Cengel, *Heat and Mass Transfer: A Practical Approach*, 3rd ed. McGraw-Hill, 2006.

[116] J. O. Hinze, *Turbulence*, 2nd ed. McGraw-Hill, New York, 1975.

[117] F. M. White, *Viscous Fluid Flow, Second Edition.* McGraw-Hill Inc., 1991.

[118] O. Singh and A. Curzon, "The effect of oxygen and hydrogen contamination on the electrical resistivity of rare earth metal films," *Thin Solid Films*, vol. 44, no. 2, pp. 233–240, 1977.

[119] Y. S. Toulokian, *Thermal Properties of Matter, The TPRC Data Series:* Vol.2, *Thermal Conductivity Non Metalic Solids*; Vol. 5, Spesific Heat Nonmetalic Solids. lfi, New York, 1970.

[120] Anonymous, "American national standard for temperature measurement thermocouples," ANSI-MC96-1, Instrument Society of America (sponsor), 1982.

[121] I. E. Beckwith and C. G. Miller, "Aerothermodynamics and transition in high-speed wind tunnels at nasa langley," *Annu. Rev. Fluid Mech.*, vol. 22, pp. 419–439, 1990.

[122] T. G. Beckwith, R. D., Marangoni, and J. H. Lienhard, *Mechanical Measurements*, 5th ed. Addison-Wesley, 1993.

[123] D. R. Buttsworth and P. A. Jacobs, "Measurement of fluctuations in a mach 4 shock tunnel nozzle flow," ser. 7th Australasian Heat and Mass Transfer Conference. Chalkface Press Pty Ltd., 3 - 6 Jul 2000, pp. 53–59, James Cook, Australia.

[124] S. W. Churchill and M. Bernstein, "A correlating equation for forced convection from gases and liquids to a circular cylinder in crossflow," *J. Heat Transfer*, vol. 99, pp. 300–306, 1977.

[125] R. J. Goldstein, P. H. Chen, and H. D. Chiang, *Measurement of Temperature and Heat Transfer. Handbook of Heat Transfer*, 3rd ed. McGraw-Hill, 1998.

[126] W. D. Harvey, P. C. Stainback, J. B. Anders, and A. M. Cary, "Nozzle wall boundary-layer transition and freestream disturbances at mach 5," *AIAA Journal*, vol. 13, pp. 307–314, 1975.

[127] M. D. Mack and J. H. McMasters, "High Reynolds number testing in support of transport airplane development," *AIAA Paper 92-3982*, 1992.

[128] S. J. Park, "A new method for measuring time constants of a thermocouple wire in varying flow state," *Experiment in Fluid*, vol. 21, pp. 380–386, 1996.

[129] S. R. Pate and C. J. Schueler, "Radiated aerodynamic noise effect on boundary-layer transition in supersonic and hypersonic wind tunnel," *AIAA Journal*, vol. 7, no. 3, 1969.

[130] P. R. N. Childs., *Practical Temperature Measurement*. Butterworth Heinemann, Oxford, 2001.

[131] C. S. Wells, "Effects of free stream turbulence on boundary layer transition." *AIAA Journal*, vol. 5, no. 1, pp. 172–174, 1967.

[132] Burr-Brown Corporation, http://www.burr-brown.com.

Appendix A

Circuit Amplifier of INA105

Figure A.1 is schematic diagram of the circuit amplifier used for the thin film heat gauge measurement.

The INA105 is a monolithic Gain = 1 differential amplifier consisting of a precision op amp and on-chip metal film resistors. The resistors are laser trimmed for accurate gain and high common-mode rejection. Excellent TCR tracking of the resistors maintains gain accuracy and common-mode rejection over temperature.

The differential amplifier is the foundation of many commonly used circuits. The INA105 provides this precision circuit function without using an expensive precision resistor network. The INA105 is available in 8-pin plastic DIP, SO-8 surface-mount and TO-99 metal packages [132].

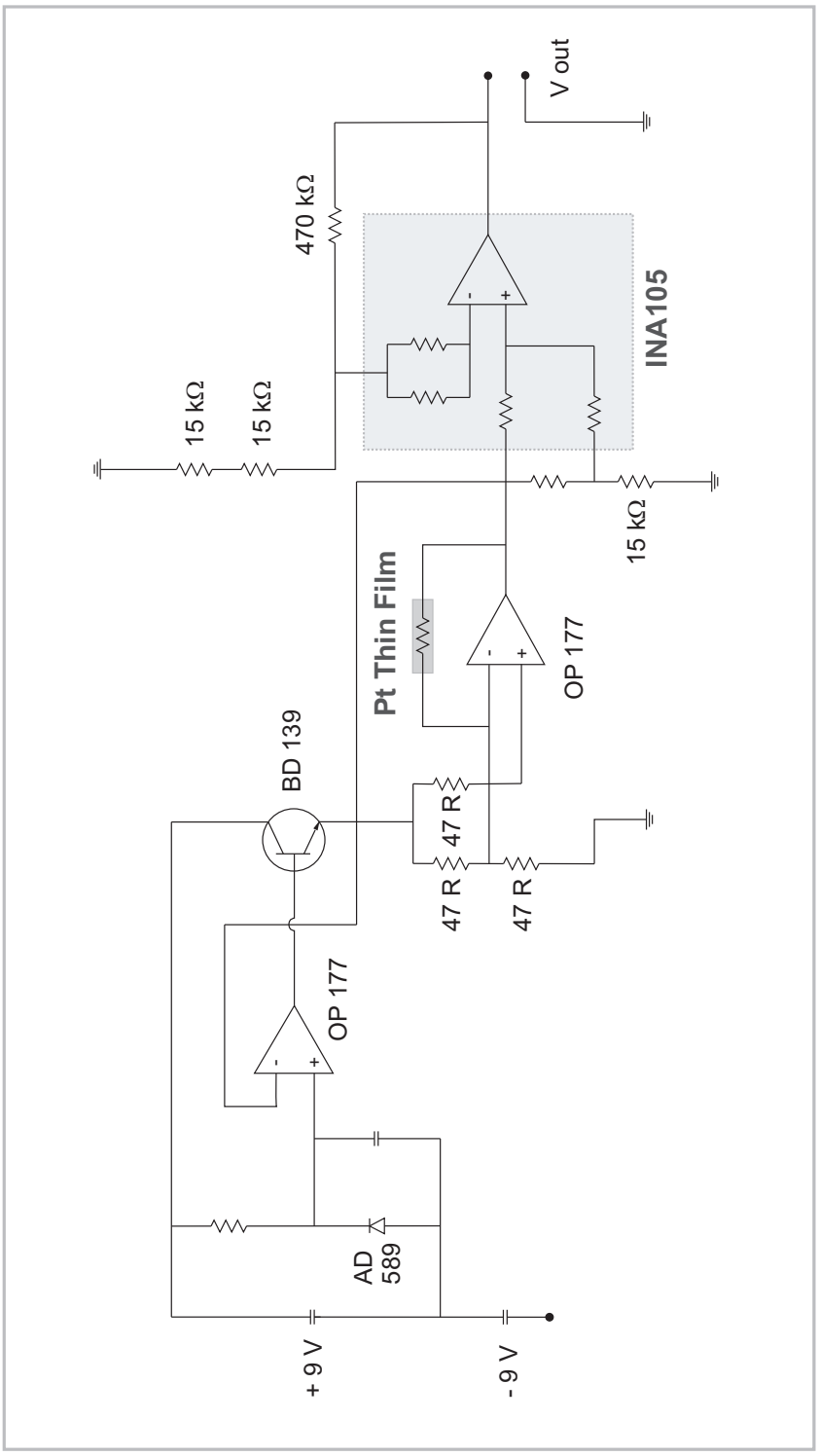

Figure A.1: Circuit amplifier based on the INA105 chip as used for the current experiments reported here in.

Appendix B

Thermocouple Position Matrix

Figure B.1 show position of the thermocouple probes during the program of spatial stagnation temperature measurements at the Mach 6 nozzle exit as reported in chapter 7. Four thermocouple probes were used simultaneously in the experiment. To obtain measurements at spatial increments of about 5 mm, the probes were repositioned between the runs. After a sequences of four runs, two thermocouples were broken, and replacements were installed. The measurements were performed until the boundary layer at the nozzle wall was resolved to some degree.

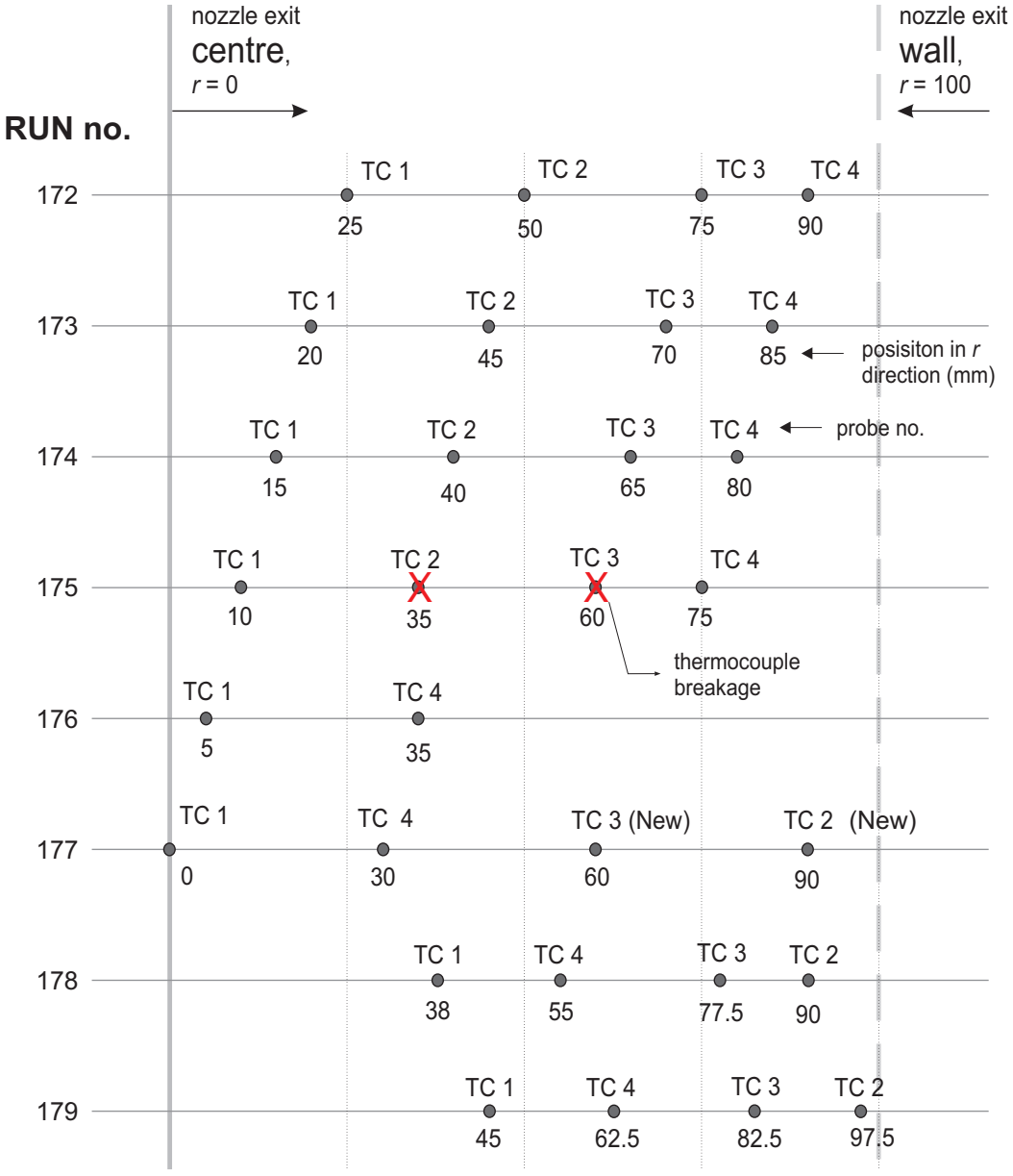

Figure B.1: Matrix showing positions of the thermocouple probes during the program of spatial stagnation temperature measurements at the Mach 6 nozzle exit of the TUSQ.

Appendix C

Photos of Experiments

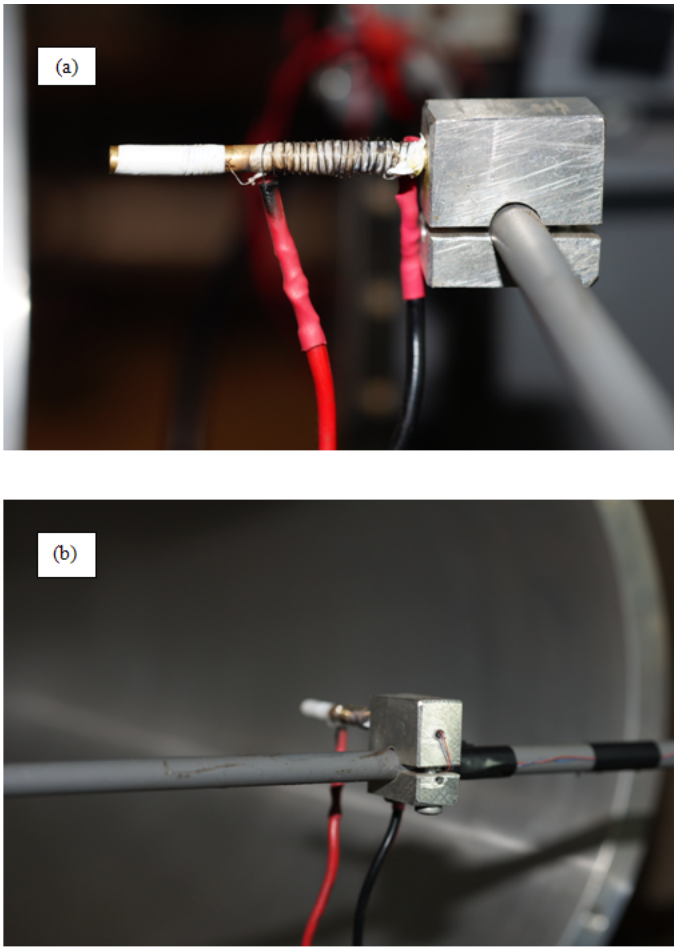

Figure C.1: Photographs showing: (a) sideview of the t-type thermocouple probe; and (b) the position of t-type thermocouple probe relative to the Mach 6 nozzle exit of the TUSQ.

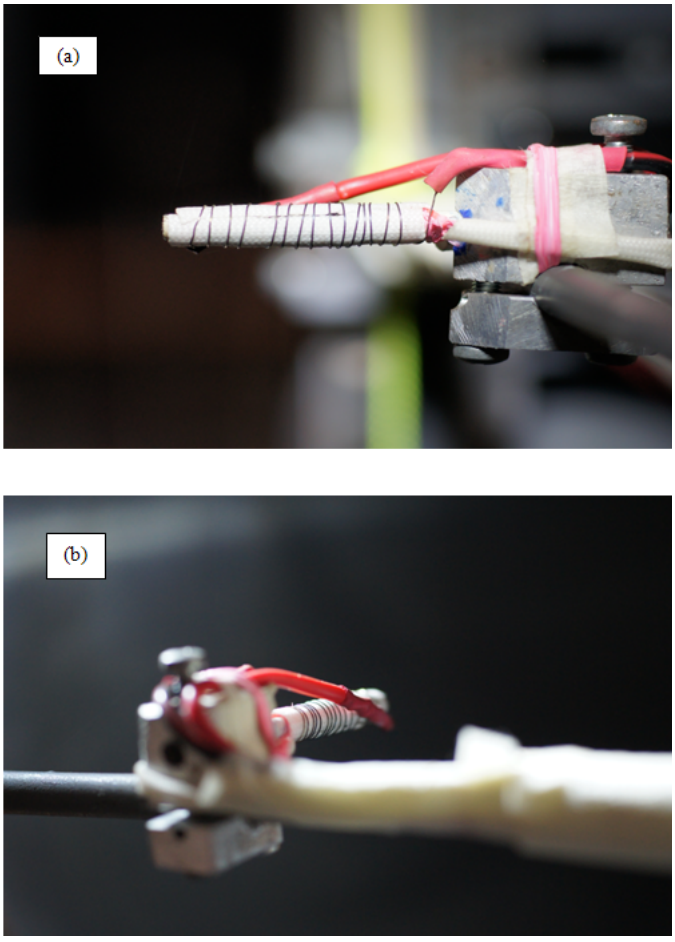

Figure C.2: Photograph of the k-type thermocouple probe showing different views in part (a) and (b).

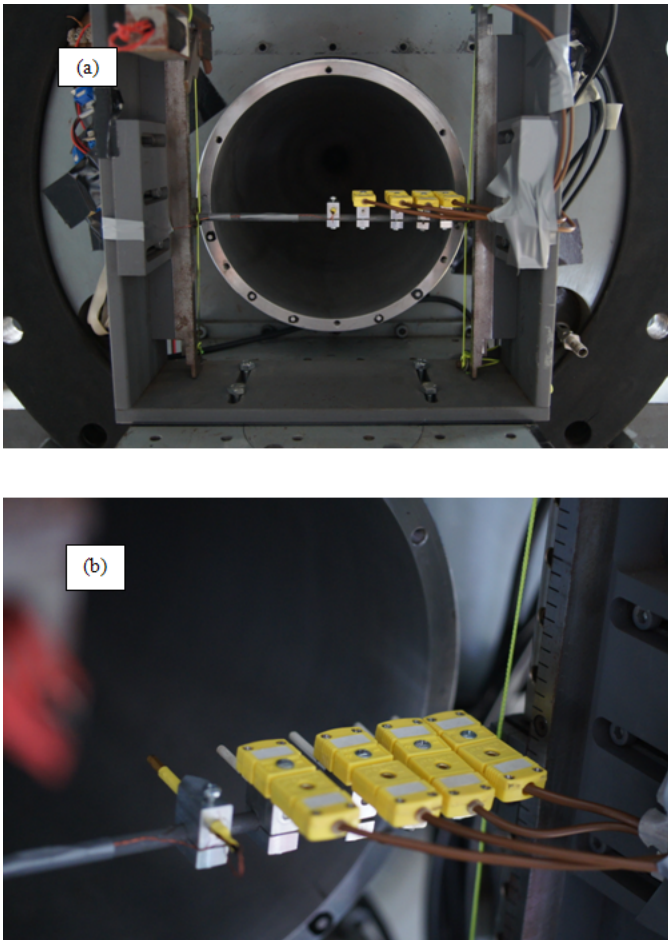

Figure C.3: Photographs of the spatial thermocouple probe rake used in the current experiments with different views in part (a) and (b).

Appendix D

Physical Properties of Thermoelement Materials

Table D.1: Physical Properties of Thermoelement Materials. (Source: Omega Corp.).

Property	Chromel	Alumel
Melting point,°C	1427	1399
Resistivity, $\mu\Omega$		
at 0^oC	70	28.1
at 20^oC	70.6	29.4
Temperature coefficient of resistance, $\Omega/\Omega.^o$C (0 to 100^oC)	4.1×10^{-4}	23.9×10^{-4}
Coefficient of thermal expansion, in./in.^{o}C (20 to 100^oC)	13.1×10^{-6}	12.0×10^{-6}
Thermal conductivity at 100^oC, Cal.cm/s.cm^2.^{o}C	0.046	0.071
Specific heat at 20^oC, cal.g^{o}C	0.107	0.125
Density, g/cm^3	8.73	8.60
Tensile strength (annealed), MPa	655	585
Magnetic attraction	none	moderate

Appendix E

Reynolds number based on friction velocity

Reynolds number base on the mean velocity of the flow is written as

$$Re = \frac{\rho \bar{u} D}{\mu} \tag{E.1}$$

where ρ is the density of the gas, $\bar{u}$ is the average velocity at the centreline of the pipe, D is the diameter of the pipe, and μ is the dynamic viscosity of the gas.

Reynolds number based on friction velocity can be defined as:

$$Re_\tau = \frac{\rho u_\tau R}{\mu} \tag{E.2}$$

where R is radius of the pipe and u_τ is the friction velocity defined as:

$$u_\tau = \sqrt{\frac{\tau_w}{\mu}} \tag{E.3}$$

τ_w is the shear stress at the wall defined as:

$$\tau_w = \frac{f\rho\bar{u}^2}{8} \tag{E.4}$$

where f is the friction factor obtained from Petukhov formula,

$$f = \frac{1}{\left(0.79\ln\left(\mathrm{Re}\right) - 1.64\right)^2} \tag{E.5}$$

Appendix F

Pitot Pressure and Normalised Pitot Pressure Outside the Core

Figures F.1. shows pitot pressure history and normalised pitot pressure outside the core indicated by +90.6 mm from the centre of the flow. Pitot pressure history and normalised pitot pressure inside the core (within 0 - $\sim$ 80 mm from the centre of the flow) are presented in section 7.3.1.

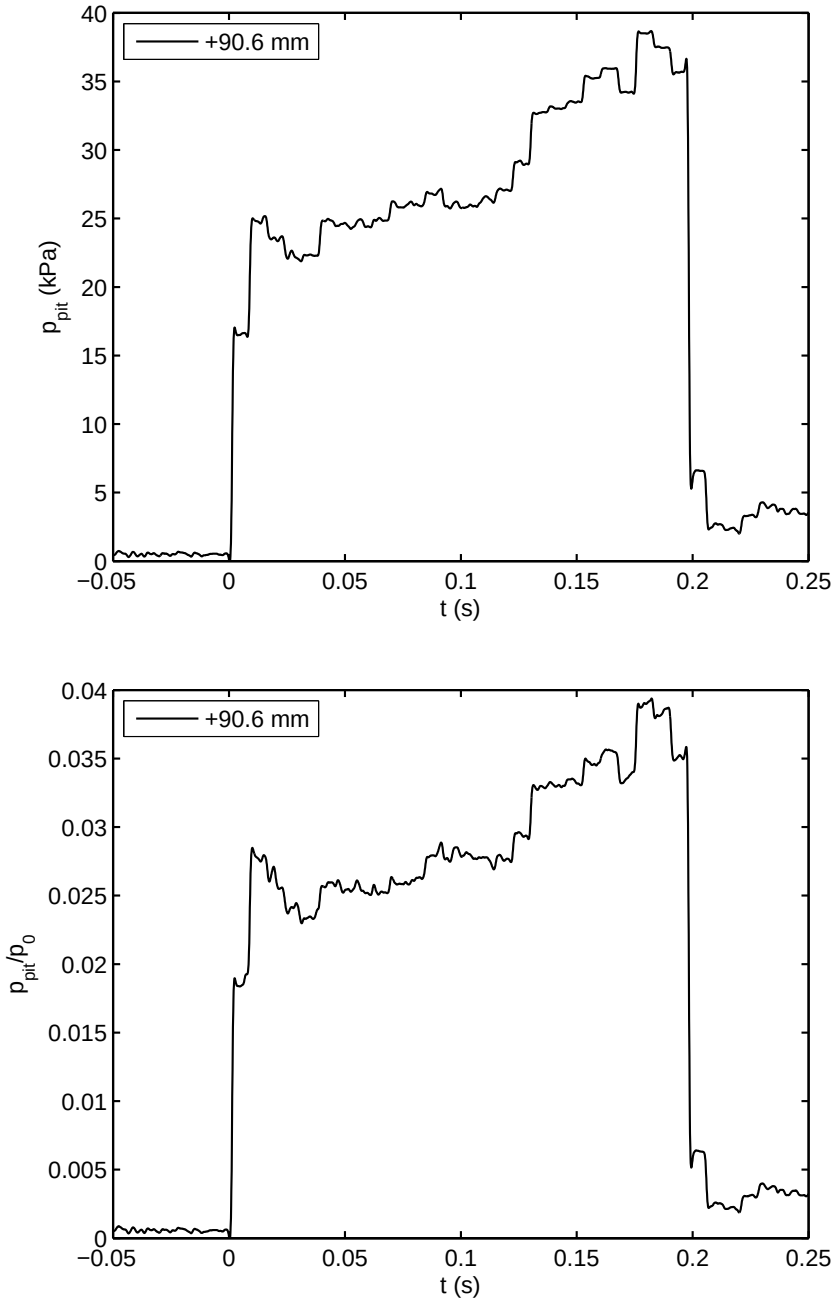

Figure F.1: Pitot pressure and normalised pitot pressure outside the core.

Appendix G

East's and Current Temperature Signals

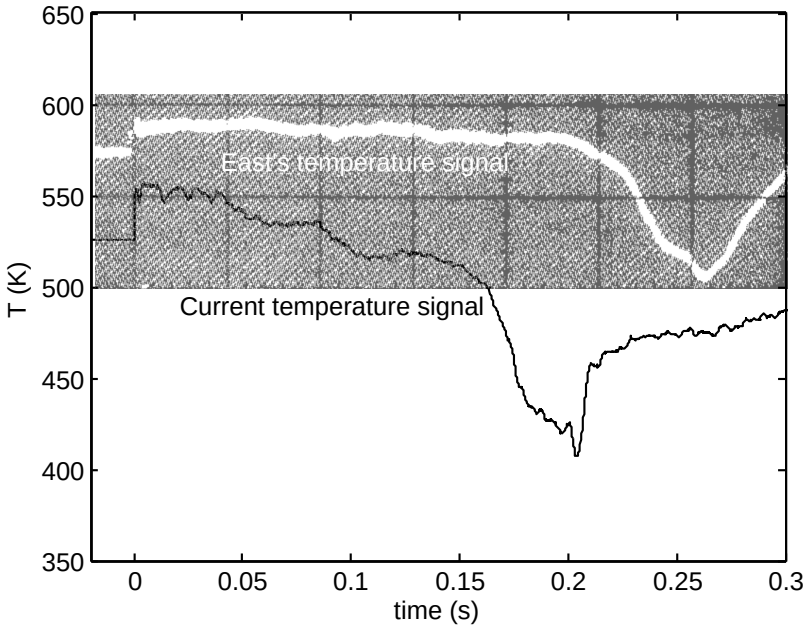

Figure G.1: East's and current temperature signals.